Università degli Studi di Palermo

AREA RICERCA E TRASFERIMENTO TECNOLOGICO
SETTORE DOTTORATI E CONTRATTI PER LA RICERCA
U. O. DOTTORATI DI RICERCA

PhD Course in Biomedicine, Neuroscience and Advanced Diagnostics
Dipartimento di Biomedicina, Neuroscienze e Diagnostica Avanzata
Settore Scientifico Disciplinare - Anatomia Umana - BIOS-12/A

Regulation of mitochondrial dynamics imbalance as a potential therapy for Spinal Muscular Atrophy

IL DOTTORE

Francesco Paolo Zummo

IL COORDINATORE

Prof. Fabio Bucchieri

IL TUTOR

Prof. Fabio Bucchieri

CICLO XXXVIII - ANNO CONSEGUIMENTO TITOLO 2025/2026

INDEX……1

INTRODUCTION…….....4

1. The human nervous system…….....4
1.1 Subdivision of the central nervous system…….4
1.2 Early brain development…….5
1.3 Spinal cord Motor Neurons differentiation…….6
1.4 Motor neurons (MNs)…….7
1.4.1 Upper motor neurons……..7
1.4.2 Lower motor neurons…….....7
1.5 Columnar organization of spinal cord motor neurons……....9

2. Mitochondria: beyond the powerhouse of the cell……11
2.1 Mitochondrial dynamics……...12
2.1.1 Mitochondrial fusion and main regulators…….……...13
2.1.2 Mitochondrial fission and main regulators……..….14
2.2 Mitochondrial dynamics in neurodegenerative disorders……15
2.3 Pharmacological strategies to modulate mitochondrial dynamics……....16
2.3.1 Teriflunomide……...……18

3. Spinal Muscular Atrophy (SMA)…….....19
3.1 Genetic basis of the disease……..19
3.2 Clinical classification of SMA……..20
3.3 SMN protein and cellular functions……..21
3.4 Development of approved therapeutic strategies for SMA…….....23
3.4.1 Limits of SMA-approved therapies……..24
3.5 The role of SMN in mitochondria……24
3.5.1 Mitochondrial dysfunction in SMA……..25

HYPOTHESIS AND AIMS……28

MATERIALS AND METHODS……29

1. Mouse model and colony maintenance……29
1.1 SMNDelta7 mice…….……..29
1.2 Genotyping…….....30

2. Primary mouse MNs…….....30
2.1 Mouse MNs isolation…….....30
2.2 Precoating plates……...31
2.3 Mouse MN plating ……...…….....32
2.4 Western Blotting (WB) analysis of mouse MNs……..32
2.5 Immunofluorescence (IF) on mouse MNs…….....32

3. Human-induced Pluripotent Stem Cells (iPSC)……..33
3.1 MN differentiation protocol……..33
3.2 Mouse MN plating and drug treatment……34
3.3 IF on human MNs……..34
3.4 WB analysis of human MNs……34
3.5 Mitochondrial Network Analysis (MiNA) toolset……35
3.6 Automated Cell Counting after drug treatment……35

4. Human fibroblast cell lines…….....36
4.1 Maintenance…….....36
4.2 Cell plating and drug treatment…….....37
4.3 WB analysis of human fibroblasts……37
4.4 Fluorescence-Activated Cell Sorting (FACS) analysis……38
4.5 MitoTracker Red CMXRos labelling……38
4.6 mACO2 enzymatic activity assay……39
4.7 IF on human fibroblasts……39
4.8 MTS assay for human fibroblasts ……40
4.9 MitoTracker Green FM labelling ……40
4.10 Colocalization rate analysis between TOM20 and LC3……41

5. Statistical analysis…….....41

RESULTS…….....……....42

1. SMA mouse and human MNs show a significant reduction in the overall mitochondrial content……..42
2. Mitochondrial network distribution is altered between soma and neurites in SMA mouse and human MNs……...43
3. Global moderate imbalance toward the fission of mitochondrial dynamic regulators in SMA mouse and human MNs……..45
4. Differential regulation of mitochondrial fusion and fission between soma and neurites in SMA human MNs…….....47
5. TFN, a fusion-promoting drug, increases mitochondrial content and upregulates SMN in SMA human MNs……...49
6. SMA human fibroblasts exhibit mitochondrial dysfunctions, despite unaltered mitochondrial content……...51
7. Mitochondrial network fragmentation is moderately increased in SMA human fibroblasts……..53
8. Fusion-promoting drug enhances mitochondrial network fusion in SMA human fibroblasts……..55
9. Enhanced mitochondrial fusion promotes organelle enrichment without suppressing mitophagy in SMA humafibroblasts…….……58
10. Mitochondrial content enhancement boosts membrane potential and upregulates Complex V and SMN in SMA human fibroblasts……60

DISCUSSION…….....62

REFERENCES…….....70

INTRODUCTION

1. The human nervous system

The human nervous system is the most complex and organized structure of the body. Like the rest of the upper vertebrates, the human nervous system is typically divided into two main parts: the central nervous system (CNS) and the peripheral nervous system (PNS).

The **CNS**, involved in the analysis and integration of sensory and motor stimuli and information, is usually divided into the **brain** (cerebral hemispheres, diencephalon, cerebellum, and brainstem) and the **spinal cord**.

The **PNS**, including **cranial** and **spinal nerves** (and their branches), can receive and send these processed signals to the effector organs thanks to the presence of two different components. In particular, the **sensory component**, receiving stimuli from the internal and external environment, is made by sensory nerves, ganglia, and sensory receptors (at the surface and within the body). The **motor component**, in turn, consists of motor axons, connecting the brain and spinal cord to skeletal muscles -resembling the **somatic motor system-,** and cells and axons innervating smooth and cardiac muscles, and glands -representing the **visceral** or **autonomic motor system-**. In the peripheral nervous system, the neuronal cell bodies (together with supporting cells) are organized in **ganglia**. Peripheral axons are organized into structures known as **nerves**. These nerves are commonly enveloped by Schwann cells, a specialized class of glial cells.

In contrast, within the CNS, the architectural organization of neurons differs substantially. Neurons are arranged either in localized clusters called **nuclei**, characterized by shared connections and functions, or in sheet-like structures forming the **cerebral** and **cerebellar cortices**. Axons within the CNS aggregate into pathways referred to as **tracts**, which function analogously to peripheral nerves. Notably, those tracts that traverse the brain's midline are termed commissures. Furthermore, a distinction is made between gray and white matter based on histological characteristics**: gray matter** comprises accumulations of neuronal cell bodies and neuropil, while **white matter**, owing to the high lipid content of myelin, contains axonal tracts and commissures and appears relatively pale in histological preparations (Nieuwenhuys et al., 2008; Purves et al., 2004).

1.1 Subdivision of the central nervous system

The CNS is usually considered to have **seven** basic parts: the medulla, the pons, the midbrain, the cerebellum, the diencephalon and the telencephalon (cerebral hemispheres), and the spinal cord.

The medulla, pons, and midbrain together form the **brainstem**, a central structure that supports numerous critical functions. Embedded within the brainstem are cranial nerve nuclei, which either receive sensory input from cranial sensory ganglia via cranial nerves or give rise to motor axons that form the cranial motor nerves. Additionally, the brainstem serves as a conduit for major CNS tracts that transmit ascending sensory information from the spinal cord and brainstem to the forebrain, as well as descending motor commands from the forebrain to motor neurons in the brainstem and spinal cord. Beyond its role as a relay system, the brainstem contains numerous nuclei involved in vital autonomic processes, including the regulation of heart rate, respiratory rhythm, blood pressure, and levels of consciousness.

Prominently situated on its dorsal aspect is the **cerebellum**, a structure essential for the coordination and planning of voluntary movements, the acquisition of motor skills, and the storage of procedural memories.

Superior to the brainstem lies the **forebrain**, comprising the diencephalon and the cerebral hemispheres. The **cerebral hemispheres** are the most visually apparent subdivisions and are markedly expanded in humans relative to other species. Despite individual variation, several sulcal landmarks consistently delineate the four lobes of the cerebral hemispheres: frontal, parietal, temporal, and occipital -names corresponding to the overlying cranial bones. Flanking this landmark are the precentral and postcentral gyri, which house the primary motor cortex and the primary somatosensory cortex, regions crucial for the execution of movement and the perception of somatic sensory input.

Located centrally within the brain, the **diencephalon** plays a pivotal role in integrating sensory and motor pathways and maintaining homeostatic balance. It is composed of the thalamus and hypothalamus, along with the epithalamus and subthalamus. The **thalamus** serves as a major relay station, channeling afferent sensory signals to the appropriate cortical regions for further processing. The **hypothalamus**, by contrast, orchestrates a vast array of autonomic and endocrine functions, regulating body temperature, appetite, circadian rhythms, and hormonal secretions via its influence over the pituitary gland. The diencephalon thus acts as a crucial interface between the nervous and endocrine systems, mediating both conscious perception and unconscious physiological regulation.

Equally central to the architecture of the central nervous system is the **spinal cord**, an elongated structure that extends from the base of the brainstem to the lumbar vertebral region, acting as the main communication conduit between the brain and the rest of the body. Organized into distinct segments -cervical, thoracic, lumbar, sacral, and coccygeal-, it gives rise to pairs of spinal nerves that innervate specific body regions. Internally, the spinal cord exhibits a central core of grey matter (containing neuronal cell bodies) surrounded by white matter (comprised of myelinated axons). The grey matter is divided into **dorsal horns** (sensory processing), **ventral horns** (motor output), and, in the thoracic region, **lateral horns** (autonomic functions). The white matter is arranged into dorsal, lateral, and ventral columns that house ascending sensory and descending motor tracts. The spinal cord is essential for relaying sensory information to the brain, transmitting motor commands to the body, and executing local processing such as reflexes and rhythmic motor patterns. It is protected by three meningeal layers and supplied by dedicated spinal arteries (Nieuwenhuys et al., 2008; Purves et al., 2004; Standring et al., 2020).

1.2 Early brain development

The adult brain emerges as a highly intricate organ shaped by the interplay of genetic programming, intercellular signalling, and continuous interaction with the external environment throughout development. Early neural development encompasses the emergence of the primordial nervous system, the differentiation of neural precursors, the regionalization of the brain, and the spatial migration of neurons to their definitive anatomical locations. Two pivotal embryonic processes underpin the initial formation of the vertebrate nervous system: the establishment of embryonic polarity (anterior-posterior and medial-lateral axes) and the specification of the three primary germ layers.

Gastrulation marks the first of these, wherein a single sheet of embryonic cells undergoes coordinated invagination to generate the ectoderm, mesoderm, and endoderm. This process not only defines the body's major axes but also lays the foundation for neural induction. At the embryonic midline, a cylindrical structure of mesodermal origin -termed the **notochord**- extends from anterior to posterior, developing via invagination through a surface depression known as the primitive pit, which elongates into the primitive streak. The notochord acts as a central organizing structure, emitting inductive signals that instruct the overlying ectoderm to form the neuroectoderm.

This specialized ectodermal region, through a process known as **neurulation**, gives rise to a thickened epithelial sheet, the **neural plate**. As neurulation progresses, the lateral edges of the neural plate elevate and converge at the dorsal midline, forming the **neural tube**, the embryonic precursor to the central nervous system. Neural precursor cells lining the neural tube undergo proliferative expansion and differentiation into neurons, astrocytes, and oligodendrocytes (Kandel et al., 2000; Purves et al., 2004).

1.3 Spinal cord Motor Neuron differentiation

During early neurodevelopment, the **neural tube** undergoes spatial patterning along two principal embryonic axes: the rostrocaudal (anterior–posterior) and dorsoventral (medial-lateral) axes. These positional axes are defined by gradients of morphogenetic signals that establish a molecular coordinate system guiding the regional specification and differentiation of neuronal subtypes (Kandel et al., 2000).

Along the **rostrocaudal axis**, the neural tube differentiates into the principal components of the CNS, including the forebrain, midbrain, hindbrain, and spinal cord. A critical driver of this patterning is caudalization, a process predominantly regulated by the paraxial mesoderm flanking the neural tube. This mesodermal tissue expresses aldehyde dehydrogenase 1A2, an enzyme responsible for the oxidative conversion of retinaldehyde to retinoic acid (RA). RA functions as a morphogen essential for the specification of posterior neural identities -particularly those of the hindbrain and spinal cord- by distinguishing them from anterior regions such as the forebrain and midbrain (Maden, 2007).

The **dorsoventral axis**, by contrast, is established through the integration of opposing signaling gradients originating from both the dorsal roof plate and the ventral midline structures. Dorsally, members of the Wnt family and bone morphogenetic proteins (BMPs), along with their antagonists -including Noggin (NOG), Chordin (CHRD), and Follistatin (FST)- are secreted from the roof plate. Ventral patterning is orchestrated by the secretion of Sonic Hedgehog (Shh) morphogen from the notochord and floor plate. Shh binds to its transmembrane receptor Patched-1 (PTCH1), relieving its inhibition of the receptor Smoothened and initiating an intracellular signaling cascade. The integration of Shh and counteracting dorsal morphogens establishes distinct transcriptional territories (p0, p1, p2, pMN, and p3), each characterized by the expression of a unique combination of transcription factors and destined to generate distinct neuronal subtypes, including **Motor Neurons** (MNs). MNs of the spinal cord originate exclusively from the **pMN progenitor domain**, whose identity is specified by Shh-induced downstream signaling cascades. This signaling activates homeodomain transcription factors such as Nkx6.1, Olig2, and Nkx2.2, while repressing dorsalizing factors including Pax6, Irx3, Dbx1, and Dbx2. Within the pMN

domain, Nkx6.1 functions to suppress the expression of non-MN progenitor programs, thereby reinforcing domain specificity. Critically, the transcription factor Olig2 promotes neurogenesis by inducing the proneural gene Neurogenin-2. This induction facilitates both cell cycle exits and the initiation of a transcriptional program characteristic of postmitotic MNs, including the expression of Hb9 (Mnx1), Isl1, Isl2, and Lhx3. The completion of MN differentiation is contingent on this precisely orchestrated sequence of transcriptional events, culminating in the transition from proliferative progenitor to mature, functional motor neuron. (Briscoe et al., 2000; Kandel et al., 2000).

1.4 Motor Neurons (MNs)

MNs are exceptional neuronal cells located within the CNS, where they are responsible for generating and transmitting the nerve impulses that can produce the contraction of the muscles. The complex and fascinating networks that control the locomotion processes are known as **motor circuits**: pathological alterations in these circuits are involved in many neurodegenerative disorders. MNs are divided into two main populations that must be considered as distinct entities: upper and lower motoneurons. Their differences regard not only their location but also their cellular characteristics and functions (Stifani, 2014).

1.4.1 Upper Motor Neurons (MNs)

Upper MNs are responsible for planning and directing body movements by sending their axons downward and connecting with lower MNs in the brainstem or spinal cord. These MNs represent a type of giant pyramidal cells known as pyramidal cells of Betz or Betz cells, specifically located in the fifth layer of the cortical grey matter and characterized by glutamatergic connections. The soma of the upper MNs is positioned in the premotor and primary motor regions of the cerebral cortex. In particular, descending projections from the Brodmann's area 4 (the primary motor cortex), the lateral part of area 6 (the lateral premotor cortex), and the medial part of area 6 (the medial premotor cortex) are essential for planning, initiating and directing sequences of voluntary movements (Purves et al., 2004; Stifani, 2014).

1.4.2 Lower Motor Neurons (MNs)

Lower MNs project their axons outside the CNS, directly forming synapses with skeletal muscles or indirectly through the basal ganglia to control muscle contraction. Lower MNs are cholinergic neurons, whose soma are positioned in the nuclei of the cranial nerves in the brainstem and the ventral horn of the spinal cord. In particular, those sending their axons out of the brainstem innervate the skeletal muscles of the head, while the others sending their projections out of the spinal cord innervate the skeletal muscles of the body. These MNs can receive inputs from upper MNs or sensory neurons and interneurons. Moreover, according to the type of target they innervate, lower MNs can be classified into three groups: branchial, visceral, and somatic MNs (Purves et al., 2004; Stifani, 2014).

Branchial MNs are MNs in the brainstem, forming together with sensory neurons the cranial nuclei. These MNs innervate the muscles of the face and neck through five cranial nuclei: the

trigeminal (V), facial (VII), glossopharyngeal (IX), vagus (X), and accessory (XI) nerves (Chandrasekhar, 2004).

Visceral MNs belong to the autonomic nervous system, and they are responsible for the control of smooth muscles (i.e., heart and arteries) and glands. These autonomic (preganglionic) MNs in the CNS connect with postganglionic neurons, which in turn target the final effector organs.

Somatic MNs, whose cell soma is located in the ventral horn of the spinal cord, control skeletal muscles (Rexed, 1954). Their remarkable characteristic is their long axonal extension. Each MN, together with the muscle fibers innervated, forms the structure known as motor unit. Depending on the muscle fiber type they innervate, somatic MNs can be distinguished, in turn, into three different groups: alpha, beta, and gamma.

1) **Alpha MNs (α-MNs)**, the most abundant type, are characterized by a large soma and specific innervation to extrafusal muscle fibers, the striated muscle generating the forces needed for posture and movement. These MNs can receive monosynaptic innervation directly from upper MNs and sensory neurons and play an important role also in the spinal reflex circuit (Eccles et al., 1960). Based on the contractile properties, size, conductivity, and excitability of the extrafusal fibers innervated, alpha MNs can be classified into:

- **Slow-twitch fatigable-resistant (SFR):** These MNs are characterized by a smaller soma with reduced axonal length. They are recruited first during muscle contraction, since they establish neuromuscular junctions (NMJs) with small and slowly contracting red muscle fibers that respond to a lower stimulation threshold. These fibers tend to have the capacity to maintain their contraction after the stimulation ceases since their rich myoglobin content, high mitochondrial mass, and rich capillarization. Therefore, SFR MNs are especially important for activities that require sustained but not excessive muscular contraction, such as the maintenance of an upright posture. The conduction velocity registered is about 85 m/s (Burke et al., 1973).
- **Fast-twitch fatigable (FF):** FF MNs present a larger soma with a remarkable arborisation and many presynaptic terminals. They are recruited after the initial recruitment of SFR MNs since they form junctions with larger and rapidly contracting pale muscle fibers that generate more force for the activated muscle. This type of fiber is characterized by sparse mitochondria and is therefore easily fatigued. Indeed, FF MNs are involved in movements that require short impulses and large force, such as running or jumping. Their conduction velocity is about 100 m/s (Burke et al., 1973).
- **Fast-twitch fatigable-resistant (FFR)**: possessing intermediate characteristics between the two previous α-MNs types, these MNs are of an intermediate size. They can generate twice the force of SFR MNs, but they are not as fast as FF MNs and therefore are more resistant to fatigue (Burke et al., 1973).

2) **Beta MNs (β-MNs)**, the less abundant type among the other somatic MN subtypes, are characterized by a smaller soma and an unspecific innervation for both extrafusal and intrafusal muscle fibers, controlling both muscle contraction and receptiveness of the sensory feedback from muscle spindles. According to the type of muscle fibers innervated, β-MNs can be distinguished in **static** for those innervating extrafusal fibres and, therefore, able to increase the firing rate, or in **dynamic** if they innervate intrafusal fibres, increasing the stretch-sensitivity (Bessou et al., 1965).

3) Gamma MNs (γ-MNs), more represented than beta-MNs and less than alpha-MNs, are defined by the smaller axon diameter and lower degree of arborisation, together with exclusive innervation of the sensitivity of muscle spindles, therefore regulating complex functions in motor control. Indeed, these MNs receive innervation from proprioceptive sensory neurons only indirectly, not participating in spinal reflexes and motor function, but contributing to the modulation of muscle contraction through direct stimulation of intrafusal muscle fibers by increasing the tension of the fibers. These MNs can be categorized, like β-MNs, as **static** if they enhance stretch sensitivity or **dynamic** for those enhancing dynamic sensitivity (Eccles et al., 1960).

1.5 Columnar organization of spinal cord MNs

Along the mature spinal cord, MNs are distributed in an organized system characterized by distinctive anatomical structures, resembling columns and extending along the rostro-caudal axis, called the motor columns. Each column possesses a specific gene expression profile and uniform axonal projection pattern. In recent years, the canonical classification into four different main columns has been modified, including two other less well-characterized motor columns.

Generally, the **median motor column (MMC)** includes MNs along the entire rostrocaudal axis of the spinal cord in the medial region of the ventral spinal cord, projecting their axons towards the axial musculature and therefore maintaining the body posture. Their gene profile is defined by the co-expression of MNX1, ISL1/2 and LHX3 (Tsuchida et al., 1994).

The **lateral motor column (LMC)** includes MNs located in the most lateral portion of the ventral spinal cord at the brachial (C5-T1) and lumbar (L1-L5) levels, innervating muscles of the extremities and defined by the expression of ISL2, FOXP1, and ALDH1A2 (Sockanathan et al., 2003).

The **hypaxial motor column (HMC)** is represented by MNs only positioned in the ventrolateral area of the thoracic segments, projecting their axons towards the intercostal and abdominal muscles, involved in breathing. Genetically, these MNs are determined by MNX1, ISL1, ETV1, and low levels of ISL2 expression (Dasen et al., 2008).

The **preganglionic column (PGC)** is defined by MNs located at the thoracic and upper lumbar spinal segments (T1-L2) and sacral segments (S2-S4), only innervating the sympathetic ganglia neurons and involved in the smooth muscle stimulation and the control of glandular secretions. Their molecular profile can be elucidated by SMAD1 expression (Dasen et al., 2008).

The **spinal accessory column (SAC)** is represented by MNs positioned in the intermedio-lateral region of the cervical segment (C1-C5), innervating the mastoid muscles and some neck muscles. Their genetic profile is distinguished from others by the expression of ALCAM, ISL1, RUNX1, and PHOX2B (Mazzoni et al., 2013).

Finally, the **phrenic motor column (PMC)** represents MNs found in the cervical segments (C3-C5) and innervating the diaphragm, therefore involved in the constant rhythmic activity of breathing. These MNs are characterized by HOX5, POU3F1, ISL1/2, and MNX1 co-expression (Philippidou et al., 2012).

A comprehensive understanding of the organization, structure, and molecular functions of spinal cord MNs is fundamental to elucidating the pathophysiology and clinical consequences of neuromuscular diseases. Damage or degeneration of MNs often results in the loss of precise control

over muscle groups, leading to muscle weakness, hypotonia, fasciculations, and progressive atrophy. This vulnerability of spinal MNs becomes especially evident in neurodegenerative diseases, such as Spinal Muscular Atrophy (SMA), specifically characterized by the progressive degeneration of lower α-MNs in the brainstem and anterior horns of the spinal cord. Notably, the high metabolic demands and sustained activity of MNs render them particularly susceptible to changes in mitochondrial function and ATP production. This vulnerability helps explain why disruptions in mitochondrial homeostasis so profoundly impact these neurons. An in-depth understanding of mitochondrial integrity and function is essential for appreciating how neuronal function is maintained under normal conditions and why its disruption can contribute so drastically to the onset and progression of neurodegenerative disorders. Therefore, mitochondria and their dysfunctions will be discussed in detail in the following sections.

2. Mitochondria: beyond the powerhouse of the cell

Mitochondria are unique intracellular organelles due to their evolutionary origin and incredibly high plasticity in eukaryotic cells. More than a billion years ago, an endosymbiotic event occurred between an anaerobic bacterial cell, a strictly hydrogen-dependent and autotrophic archaeon, and an α-Proteobacterium, an obligate intracellular parasite possessing elements of oxidative respiration and producing molecular hydrogen as a waste product (Gray et al., 1999). The relationship between the host (the archaebacterium) and the symbiont (the eubacterium), eventually became the mitochondrion, represented a form of anaerobic syntrophy, involving hydrogen dependence. This scenario, proposed by William F. Martin and Miklos Muller in 1998 and described as the "**hydrogen hypothesis**", considers hydrogen as the selective principle and the evolutionary driver in the development of the common ancestor of eukaryotic cells (Martin et al., 1998). This fascinating and always more emerging theory gained prominence over the "serial endosymbiosis theory", proposed by Lynn Margulis in the 1960s, who explained the origin of eukaryotic cells as a result of multiple symbiotic events. From an evolutionary perspective, mitochondria are considered pivotal to the origin of the first eukaryotic cell, primarily due to the substantial bioenergetic gene contributions that facilitated the integration of the eukaryotic genome. It is no coincidence that the most widely recognized and fundamental function of mitochondria is their capacity to generate energy for the cell, primarily through the synthesis of adenosine triphosphate (ATP) in the process known as oxidative phosphorylation (OXPHOS) (Wadkins et al., 1958). This energy production is crucial for numerous cellular and physiological activities, especially in highly specialized and energy-demanding cells such as neurons, where even minor disruptions in mitochondrial function can have far-reaching consequences for cellular health and overall neural function.

However, the multifaceted role of mitochondria extends beyond the production of simple ATP. Depending on cell type, a variable number of hundreds or thousands of highly dynamic mitochondria form an elaborate tubular reticulum called the **mitochondrial network** (**Figure 1**).

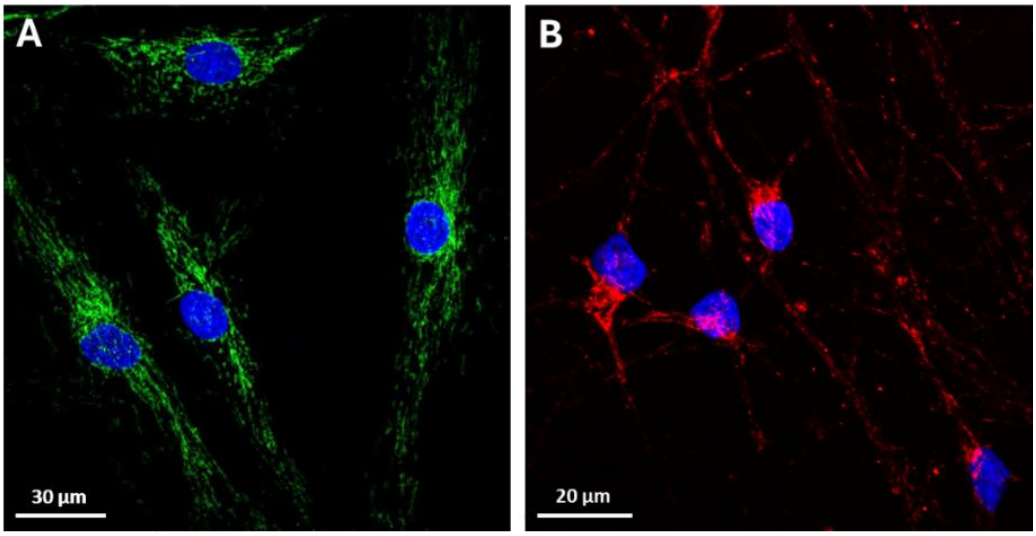

Figure 1. ***Mitochondrial network shape is dependent on cellular type***. Mitochondrial network of healthy human fibroblasts (**A**) and MNs differentiated from healthy human iPSCs (**B**). Mitochondria were labelled with TOM20 antibody, while nuclei were marked with DAPI.

This structure possesses the capacity to rapidly change the number, distribution, size, and shape of mitochondria in response to cellular demands under physiological and pathological conditions (Bahat et al., 2019). Thanks to this singular behavior for cellular organelles, mitochondria can play crucial roles in the metabolism of macromolecules, calcium signalling, membrane potential homeostasis, cytoskeleton dynamics, apoptotic and autophagic processes, and production/scavenging of free radicals (Behringer et al., 2017; Jeong et al. 2008; Angelova et al. 2018). To efficiently mediate these several functions, mitochondria constantly undergo two opposite processes, called fusion and fission (or division), also known as **mitochondrial dynamics.** While this behavior is regulated by eukaryotic proteins that will be discussed in the following paragraphs, it reflects a deeper evolutionary legacy. The ancestral α-proteobacterium that entered symbiosis with a hydrogen-dependent archaeon likely possessed membrane plasticity and interaction capabilities that facilitated its engulfment and integration. This membrane adaptability may have laid the groundwork for the dynamic behaviors seen in mitochondria in eukaryotic cells.

2.1 Mitochondrial dynamics

While mitochondrial **fusion** allows two or more separated organelles to unify, **fission** generates morphologically and functionally distinct mitochondria (Xie et al., 2018). Regulating the network structure, the **fusion-fission balance** establishes the mitochondrial turnover, the organelle distribution, and bioenergetics (Kraus et al., 2021). Indeed, generating sane mitochondria from pre-existing damaged mitochondria or isolating damaged network fractions to commit them to mitophagy, promoting the network tabularization or inhibiting the mitophagy promotion, the mitochondrial dynamics work like a quality control mechanism to maintain a healthy mitochondrial population (Ni et al, 2015) (**Figure 2**).

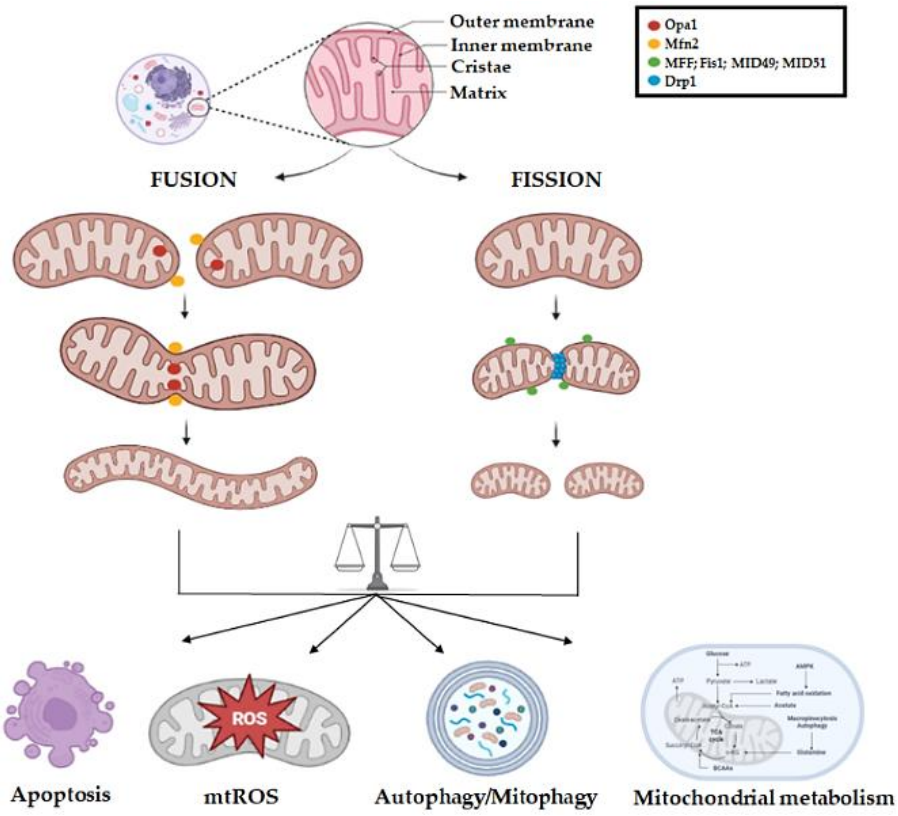

Figure 2. ***Mitochondrial dynamics balance***. The balance between fission and fusion is essential to regulate phenomena like mitochondrial metabolism/function, mitochondrial ROS production, mitochondrial turnover, and cell death processes (Cantafio et al., 2023).

Both fusion and fission are finely orchestrated by the presence of several mitochondrial and cytosolic proteins, also known as **mitochondrial shaping proteins**, cooperating in highly conserved machineries across the species.

2.1.1 Mitochondrial fusion and main regulators

The primary regulators of the fusion machinery are mitofusins (Mfn 1/2) and optic atrophy 1 (OPA1), which are involved in the fusion of the outer mitochondrial membrane (OMM) and the inner mitochondrial membrane (IMM), respectively (**Fig. 3**).

Mfn1/2 are homolog proteins of the *Drosophila* fuzzy onions (Fzo) (Hales et al., 1997) and yeast Fzo1p (Hermann et al., 1998); integral proteins of the OMM of around 86 kDa with the N-terminal GTPase domain facing the cytoplasm, a first coiled-coil heptad repeat (HR1), two adjacent transmembrane domains, and the C-terminal heptad-repeat domain (HR2). While the HR2 domains of two opposing mitochondria physically interact for the initial tethering, the GTP hydrolysis-dependent power stroke is essential for pulling the membranes together (Filadi et al., 2018). The deletion of either Mfn1 or Mfn2 results in impaired mitochondrial fusion, causing embryonic lethality in mice (Chen et al., 2003). In humans, more than 100 MFN2 mutations have been detected in patients with Charcot-Marie-Tooth type 2A (CMT2A), the axonal form of a wide spectrum of primary inherited sensory motor neuropathies (Zuchner et al., 2004). Most of these mutations have been located close to or within the GTPase domain, and the use of agonist drugs seems to reverse the mitochondrial defects, suggesting that the impairment in mitochondrial fusion is one of the pathogenetic mechanisms associated with the CMT2A neuronal die-back and degeneration (Abati et al., 2022). Furthermore, tissue-specific deletion of mitofusins in the CNS, heart, muscle, or liver impairs both metabolic and organ function, underscoring the distinct roles these proteins play across different tissues.

OPA1 is the homolog protein of yeast Mgm1 (Herlan et al., 2003); similarly to Mfn, it is an integral protein of around 100 kDa with a N-terminal mitochondrial targeting sequence domain (MTS), a transmembrane domain that anchors it to the IMM, the GTPase domain facing the cytoplasm, a stalk domain, the paddle domain (PD) and a C-terminal stalk domain (Gao et al, 2021). In humans, the long form (L-OPA1) molecules initiate membrane remodeling and recruit soluble short form (S-OPA1) to rapidly polymerize into a flexible cylindrical scaffold, which becomes an unstable membrane prone to fusion when the GTPase domain perturbs lipid leaflets, removing the PD from the lipid bilayer (Von der Malsburg et al., 2023). Genetic ablation of OPA1 blocks fusion, causing mitochondrial fragmentation. Recently, it was shown that L-OPA1 is sufficient for the maintenance of tubular mitochondria, while the short form is associated with mitochondrial fission (Anand et al., 2014). The human OPA1 gene has been mapped in genetic studies of patients affected by autosomal dominant optic atrophy (ADOA), a hereditary neurodegenerative disease characterized by progressive retinal ganglion cell loss and optic nerve degeneration. Over 400 different OPA1 variants have been described, and those involving the GTPase domain are associated with a higher risk of developing ADOA (Cartes-Saavedra et al.,

2023). Like mitofusins, the abundance of L-OPA1 and S-OPA1 varies significantly among tissues, underscoring the distinct requirements of different tissue types. Moreover, independently of its crucial role in mitochondrial fusion events, OPA1 is a master regulator of cristae shape and indirectly of mitochondrial function (Frezza et al., 2006). Indeed, genetic models of OPA1 ablation and mild overexpression show, along with apoptotic cristae remodeling, also respiratory chain complexes assembly defects and, ultimately, respiratory efficiency compromise (Cogliati et al., 2013).

Interestingly, the **ATP synthase** is the only protein complex so far reported as sufficient to induce a positive curvature at the apex of IMM invaginations, contributing to the origin of cristae (Paumard et al., 2002). During mitochondrial fusion, ATP synthase dimers can pinch the inner mitochondrial membrane and expand it to form rows. The genetic ablation of dimerization subunits results in the loss of cristae or the generation of aberrant shapes, highlighting the intertwining role of the ATP synthase in mitochondrial ultrastructure and bioenergetics (Arselin et al., 2004).

2.1.2 Mitochondrial fission and main regulators

The main regulator of fission machinery is Drp1 (dynamin-related protein 1) in association with a wide range of its receptors/adaptors (FIS1, MFF, MiD49) anchored to mitochondrial membranes (**Figure 3**).

Drp1 is a cytoplasmic protein of around 80 kDa that is comprised of four distinct domains: the C-terminal GTPase effector domain (GED), a variable domain that can interact with lipids, a stalk domain responsible for the Drp1 homo-oligomerization, and a BSE domain connecting the GTPase domain to the stalk domain. In the fission process, Drp1 is initially recruited from the cytoplasm through interaction with its receptors on OMM and forms polymers resembling linear filaments around mitochondrial tubules, called fission sites. GTP hydrolysis then triggers the dissociation of these polymers, leading to the formation of ring-shaped Drp1 polymers that constrict mitochondrial tubules (Loson et al., 2013; Kalia et al., 2018). Drp1 levels can be regulated transcriptionally or by controlling their recruitment to mitochondrial membranes. For instance, studies have shown that MiR-30 plays a pivotal role in stimulating the expression of Drp1. This regulation occurs through the modulation of the p53 signaling pathway, ultimately influencing the rate and extent of mitochondrial division (Li et al., 2010). The action of mitophagy E3 ligases further underscores the delicate balance of fission and fusion. The loss of these ligases has been found to amplify Drp1-dependent mitochondrial fission, largely by affecting Drp1 levels within the cell (Lutz et al., 2009). Concurrently, when its adaptor proteins are knocked down or their function is compromised, the ability of Drp1 to localize to mitochondria is significantly impaired, thereby reducing the frequency of mitochondrial fission events (Otera et al., 2010; Shen et al., 2014).

Since the significant role of these regulator proteins in mitochondrial dynamics, alterations in their expression and/or activation have been frequently associated with the progression of several pathologies, such as **neurodegenerative disorders**, cancer, and cardiovascular diseases (Chan, 2020).

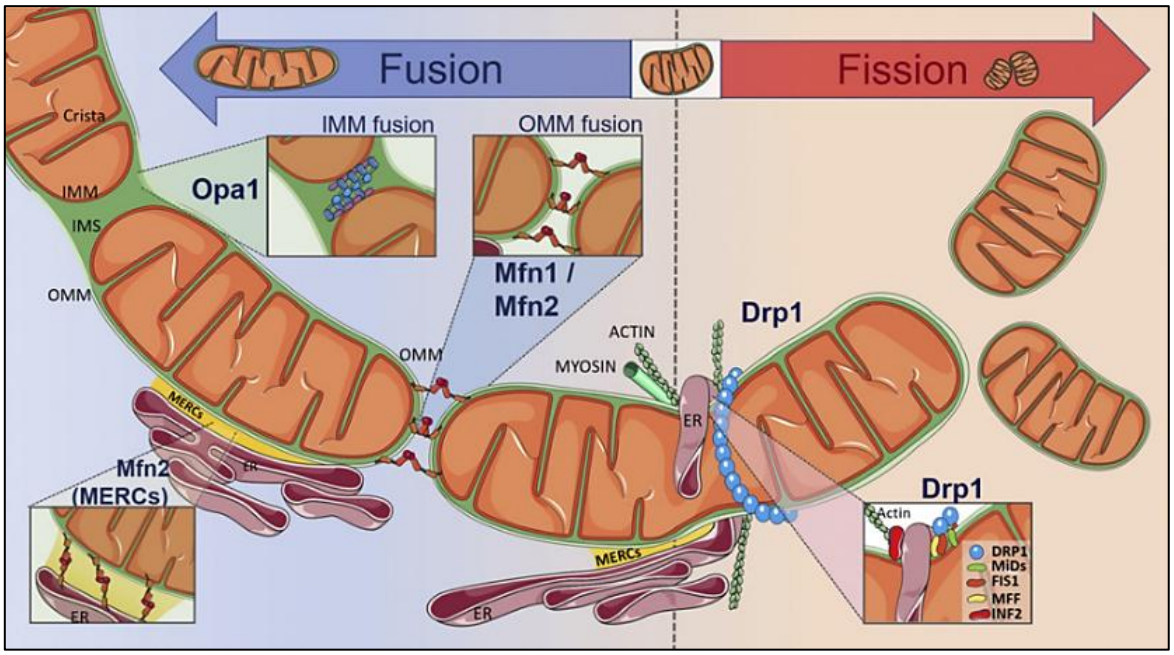

Figure 3. ***Mitochondrial shaping proteins.*** Graphical representation of pro-fusion (Opa1, Mfn1/Mfn2) and pro-fission (Drp1) proteins (Quintana-Cabrera et al., 2023).

2.2 Mitochondrial dynamics in neurodegenerative disorders

Due to their limited glycolytic capacity and extremely metabolically active nature, **neurons** are strictly dependent on the maintenance of mitochondrial function. Moreover, considering the highly polarized nature of these cells possessing processes like dendrites and axons, mitochondria are a key organelle involved in many neuronal cell activities such as Ca2+ regulation, plasmatic membrane maintenance, axonal and dendritic transport, and release and reuptake of neurotransmitters at synapses (Trigo et al., 2022). Moreover, in post-mitotic cells such as neurons, the role of mitochondrial dynamics to maintain the mitostasis (mitochondrial homeostasis) becomes even more crucial (Cagalinec et al., 2013). A comprehensive analysis of mitochondrial fusion and fission in healthy cortical and cerebellar neurons has already been elaborated. Cagalinec and collaborators found that the fusion rate matches the fission rate even if the rates change based on neuronal cell type. Moreover, the fusion rate in soma is significantly higher than in axons since mitochondria are usually strictly packed in the small soma area. Interestingly, calculating the fusion-fission cycle duration of the active mitochondrial population, the entire cycle has been estimated at 20 min, and it seems that mitochondria spend just a quarter of their lifetime in between fusion and fission and three-quarters in between fission and fusion. But one of their main findings has been to understand how specific rules, like mitochondrial length or motility, govern the crosstalk between these two processes, which are sequential events in 85% of cases, with just 15% deviations from this rule (Cagalinec et al., 2013).

What can occur is a significant deviation from the principles governing mitochondrial dynamism. Terms such as **hyperfusion** and **hyperfission** have been coined to describe how excessive/decreased activity of these mechanisms can harm mitochondrial health in the pathogenesis also of several neurodegenerative diseases, like Amyotrophic Lateral Sclerosis (ALS), Alzheimer's disease (AD), Parkinson's disease (PD), and Huntington's disease (HD)

(Nunnari et al., 2012). For example, Aβ oligomers have been associated with cognitive decline and neuronal death in AD by promoting networks of highly fragmented mitochondria through the downregulation of the *Mfn2* gene and increased interactions between FIS1 and DRP1 (Joshi et al, 2018; Wu et al., 2014). At the same time, the overexpression of MFN2 has been observed to reduce neuronal death induced by Aβ oligomers (Park et al., 2015). In Charcot-Marie-Tooth disease Type 2A (CMT2A), loss-of-function mutations in the *Mfn2* gene result in decreased mitochondrial fitness and motility in neurons, leading to neuronal degeneration (Barbullushi et al., 2015). Additionally, missense mutations in the *Opa1* gene that affect bioenergetics, calcium homeostasis, and increase apoptosis sensitivity are frequently identified in autosomal dominant optic atrophy, severe neuromuscular phenotype, and syndromic Parkinsonism and dementia (Delettre et al., 2000; Schaaf et al., 2011; Carelli et al., 2015).

2.3 Pharmacological strategies to modulate mitochondrial dynamics

Therefore, there is a new opportunity to develop therapies for these diseases by focusing on mitochondrial dynamics. As aberrant mitochondrial fission and fusion often result from dysregulated mitochondrial dynamics proteins, considerable efforts have been directed towards targeting these proteins through genetic and pharmacological means over the past two decades. Significant progress has been made in developing new modulating molecules and repurposing drugs already approved for other neurodegenerative conditions (Zacharioudakis et al., 2022). A previous, outdated classification divided mitochondrial dynamics drugs into two classes, namely mitochondrial fission inhibitors and mitochondrial fusion activators, without considering the specific modes of each drug (Miret-Casals et al., 2022). However, contemporary research has led to a refined classification of these compounds into **five categories**: protein oligomerization modulators able to counteract the oligomerization and activation of some dynamics regulators (I); GTPase inhibitors able to block their GTPase activity (II); modulators of proteins translocation (III); agents that affect the transcription of fusion and fission machinery (IV); compounds that indirectly impact the fusion and fission machinery (V) (Zacharioudakis et al., 2022). The chemical probes identified have been included in the following table (**Table 1**).

Chemical probe	Target	Effects on mitochondrial dynamics	Activity in cells/in vivo
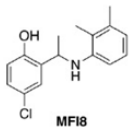 MFI8	MFN1/2	Inhibits fusion	Decreases mitochondrial functionality. Induces minority MOMP and sensitizes to apoptosis
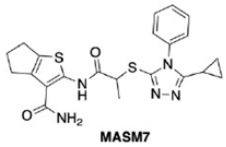 MASM7	MFN1/2	Promotes fusion	Improves mitochondrial functionality
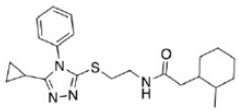 Chimera B-A/I	MFN1/2	Promotes fusion	Restores mitochondrial motility in neurons modeling CMT2A
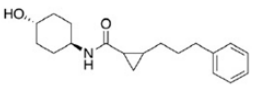 Compound 5	MFN1/2	Promotes fusion	Restores mitochondrial motility in neurons modeling CMT2A
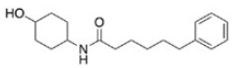 MiM-111	MFN1/2	Promotes fusion	Improves mitochondrial functionality and transport in sciatic nerves
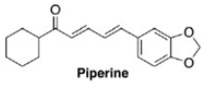 Piperine	MFN1/2	Promotes fusion	Improves mitochondrial functionality and transport in sciatic nerves
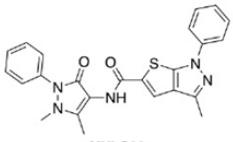 MYLS22	OPA1	Inhibits fusion	Induces apoptosis and inhibits tumor growth in vivo
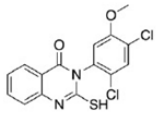 mdivi-1	DRP1/complex I	Inhibits fission	Protective effects in vivo in brain ischemia reperfusion injury
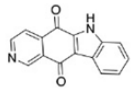 Drpitor1a	DRP1	Inhibits fission	Inhibits tumor growth in vivo
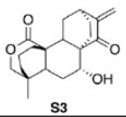 S3	USP30	Promotes fusion	Improves mitochondrial functionality
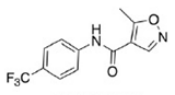 Leflunomide	DHODH	Promotes fusion	N/A

Table 1. ***Chemical probes and pharmacological compounds modulating mitochondrial fusion and fission*** (Based on Zacharioudakis et al., 2022).

2.3.1 Teriflunomide

Among the compounds regulating the protein levels of the fusion/fission machinery (category IV of mitochondrial dynamics regulators), Teriflunomide (TFN) stands out not only as a modulator of mitochondrial dynamics but also as an example of drug repurposing, since already approved for the relapsing forms of multiple sclerosis in 2012.

TFN is the main metabolically active form of Leflunomide, an isoxazole derivative with immuno-suppressive capacities and approved by the FDA for treating rheumatoid arthritis and psoriatic arthritis since 1998 (Aly et al., 2017). The compound is a malononitrilamide boosting **Mfn 2 expression** by blocking *de novo* pyrimidine biosynthesis through the selective and reversible inhibition of mitochondrial enzyme dihydroorotate dehydrogenase (DHODH). The reduced proliferation of B and T lymphocytes resulting from inhibition of pyrimidine biosynthesis appears to be a key mechanism of action, but the exact mechanism is still not completely known (Pellattiero et al., 2018). Indeed, in both a model of peripheral spinal root explants and acute hippocampal sections in mice, the increased Mfn2 levels have been shown to protect CNS tissue from oxidative damage while regulating neuronal activity and mitochondrial dynamics, without significantly compromising ATP synthesis (Malla et al., 2020; Malla et al., 2022).

Unlike many experimental compounds, TFN is already clinically approved, which significantly accelerates its potential for repurposing and clinical translation. Its well-characterized pharmacokinetics, safety profile, and oral bioavailability make it an ideal candidate for long-term administration in neurodegenerative conditions. Moreover, TFN has demonstrated the ability to modulate mitochondrial fusion machinery, counteracting oxidative damage and neuronal dysfunction, two particularly relevant hallmarks of disease in neurodegenerative disorders. The dual benefit of targeting mitochondrial dynamics and leveraging an existing therapeutic framework positions TFN as a promising option compared to other less characterized or preclinical drugs. For these reasons, in this project, the beneficial potential of TFN has been tested in different models of SMA, a neurodegenerative disorder characterized by mitochondrial dysfunction. Hence, the following section will provide an in-depth discussion of SMA and mitochondrial dysfunctions linked to it.

3. Spinal Muscular Atrophy (SMA)

The history of Spinal Muscular Atrophy (SMA) began with the case reports of two brothers affected by a progressive muscular atrophy more than a century ago (Hoffmann, 1893; Werdnig, 1891). Nowadays, SMA is considered one of the most frequent monogenic neurodegenerative diseases with a prevalence of 1-2 per 100,000 persons, an incidence of approximately 1:6,000-1:10,000 in live births, and a carrier frequency of around 1:40-1:60 when examining all types of SMA together (Lunn et al., 2008; Verhaart et al., 2017). The pathology is characterized by the fatal degeneration of lower α-MNs, resulting in progressive and symmetrical proximal muscle weakness and atrophy, and premature death. SMA has historically been recognised as the primary cause of genetic mortality in infants globally, second only to cystic fibrosis. The introduction and widespread adoption of newly approved treatments have significantly altered the prognosis and management of SMA. However, many cellular and molecular alterations involving MNs and other tissues affected by SMA pathology, must be in-depth understood. Indeed, in recent years, research has concentrated on identifying new targets to develop treatments that improve outcomes for patients and their families.

The following sections delve into the genetic underpinnings, clinical classification, SMN protein functions, and current therapeutic strategies relevant to SMA.

3.1 Genetic basis of the disease

SMA is a recessive autosomal genetic disease, caused by homozygous deletion, conversion, or mutation of the telomeric **survival motor neuron 1** (***SMN1*** or ^{T}*BCD541*) gene that induces a defective production of the SMN protein. In 1990, thanks to linkage analysis, the locus of the *SMN1* gene was mapped on the chromosome 5q13 (Brzustowicz et al., 1990; Melki et al., 1990); some years later, in 1995, Judith Melki's group pinpointed and characterized the SMA-determining gene, *SMN1*, as the mutated gene in more than 95% of the patients (Lefebvre et al., 1995). The remaining cases must be attributed to the presence of SMA mutations in other genes that can also be causative and therefore indicated as non-5q-SMA. At present, 20 different genes are associated with proximal non-5q forms, having high phenotypic variability and diverse inheritance patterns. (Peeters et al., 2014).

The *SMN1* gene is approximately 34 kb in length, consists of ten exons (exons 1, 2a, 2b, 3, 4, 5, 6a, 6b, 7, and 8), and the translation initiation codon (ATG) and termination codon (TAA) are located within exons 1 and 7, respectively. Interestingly, humans are the only species that carry two different *SMN* paralogs, *SMN1* and ***SMN2*** (or ^{C}*BCD541*), while all other species have only the *SMN1* gene. Indeed, although *SMN* duplication has been described in primates, long-read next-generation sequencing has demonstrated that they have only one *SMN* copy, suggesting that a duplication of *SMN* occurred during evolution from primates to humans (Dennis et al., 2017; Rochette et al., 2001).

In humans, these two *SMN* genes differ by only five nucleotides. Among these, the C>T transition at position +6 in the coding region of exon 7 (c.840C>T) is a silent variant that causes exon skipping from most (90%) *SMN2* pre-mRNA transcripts. These latter result in a truncated and non-functional variant (**SMNΔ7**) instead of the full-length protein SMN (Lorson et al., 1999; Monani et al., 1999).

However, being able to produce around 10% of functional SMN protein, the phenotypic spectrum of SMA is attributable to variable copy numbers of the *SMN2* gene (**Figure 4**).

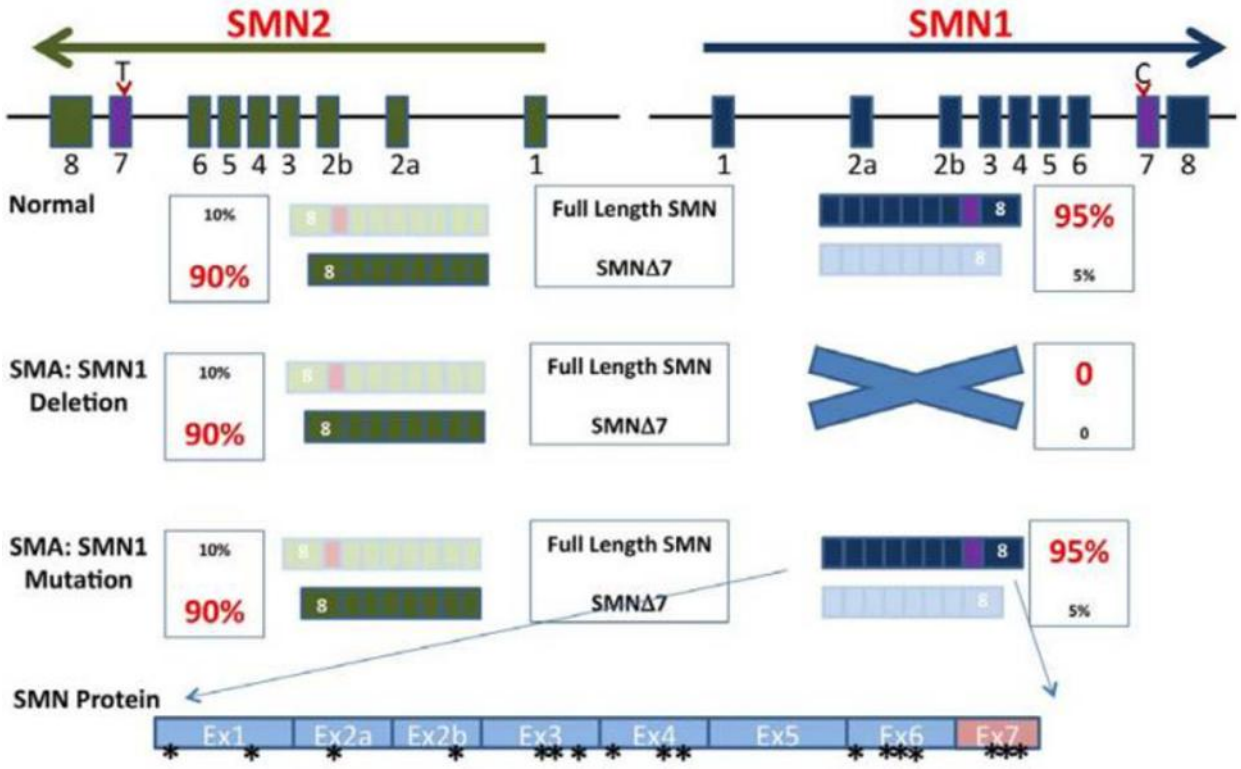

Figure 4. ***SMN genes and their products.*** The top section displays the genomic structure of the two genes. The critical difference is that C in *SMN1* promotes normal splicing via an exon splicing enhancer, while T in *SMN2* creates a silencer, resulting in exon 7 exclusion in most (around the 90%) SMN2 transcripts. Under normal conditions, > 95% of SMN1 mRNA includes exon 7, whereas only 10% of SMN2 mRNA has exon 7. Most patients with SMA have a deletion of the *SMN1* gene. In these patients, 10% of full-length mRNA is produced from the *SMN2* gene, which mainly generates an unstable, truncated form lacking exon 7 (SMNΔ7). In addition to deletion events, SMA can also result from point mutations in *SMN1*. Multiple missense variants have been reported throughout the gene, here marked by asterisks (*) on the respective exons (Zhou et al., 2012).

3.2 Clinical classification of SMA

The first reports of infants with SMA date back more than a century, by physicians Guido Werdnig and Johann Hoffmann, respectively, in 1891 (Werdnig, 1891) and 1893 (Hoffmann, 1893). Their cases were of intermediate severity, although the etymon of Werdnig-Hoffmann disease was later attributed to the severe childhood form of SMA type I. By contrast, the intermediate form of SMA type II is currently known also as Dubowitz Disease, for the name of the professor who detailed this phenotype in 1964 (Dubowitz, 1964). Milder forms of SMA, which were documented by Kugelberg and Welander in 1956 (Kugelber et al., 1956), were eponymized in Kugelberg-Welander disease to refer to mild SMA (SMA type III).

A first clinical classification was proposed at the 134th European Neuromuscular Centre (ENMC) International Workshop 2005 (Naarden, The Netherlands), where SMA type I was

subdivided into three types, SMA type II was not subclassified, and SMA type III was subdivided into the other two types (Bertini et al., 2005). In 2014, during the 209th ENMC International Workshop 2014 (Heemskerk, The Netherlands), SMA type 0 and SMA type IV were finally adopted into the disease classification (Finkel et al., 2014). However, due to the difficulty in remembering this detailed subclassification and in differentiating between neighboring subtypes, in 2015 Arnold et al. proposed a simple classification without subtypes and based basically on the disease onset, survival, and SMN2 copy number (Arnold et al., 2015).

The above provides a detailed overview of Arnold et al.'s SMA classification:

- **SMA Type 0**: the prenatal form of SMA and the most severe. These infants usually present only one copy of *SMN2.* The respiratory failure at birth leads to premature death within some weeks.
- **SMA Type I** (Werdnig-Hoffmann Disease): the severe form of SMA, consisting of the majority of SMA *nonsitters*. These "floppy infants" of less than 6 months old present 2 or 3 copies of *SMN2*. Respiratory insufficiency, fasciculations, and proximal muscle weakness are the most common disease markers. The survival is less than 1 year.
- **SMA Type II** (Dubowitz Disease): the intermediate form of SMA, which includes the majority of SMA sitters. These infants who are less than 18 months old have 3 copies of *SMN2*. They are characterized by a delay in motor development and weaknesses. These patients usually become adults with a survival of less than 25 years.
- **SMA Type III** (Kugelberg-Welander Disease): the mild form of SMA, consisting of the major part of SMA walkers, but also some sitters. These children of more than 18 months old present 3 or 4 copies of the *SMN2* gene. They exhibit a variable degree of weakness, become adults, and their life expectancy does not change significantly.
- **SMA Type IV**: the adult-onset and milder form of SMA, consisting of SMA walkers. These adults of more than 30 years old have 4 or more copies of *SMN2*. They are characterized by mild muscle weakness, and their life expectancy does not change significantly.

3.3 SMN protein and cellular functions

SMN is a ubiquitously expressed protein essential for every cell and species, and its deletion is early embryonic lethal. Liu and Dreyfuss originally described the subcellular localization of the SMN protein in HeLa cells as present in discrete nuclear structures and the cytoplasm (Liu et al., 1996). Moreover, they termed SMN protein-containing nuclear structures "gems" according to the Gemini of Cajal bodies for the number (2-6) and size (0.1-1) similarities. Only one year later, the same group demonstrated that the SMN protein was associated with snRNP biogenesis and splicing of pre-mRNA. Just a few years later, the model of the SMN protein complex shuttling between the nucleus and cytoplasm related to small nuclear ribonucleoprotein (snRNP) biogenesis was proposed (Yong et al., 2004). In the following period, the central question surrounding the SMN protein has been: why does a reduction in its levels lead to the selective degeneration of MNs in patients affected by SMA? Several hypotheses were presented over the years. Among these, the two main ones have been: (1) SMA is a consequence of a defect in snRNP biogenesis and pre-mRNA splicing, or (2) SMA is a consequence of a defect in the transport of mRNA in neurons

(Burghes et al., 2009; Monani et al., 2005).

However, although MNs seem to be the most affected cells by SMN reduction, in recent years, many peripheral alterations have been described in both mouse models and humans, leading SMA to be considered not only a motor neuron disease but also a multisystemic disorder. Indeed, early involvement of organs such as the heart, liver, and connective tissues has been observed, supporting the concept that dysfunctions in non-neuronal tissues appear before or alongside motor symptoms (Yeo et al., 2020) (**Figure 5**). This is because SMN protein is now known to participate in different protein complexes in a plethora of cellular processes, such as small nuclear ribonucleoprotein (snRNP) biogenesis, translation, transcription, microRNA metabolism, stress granule formation, DNA damage response, actin cytoskeleton dynamics, vesicle trafficking, autophagy, mitochondrial dysfunction, and energy homeostasis (Chaytow et al., 2018). The canonical function of SMN is **snRNP biogenesis** and splicing, and its depletion has been reported to be early embryonic lethal because it affects the U12 minor spliceosome, leading to an accumulation of U12-dependent intron-retention transcripts (Boulisfane et al., 2011). However, it remains difficult to elucidate all SMN functions and to understand which functions are related to the pathogenesis of SMA.

Regarding **MNs**, it has been demonstrated that the SMN protein, with its binding partner hnRNP R, interacts with beta-actin mRNA, playing a central role in axonal RNA metabolism and axonal transport granules (Rossoll et al., 2003). Moreover, a study pointed out the maturation impairment in acetylcholine receptor (AChR) cluster formation in the NMJs, probably related to the same axonal trafficking defects in MNs (Kariya et al., 2008). Also in **skeletal muscles**, Ikenaka found that the downregulation of SMN might reduce the production of myoblast determination protein 1, miR-1, and miR-206, causing mitochondrial dysfunction and subsequent cell death (Ikenaka et al., 2023).

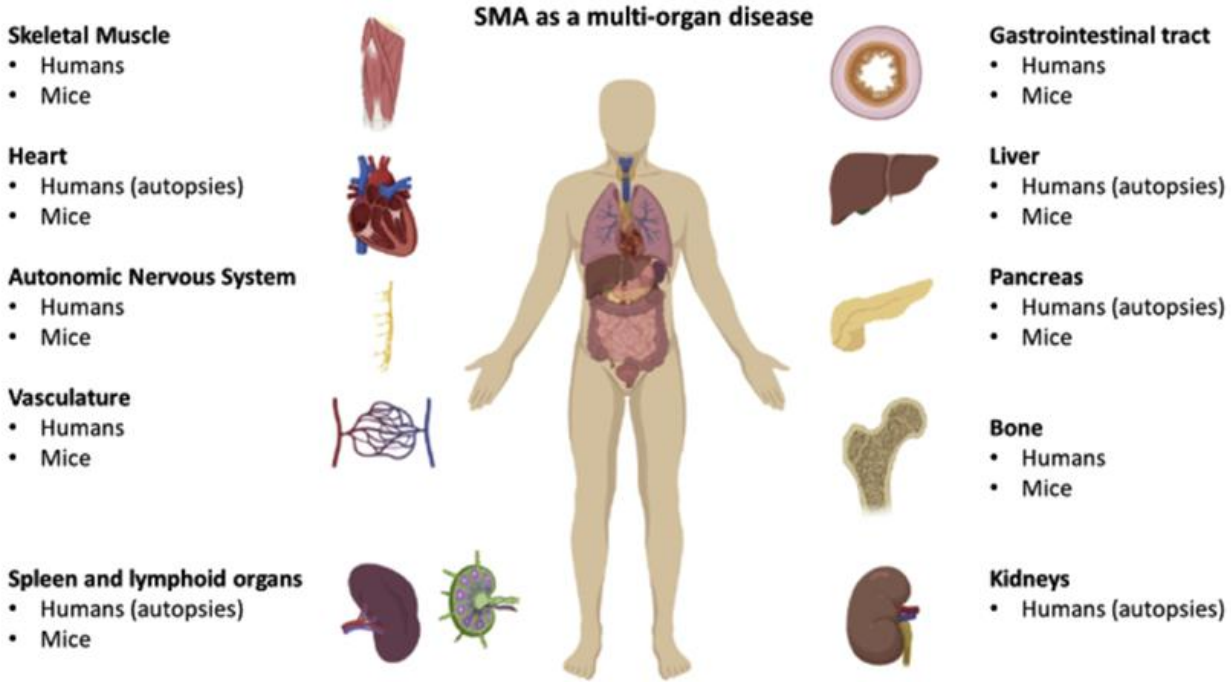

Figure 5. ***SMA as a multisystemic disease.*** Graphical representation of various tissues and organs involved in the SMA pathology in humans and mice (Yeo et al., 2020)

3.4 Development of approved therapeutic strategies for SMA

As described above, there is an inverse correlation between the severity of SMA phenotype and the *SMN2* copy number, since *SMN2* can compensate for the loss of *SMN1*, producing a low abundance of full-length SMN protein. From the report of Lefebvre in 1995 about the *SMN* genes, an incredible amount of research was conducted.

Already in 2000, Monani et al. demonstrated that *SMN2* overexpression was able to rescue the embryonic lethality in *Smn (-/-)* mice, leading to the birth of mice with SMA (Monani et al., 2000). In 2003, two artificial compounds, the exon-specific enhancement by small chimeric effectors (ESSENCE) and targeted oligonucleotide enhancers of splicing (TOES), both targeting the splicing of *SMN2* exon 7, were reported (Cartegni et al., 2003; Skordis et al., 2003). In 2004, Azzouz and colleagues constructed lentivector-SMN (a lentivector carrying *SMN* cDNA) and injected it into the muscles of SMA model, reducing motor neuron death and prolonging the average survival of SMA mice (Azzouz et al., 2004). In 2006, a cis-acting element (ISS-N1) regulating the *SMN2* exon 7 splicing in intron 7 was identified (Singh et al., 2006). In 2010, Foust et al. reported that the scAAV9 vector carrying the *SMN* gene (scAAV9-SMN) was injected into the facial vein of neonatal SMA model mice, resulting in prolonged survival of one of the treated mice (Foust et al., 2010). The next year, in animal studies, an ISS-N1-targeting ASO drug stimulated the inclusion of exon 7 in SMN2 mRNA transcripts, increasing the full-length SMN amount (Passini et al., 2011).

Nusinersen (Spinraza®; Biogen, Cambridge, MA, USA) was the first treatment approved for 5q-SMA patients in the US in 2016 and Europe and Japan in 2017. It is an intrathecally administered antisense oligonucleotide (ASO) that incorporates the exon 7 into the mRNA transcript of the *SMN2* gene, thus promoting increased production of full-length SMN protein (Finkel et al., 2017). Nusinersen is now available for all 5q-SMA patients, regardless of age or disease form, by a lumbar puncture at the fixed dose of 12 mg with 4 loading injections in the first 2 months, followed by a maintenance dose every 4 months thereafter.

Onasemnogene abeparvovec (Zolgensma®; Novartis Gene Therapies, Bannockburn, IL, USA) was the next drug introduced into clinical practice for the treatment of SMA after Nusinersen and approved in the US in 2019 and in Europe and Japan in 2020. It consists of a non-replicating recombinant adeno-associated virus serotype 9 (AAV9) containing the wild-type *SMN1* gene. After entering the host, the AAV vector translocates into the nucleus, where the transgene acts as an episome (a stable chromosome separated from the native chromosome) (Mendell et al., 2017). Onasemnogene abeparvovec is now available for 5q-SMA patients who are less than 2 years of age at the time of dosing, regardless of the form of SMA. This drug is one-time treatment given through an intravenous infusion that takes 1 hour.

Risdiplam (Evrysdi®; Roche, Basel, Switzerland) was the third drug introduced into clinical practice after nusinersen and onasemnogene abeparvovec and approved in the US in 2020 and Europe and Japan in 2021. This drug consists of an oral solution containing a small-molecule compound that modifies the *SMN2* pre-mRNA splicing. It may influence the stem-loop structures of exon 7 in the *SMN2* gene, promoting the inclusion of the same exon. Ridisplam is now available for all 5q-SMA patients, regardless of age and disease form, who can receive the treatment without leaving their homes. The drug is given once a day and the dosing is dependent on age and body

weight: adults and children aged > 2 years and weighing ≥ 20 kg take 5 mg of risdiplam; children ≥ 2 years of age weighing < 20 kg, the dose is based on body weight (usually 0.25 mg/kg).

3.4.1 Limits of SMA-approved therapies

All three approved drugs currently available can significantly change the disease trajectory from the known natural course of SMA, especially when early administered. However, despite their remarkable benefits, current SMA treatments still have important **limitations**.

Older children and adults living with SMA, representing two-thirds of the overall SMA population, may not have been treated early in their disease course because of the lack of treatment availability. These patients also worry about choosing nusinersen or risdiplam, as both may offer limited efficacy for them.

Despite the improved survival and motor development of symptomatic patients with early-onset SMA, the therapies are **highly costly**, with Zolgensma being the second most expensive drug in history, priced at $2.1 million per treatment (Thielen et al., 2022).

Additionally, clinical and age **restrictions** may preclude certain patients from accessing these treatments.

The intrathecal administration of nusinersen poses challenges for many SMA patients due to contractures, scoliosis, and spinal fusion, necessitating multiple injections annually.

As a splicing modifier, risdiplam may influence transcripts beyond its intended target, resulting in potential **off-target effects** that remain poorly characterized. Furthermore, Zolgensma therapy has been associated with **acute liver injury** (Chaytow et al., 2021).

Recent research indicates that SMN deficiency affects not only MN function but also additional organs and tissues. Current therapies predominantly yield CNS-specific distribution and have limited multisystemic availability.

Notably, the long-term adverse effects of these treatments remain uncertain and could arise years post-administration (Chaytow et al., 2021; Day et al., 2022). Given these limitations, ongoing research on SMA is essential to identify **novel therapeutic candidates**, including those suitable for use in combination with existing treatments to enhance efficacy and mitigate side effects.

3.5 The role of SMN in mitochondria

Among the most relevant functions of the SMN protein, the ones related to **mitochondria** have been largely studied in recent years. In the very early stages of SMA disorder, a switch in mitochondrial morphology and function contributes to the transition from physiological to degenerative condition that takes place not only in MNs but also in peripheral tissues (Stanga et al., 2021). This can be attributed to the impact of several SMN protein functions on mitochondrial homeostasis. For example, RNA metabolism is involved in nuclear-encoded mitochondrial transcripts, the calcium homeostasis impacts the mitochondrial calcium signaling, and the cytoskeleton is implicated in mitochondrial transport (Zilio et al., 2022) (**Figure 6**).

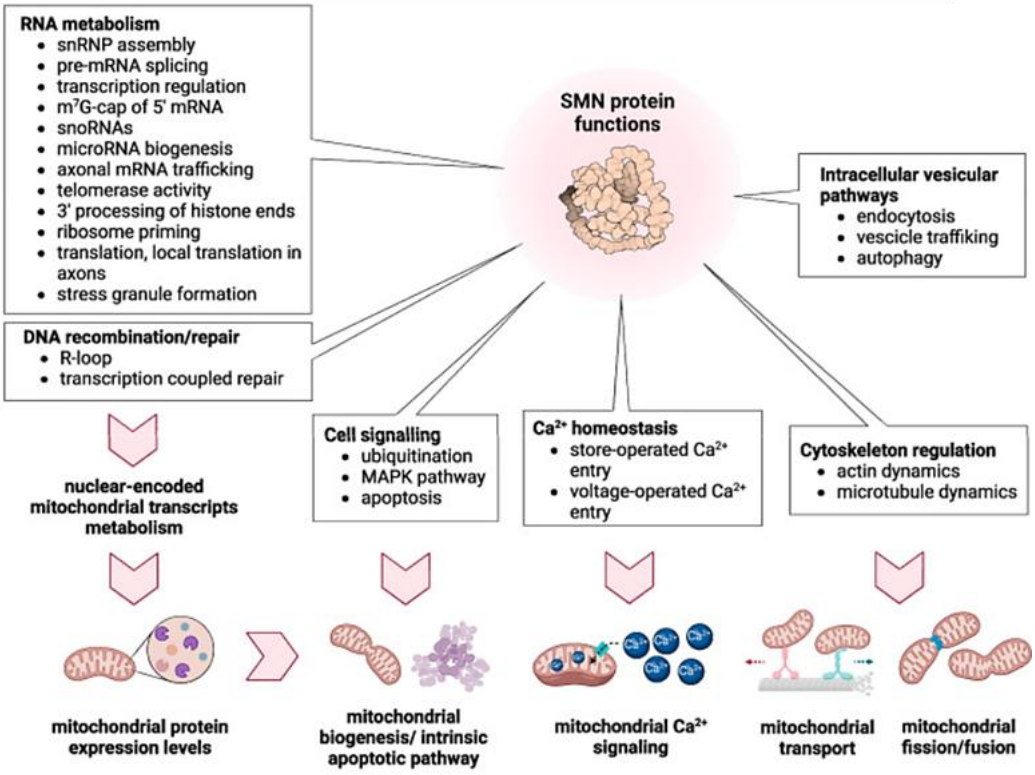

Figure 6. ***SMN functions and mitochondrial homeostasis***. From left to right, SMN protein is involved in RNA metabolism and DNA recombination/repair, cell signaling, Ca^{2+} homeostasis, cytoskeleton regulation, and intracellular vesicular pathways. All these SMN functions are crucial for mitochondrial biogenesis, mitochondrial Ca^{2+} signalling, mitochondrial transport, and mitochondrial dynamics (Zilio et al., 2022).

3.5.1 Mitochondrial dysfunction in SMA

Recent research has underscored that, in the context of SMA, mitochondria within **MNs** display striking morphological abnormalities and functional deficits. Miller was among the first to document that these organelles become markedly fragmented and lose their structural integrity in MNs from the SMNΔ7 mice, a severe SMA murine model (Miller et al., 2016). A general reduction in mitochondrial size and density was observed in both murine and human *in vitro* models of SMA (Xu et al., 2016). More recently, ultrastructural alterations, i.e., reduced cristae density and/or lamellar inclusions, were observed in the MNs from the SMNdelta7 and Type III SMA murine models (Fulceri et al., 2021). Functionally, an intrinsic reduction in mitochondrial Ca^{2+} influx capacity, as well as a remarkable decrease in mitochondrial membrane potential, has been demonstrated (Kong et al., 2009; Xu C.C. et al., 2016). These defective mitochondria exhibit significantly decreased activity of key respiratory chain complexes, impairing their capacity to generate adequate ATP and sustain proper neuronal energy metabolism (Thelen et al., 2020). Consequently, this altered mitochondrial respiration has been associated with increased cellular oxidative stress and mitochondrial ROS production found in SMA human stem cell-derived MNs (Wang et al., 2013).

Like neuronal cells, SMA **muscle cells** are characterized by heterogeneous mitochondrial defects, showing that mitochondrial dysfunction is not confined to neurons alone but is also evident in peripheral tissues. In *C. elegans*, muscle-specific knockout of *smn-1* leads to

mitochondrial defects in sarcomeres (Schultz et al., 2017). Reduced ADP-dependent O_2 consumption, reflecting impaired mitochondrial respiration and OXPHOS, has been observed in mitochondria from mouse SMA muscles and human SMA myoblasts (Hellbach et al., 2019). Muscle biopsies from individuals with SMA further confirm these findings (Ripolone et al., 2015). Mitochondrial dysfunction can lower SMN protein levels and increase oxidative stress, together speeding up cell death and contributing to muscle atrophy and cardiovascular problems in SMA patients (Wijngaarde et al., 2017) (**Figure 7**).

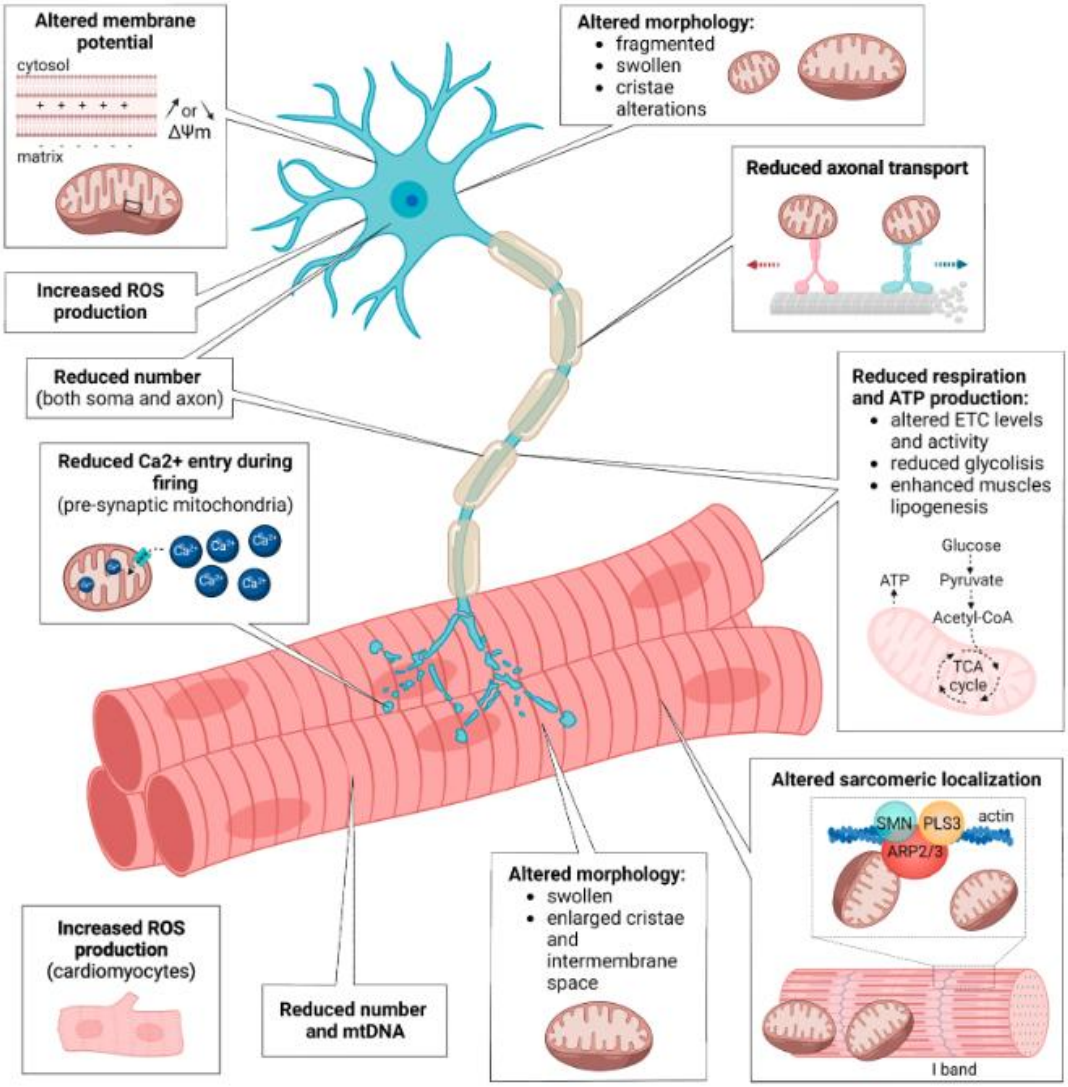

Figure 7. ***Mitochondrial dysfunctions in SMA MNs and muscles***. Summary of mitochondrial alterations found both in SMA MNs (upper part) and muscles (lower part). SMN loss causes mitochondrial morphology aberrations, reduced mitochondrial content, decreased axonal transport, altered respiration, decreased ATP production, increased ROS production, decreased mitochondrial membrane potential, and altered sarcomeric localization (Zilio et al., 2022).

Such defects likely contribute to the systemic nature of SMA pathology, exacerbating muscle weakness and degeneration beyond what is caused by loss of MNs alone. These insights highlight the importance of considering mitochondrial health in the ongoing development of more

comprehensive SMA therapies.

Currently, olesoxime is the only mitochondrial-targeted pharmacological therapy for SMA patients that has reached clinical trials (Bordet et al., 2010). While it modulates the mitochondrial permeability transition pore to prevent cell death, its phase II trial was unsuccessful due to a lack of long-term efficacy (Muntoni et al., 2020). However, its positive effects in various MN disease models suggest potential for use in combination therapies. Research in mitochondrial drugs for SMA continues to progress, with new candidates emerging. These include agents that promote mitochondrial biogenesis, antioxidants designed to reduce mitochondrial oxidative stress, and molecules aimed at restoring mitochondrial membrane potential. There is also growing interest in leveraging metabolic modulators to support energy production and improve overall cellular resilience to stress. Moreover, considering the systemic manifestations of spinal muscular atrophy (SMA), which call for therapeutic strategies aimed not only at preserving motor neurons (MNs) but also at protecting and restoring peripheral organ function, mitochondrial dysfunctions may represent a promising therapeutic target for the development of new combinatorial treatments for SMA.

HYPOTHESIS AND AIMS

Mitochondrial homeostasis is closely linked to mitochondrial dynamics, which can rapidly alter the appearance, quality, and function of mitochondria within their network. Above all, the role of mitochondrial fusion appears pivotal in promoting the biogenesis of new and functional mitochondria, increasing mitochondrial mass, membrane potential, matrix component exchange, as well as ATP production (Tàbara et al., 2025). On the other hand, mitochondrial hyperfusion has emerged as a critical pathological condition that disrupts the physiological balance between fusion and fission. This state impairs mitophagy by preventing the segregation and degradation of dysfunctional mitochondria, and also negatively affects cytoskeletal organization and cellular homeostasis (Ma et al., 2020). Considering that the morphological, ultrastructural, and functional defects already observed in SMA could be attributed to a remarkable shift of dynamics toward fission, we **hypothesize** that mitochondrial fusion may represent a promising novel molecular target. As reported for other neurodegenerative disorders, which are characterized by similar mitochondrial dysfunctions, increasing mitochondrial fusion may preserve mitochondrial integrity, supporting neuronal survival by counteracting the fragmentation and bioenergetic failure commonly observed in these conditions (Nunnari et al., 2012). Moreover, among the pharmacological compounds already developed or repurposed to enhance mitochondrial fusion, TFN not only upregulates MFN2 expression but also benefits from existing approval for oral and long-term administration in patients with multiple sclerosis.

Based on these findings, the **first aim** of our study was to in-depth characterize the mitochondrial network and dynamics in two different models of SMA MNs, primary mouse MNs from SMNΔ7 mice and human MNs differentiated from SMA patients' iPSCs. The mitochondrial content/mass, its distribution within MNs' compartments (soma and neurites), protein levels of mitochondrial dynamics regulators (DRP1, MFN2, and OPA1), and the mitochondrial network morphology will be investigated to confirm the imbalance in fusion/fission rates toward fission in our SMA MNs models. Subsequently, the TFN compound will be preliminarily tested to evaluate its effect in increasing mitochondrial fusion and mass. Moreover, given the relevance of systemic manifestations in the context of SMA and the goal of translating this drug into in vivo applications, our **second aim** was to characterize the mitochondrial network and dynamics in a peripheral SMA model, i.e., fibroblasts derived from SMA patients. Similarly, the mitochondrial content/mass and function, together with the protein levels of mitochondrial dynamics regulators (DRP1, MFN2, and OPA1) and the mitochondrial network morphology, will be evaluated to assess mitochondrial alterations related to mitochondrial dynamics in SMA human fibroblasts. TFN will be tested, first of all, to confirm its effect in increasing mitochondrial fusion and mass also in this model, and to evaluate if the drug reverses the previously found mitochondrial defects.

Overall, the outcomes of this study will contribute to the identification of a potential mitochondrial-targeted therapy, complementing existing SMN-replacement therapies, thereby addressing the urgent need for combined and systemic treatments for SMA patients.

MATERIALS AND METHODS

1. Mouse model and colony maintenance

SMNΔ7 mice were kindly provided by Dr Josep Esquerda and Dr Jordi Caldero (Universitat de Lleida-IRBLLEIDA), collaborating with Prof Rosa Maria Soler (Universitat de Lleida-IRBLLEIDA). The procedures were approved by the Universitat de Lleida Advisory Committee on Animal Services (CEEA02-02/23) and by the Departament d'acció climàtica, alimentació i agenda rural (CEA-OH/12150/2, project number 12150), Generalitat de Catalunya (Catalunya, Spain). Mice were housed in polypropylene cages at room temperature (RT) (22 ± 2 °C), humidity of 40±10%, and with a 12/12-hour light/dark cycle. Water and rodent chows were given ad libitum.

1.1 SMNDelta7 mice

Mutant mice that are homozygous for the targeted mutant Smn allele and homozygous for the two transgenic alleles, FVB.Cg-Grm7Tg (SMN2)89AhmbSmn1tm1Msd Tg (SMN2*delta7) 4299Ahmb/J (Smn-/-; SMN2+/+; SMNΔ7 +/+), referred here as SMA, exhibit symptoms and neuropathology comparable to a severe type of SMA. Two other SMNΔ7 mouse genotypes were generated: heterozygous (Smn+/-; SMN2+/+; SMNΔ7 +/+, used for colony maintenance) and wild-type (Smn+/+; SMN2+/+; SMNΔ7 +/+, used as control and referred to in this work as WT). At birth, mutants are noticeably smaller than normal littermates, and starting at day 5, they show progressive muscle weakness that gets more pronounced over the following week, presenting a typically abnormal gait, shakiness in the hind limbs, and a tendency to fall over. Mean survival was originally reported to be ~13 days (Le et al., 2005). A timeline of the major cellular and symptomatic events from the embryonic day (E10) to postnatal day (P14) development of the SMNΔ7 mouse model used in this study is illustrated in **Figure 8**. For each experiment, a mean of 3 heterozygous pregnant adults was sacrificed, and a total of 4 SMA embryos and 4 WT embryos were used to obtain each SMA or WT MN culture.

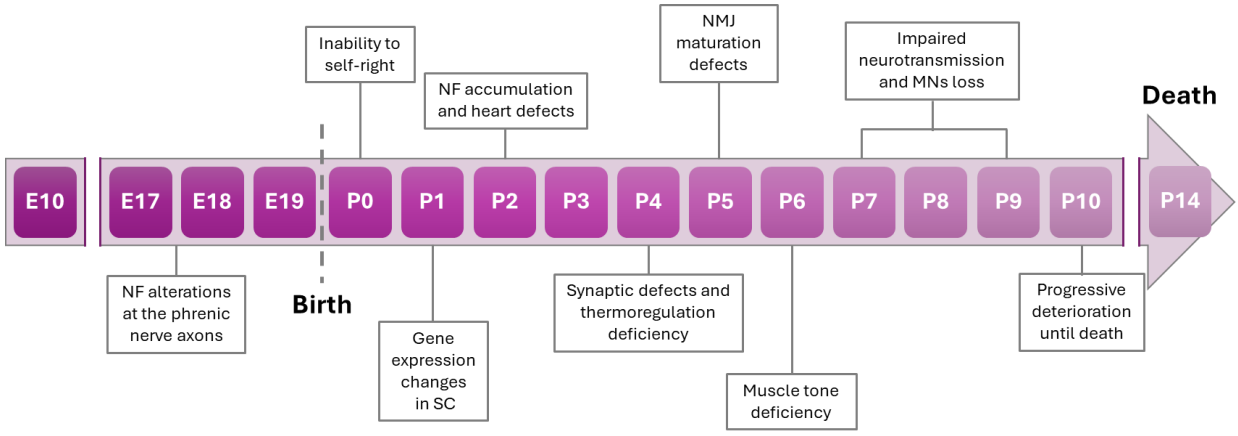

Figure 8. ***Timeline of the major cellular and symptomatic events during the embryonic and postnatal development of the SMNΔ7 (Smn-/-; SMN2+/+; SMNΔ7 +/+) mouse model of SMA***. E: embryonic; NF: neurofilament; P: postnatal; SC: spinal cord; NMJ: neuromuscular junction; MNs: motor neurons (Based on Sleigh et al., 2011).

1.2 Genotyping

To perform the SMA MN purification, a fragment of the tail or head was obtained from E13 (embryonic day 13) mice for genotyping, and the REDExtract-N-Amp Tissue PCR kit (Sigma, St Louis, MO, USA) was used for genomic DNA extraction. The tissue was incubated with the extract solution for 10 minutes at RT. After heating the samples to 95 °C for 3 minutes, the neutralization buffer was added to each sample, and the mix was centrifuged for 10 minutes to collect the supernatant. The REDExtract-N-Amp Tissue PCR Kit contains the buffer, salts, dNTPs, and the Taq polymerase. It also includes a JumpStart™ Taq antibody for hot start PCR, which prevents the premature activation of the DNA Taq polymerase at RT and enhances specificity. The primers, designed for the Jackson Laboratory, were the following:

- WT forward (Fwd): **5′-CTCCGGGATATTGGGATTG-3′.**
- SM reverse (Rev1): **5′-GGTAACGCCAGGGTTTTCC-3′.**
- WT reverse (Rev2): **5′-TTTCTTCTGGCTGTGCCTTT-3′.**

After preparing the PCR reaction mix with the extraction buffer, Fwd/Rev1/Rev2 primers, the DNA sample, and sterile MilliQ water (up to the final volume), the PCR cycling was started using specific parameters. For the electrophoresis, the REDExtract-N-Amp PCR ReadyMix containsREDTaq®dye, an inert dye that acts as a tracking dye and allows for convenient laddering of PCR reactions directly onto agarose gels for analysis. Using 1% agarose gel for the DNA separation and SYBR Safe (1:10,000; added to the gel) as a dye. After the electrophoresis, the gel was developed using the ultraviolet sample tray support on a Gel Doc™ EZ Imager. As a result, we obtained: an amplification of 800Kb DNA product that corresponds to the endogenous Mouse Smn gene (WT (+/+)); a single fragment of 500Kb corresponding to the neomycin resistance cassette (mutants (-/-)); and a combination of both fragments in the heterozygous samples (+/-).

2. Primary mouse MNs

The most common source of primary MNs is obtained from the dissociation of the spinal cord from E12.5-13 embryos. We obtained our MN primary cultures from the spinal cord of E13 SMA and WT mice embryos at E13 as already described (Gracer et al., 2011), using a two-step centrifugation based on two density gradients that allows us to maintain a 97% culture purity for up to 2 weeks. All experiments involving primary mouse MN were performed at the IRBLleida (Llieda, Spain), under the supervision of Prof Rosa Maria Soler.

2.1 Mouse MN isolation

To collect the MNs, adult-pregnant mice were sacrificed by cervical dislocation, and all the embryos were removed from the uterus. The head was cut (and, together with the tail, used for genotyping, as previously described), and the remaining body was moved, fixing the upper and lower limbs with small needles, in a silicon support plate with GHEBS solution. By opening the dorsal part of each embryo with a longitudinal cut in the middle of the spinal cord area (1-2 mm of depth) and removing the dorsal horns, the ventral part of the spinal cord was separated with thin dissection tweezers from the rest of the body (**Figure 9**). Then also the meninges were carefully

removed, and each spinal cord was cut into 4-5 pieces and pooled in groups of 4 in GHEBS solution to start the purification process.

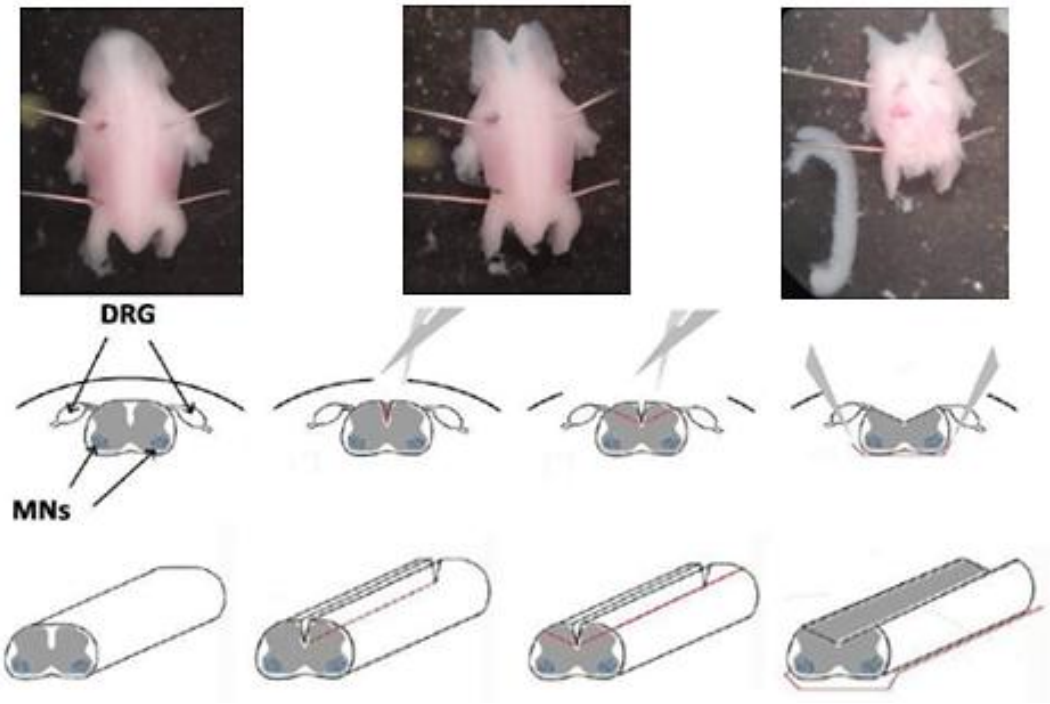

Figure 9. ***Dissection phases of the embryonic spinal cord*** (Based on Sandra De la Fuente, 2020).

The purification process started by cleaning the spinal cord pieces three times with GHEBS solution and a Pasteur pipette, then incubating in GHEBS solution containing trypsin (at a concentration of 0.025%) for 8 minutes at 37 °C, shaking frequently. After that, the tissue was transferred to Leibovitz's L15 medium Complete supplemented with BSA 4% (Sigma, Ref. A8412) and DNase (Sigma, Ref. 10104159001), manually shaken for 2 min, and then mechanically dissociated using a P1000 tip. After tissue disaggregation, the supernatant was collected in a tube, and the remaining tissue was resuspended in the same medium to repeat the process until the tissue was fully disaggregated. The first gradient was created using a Pasteur pipette containing BSA 4% at the bottom of a conical tube and centrifuging at 1000 rpm for 5 min. The supernatant was discarded, and the cells inside the pellet were resuspended in L15 medium. To specifically isolate MNs, a solution with GHEBS and OPTIPREP (Axis-Shield) was added to the suspended cells creating two different phases. After the centrifugation at 1650rpm for 10 min a three-phase solution was visible with the middle one, between OPTIPREP and L15 medium, corresponding to the isolated MNs. This cellular interphase was collected and suspended in an L15 medium for cell counting.

2.2 Precoating plates

To prepare the culture dishes 35 μg/ml solution of poly-DL-ornitin (P/O) (Sigma, Stock solution of 10mg/ml) was prepared in Boric-Borate buffer (150mM sodium tetraborate, 150mM boracic acid, pH 8.3). Four-well tissue culture plates (M4 plates) were covered overnight at RT. After

incubation, plates were washed three times with sterile MilliQ water and air-dried at RT for 15 minutes. After P/O coating, plates were treated with laminin (Sigma, stock solution 1mg/ml) diluted in L-15 medium at a final concentration of 3.8 µg/ml. Laminin was incubated for a minimum of 2 hours at 37ºC in a CO2 incubator. Laminin solution was removed before plating.

2.3 Mouse MN plating

Primary mouse MNs were plated in laminin-coated four-well tissue culture dishes for western blot analysis (100.000 cells/well) or on 1 cm2 laminin-coated glass coverslips for immunofluorescence experiments (25.000 cells/well).

2.4 Western Blotting (WB) analysis of mouse MNs

After six days of culture, mouse MN cultures were rinsed with cold PBS 1X buffer and collected using lysis buffer (125 mM Tris, pH 6.8, and 2% SDS). The total cell protein lysates were collected in sterile Eppendorf tubes, boiled for 5 min at 95°, and stored at -20° until use. Lysate sonication and short centrifugation were also performed before using the NanoPhotometer® for protein quantification. The same amount of 35 µg of proteins was always loaded in SDS polyacrylamide gels and transferred onto polyvinylidene difluoride Immobilion-P transfer membrane filters using a semi-dry trans-blot. Membranes were blocked in 5% milk (diluted in TBS-T) for 1h at RT under shaking. Then, membranes were incubated at 4 °C overnight with the following primary antibodies: anti-tubulin (anti-mouse, 1:50,000, #T5168, Sigma Aldrich), anti-SMN (anti-mouse, 1:5,000, #610646, BD Biosciences), anti-LONP1 (anti-rabbit, 1:1,000, #15440-1-AP, Proteintech), anti-DRP1 (anti-mouse, 1:1,000, #sc-271583, Santa Cruz Biotechnology, Inc.), anti-Mfn2 (anti-rabbit, 1:1,000, #M6319, Sigma Aldrich), and anti-OPA1 (anti-rabbit, 1:1,000, #ABN95, Thermo Fischer Scientific). Anti-mouse and anti-rabbit secondary antibodies (1:10,000, #1706515, #1706516, Bio-Rad) were used to bind primary antibodies, and finally, blots were developed using LuminataTM ForteWestern HRP Substrate.

2.5 Immunofluorescence (IF) on mouse MNs

After six days of culture, mouse MN cultures were fixed with 4% PFA for 10 min and then with cold methanol (-20 °C) for 10 min. Fixed MNs were washed with PBS 1X and were permeabilized with permeabilizing solution, 0.5% Triton-PBS 1X solution for 30 min at RT under shaking. After three washes with PBS 1X, the cells were incubated with a solution containing 5% BSA and 0.5% Triton-PBS 1X for 30 min at RT under shaking, to block unspecific binding sites. After three washes with PBS 1X, mouse MNs were incubated overnight at 4 °C under shaking using anti-βIII tubulin (anti-rabbit, 1:400, #5568, Cell Signaling Technology) and anti-LONP1 (anti-rabbit, 1:300, #15440-1-AP, Proteintech) antibodies. The anti-rabbit ALEXA488 and the anti-mouse ALEXA555 secondary antibodies (1:400) incubations were carried out for 1h at RT under shaking. Hoechst staining (1:500) was performed to localize the nuclei inside MNs soma. Finally, after three washes with PBS 1X, samples were mounted using Mowiol embedding medium. Image acquisition was performed in an Olympus FV1000 confocal microscope, using the blue 405 channel for Hoechst and the green 488 channel for LONP1, with a 60× magnification oil immersion objective and 1.5 zoom.

3. Human-induced Pluripotent Stem Cells (iPSCs)

Human MNs were obtained from the differentiation of specific cell lines. The differentiation owas performed following the protocol described previously with minor modifications established by Dr Manuel Portero's laboratory (Universitat de Lleida-IRBLLEIDA) (Gou Fabregas et al., 2009). All experiments involving human-induced Pluripotent Stem Cells were performed at the IRBLleida (Llieda, Spain), under the supervision of Prof Rosa Maria Soler. In particular, CTRL (control) human MNs were obtained from the non-SMA GM23411*B cell line, HET (heterozygous) human MNs from the SMA carrier GM24474 cell line, SMA I human MNs from the SMA type I CS85iSMA-nxx cell line, and SMA II human MNs from the SMA type II GM23240*B cell line. Cell lines' details, including identification codes, nicknames, and clinical features like age, SMN1/SMN2 copy number and condition, were described in **Table 2**.

CELL LINE	CONDITION	SMN1/SMN2 COPY NUMBER	AGE	NICKNAME
GM23411*B	NON SMA	SMN1: 2 SMN2: not reported	3 mo.	CTRL
GM24474	SMA carrier	SMN1: 1 SMN2: 5	Not reported	HET
CS84iSMA-nxx	SMA type I	SMN1: 0 SMN2: 2	6 mo.	SMA I
GM23240*B	SMA type II	SMN1: 0 SMN2: 3	3 yrs.	SMA II

Table 2. ***Human-iPSCs' details.***

3.1 MN differentiation protocol

On day 0, human iPSCs were dissociated with Accutase (Gibco) following the manufacturer's instructions and cultured on a layer of irradiated mouse embryonic fibroblasts in hES media to facilitate the growth of large colonies. After two days, hiPSCs were dissociated and plated on Geltrex-coated plates with MEF-conditioned hES media (for 24 hours) and neuroepithelial induction medium (NEPIM) to induce their differentiation into neuroepithelial progenitors. After 6 days, cells were dissociated with Accutase and plated on matrigel-coated dishes and MNP (MN progenitor) medium to differentiate into MN progenitors I, and then in the same medium supplemented with valproic acid (VPA) to differentiate into MN progenitors II. After other 12 days, MNPs were detached with Accutase and cultured in non-cell-culture-treated plates with MN induction medium (NEPIM plus Retinoic Acid and purmorphamine) to obtain neurospheres. Finally, after 6 days, neurospheres were dissociated using Accumax Dissociation Medium

(Invitrogen) and plated on laminin-coated plates in MN maturation medium (MN induction medium supplemented with Compound E, CNTF, and IGF-1).

3.2 Human MN plating and drug treatment

For western blot analysis, 100,000 cells/well were plated on laminin-coated four-well dishes and maintained in the MN maturation medium, while for IF experiments, 25,000 cells/well were plated on laminin-coated 1 cm2 glass coverslips, maintained in the MN maturation medium, and then fixed in 4% paraformaldehyde (PFA) in PBS. Teriflunomide (TFN) or DMSO (vehicle) was added for 48h at 50 μM final concentration to treat the cells.

3.3 IF on human MNs

Human iPSC-derived MN cultures were fixed with 4% PFA for 10 min and then with cold methanol (-20 °C) for 10 min. Fixed MNs were washed with PBS 1X and were permeabilized with permeabilizing solution 0.5% Triton-PBS 1X solution for 30 min at RT under shaking. After three washes with PBS 1X, fixed and permeabilized cells were blocked with a solution containing 5% BSA and 0.5% Triton-PBS 1X for 30 min at RT under shaking. After three washes with PBS 1X, MNs were incubated overnight at 4 °C under shaking using anti-Hb9 (anti-rabbit, 1:500, #PA5-23407, Invitrogen) , anti-ChAT (anti-mouse, 1:500, #MA5-31383, Invitrogen) , anti-βIII tubulin (anti-rabbit, 1:400, #5568, Cell Signaling Technology), and anti-Tom20 (anti-mouse, 1:300, #17764, Santa Cruz Biotechnology) antibodies. The anti-rabbit ALEXA488 and the anti-mouse ALEXA555 secondary antibodies (1:400) incubations were carried out for 1h at RT under shaking. Hoechst staining (1:500) was performed to localize the nuclei inside MN soma. Finally, after three washes with PBS 1X, samples were mounted using Mowiol embedding medium. Image acquisition was performed in an Olympus FV1000 confocal microscope, using the blue 405 channel for Hoechst, the green 488 channel for Hb9 and βIII tubulin, and the red 555 channel for ChAT and TOM20, with a 60× magnification oil immersion objective and 1.5 zoom.

3.4 WB analysis of human MNs

Human MN cultures were rinsed with cold PBS 1X buffer and collected using lysis buffer (125 mM Tris, pH 6.8, and 2% SDS). The total cell protein lysates were collected in sterile Eppendorf tubes, boiled for 5 min at 95°, and stored at -20° until use. Lysate sonication and short centrifugation were also performed before using the NanoPhotometer® for protein quantification. The same amount of 35 μg of proteins was always loaded in SDS polyacrylamide gels and transferred onto polyvinylidene difluoride Immobilion-P transfer membrane filters using a semi-dry trans-blot. Membranes were blocked in 5% milk (diluted in TBS-T) for 1h at RT under shaking. Then, membranes were blotted at 4° overnight with the following primary antibodies: anti-tubulin (anti-mouse, 1:50,000, #T5168, Sigma Aldrich), anti-SMN (anti-mouse, 1:5,000, #610646, BD Biosciences), anti-Tom20 (anti-mouse, 1:1,000, #17764, Santa Cruz Biotechnology), anti-DRP1 (anti-mouse, 1:1,000, #sc-271583, Santa Cruz Biotechnology, Inc.), anti-Mfn2 (anti-rabbit, 1:1,000, #M6319, Sigma Aldrich), anti-OPA1 (anti-rabbit, 1:1,000, #ABN95, Thermo Fischer Scientific) and anti-LONP1 (anti-rabbit, 1:1,000, #15440-1-AP, Proteintech). Anti-mouse and anti-rabbit secondary antibodies (1:10,000, #1706515, #1706516,

Bio-Rad) were used to bind primary antibodies and finally blots were developed using LuminataTM ForteWestern HRP Substrate.

3.5 Mitochondrial Network Analysis (MiNA) toolset

Mitochondrial morphology of human MNs was performed *in silico* using MiNA, as described by Valente et al. (Valente et al., 2017). MiNA is a free tool for ImageJ that incorporates optional pre-processing steps to enhance the quality of images before converting the images to binary and producing a morphological skeleton for calculating descriptive parameters to quantitatively capture the morphology of the mitochondrial network. MiNA was used, including all optional pre-processing steps, after the scale was set: Unsharp Mask to enhance sharpness, Enhance Local Contrast to adjust the pixel intensities to equalize the histogram, and Median Filtering to provide a convenient way to reduce or eliminate noise. For human MNs, at least 5 images were captured for CTRL and SMA I cell lines to obtain a comparable number of 16 MNs for each experiment. All images acquired were converted to binary images through the step Make Binary. Using binary images, through the step MiNA Analyze Morphology, it is possible to obtain one parameter, the Mitochondrial Footprint. This is the number of pixels in the binary image containing signal multiplied by the area of a pixel, i.e., the total area in the image of the mitochondrial network consumed by signal after being separated from the background. Then, from binary image through the step Skeletonize the image is converted to a skeleton image that can be analyzed, obtaining principal descriptive parameters: Individuals (the number of objects in the image that do not contain junction pixel, comprised of 1 or 0 branches, and that can be round, rod or puncta), Network (the number of objects in the image that contain at least 1 junction and more than 1 branch), Mean Branch Length, Median Branch Length and Standard Deviation of Branch Lengths (that describe branch length), and Mean Branches, Median Branches and Standard Deviation Branches (that describe branches of network).

3.6 Automated Cell Counting after drug treatment

To compute the IC50 of TFN in human iPSC-derived MNs, the cell viability was established using an automated cell counting based on quantification of the number of nuclei, as described by Shihan with minor modifications (Shihan et al., 2021). Indeed, after each treatment with four different concentrations (0, 25, 50, 75 μM) of TFN or DMSO (as vehicle), human MNs were rinsed with ice-cold PBS 1X buffer, and fixed with 4% PFA for 10 min and then with cold methanol (-20 °C) for 10 min. Fixed cells were washed with PBS 1X buffer and were permeabilized using a 0.5% Triton-PBS 1X solution for 30 min at RT under shaking. Then, the cells were incubated in a solution containing 5% BSA and 0.5% Triton in PBS 1X for 30 min at RT under shaking, to block unspecific binding sites. Finally, the cells were incubated with DAPI to count the number of live cells. At least 7 images for each condition were taken using a fluorescence microscope and a 20X objective. After that, each image was loaded on ImageJ, the contrast was increased using "Enhanced Local Contrast", a different threshold was set to visualize all the nuclei in each image, the images were converted to binary images, and near nuclei were divided using the "Wotersheed" selection. Finally, using "Analyze particles", nuclei were automatically counted.

4. Human fibroblast cell lines

Human fibroblast cell lines were obtained from the biobank of the UO Medical Genetics and Neurogenetics Fondazione IRCCS Istituto Neurologico "Carlo Besta" (FINCB), located in Milan, Italy. All experiments involving human fibroblast cell lines were performed at the Neuroscience Institute Cavalieri Ottolenghi (NICO; Turin, Italy), under the supervision of Prof Marina Boido and Serena Stanga. Primary skin fibroblasts were isolated from skin biopsies derived from the arm of three CTRL (control) subjects, with the following identification codes 1890CL, 1892SE, 1891SC, and three SMA patients, with the subsequent identification codes 1279ZF, 1110RS, and 1123DLR. Patients' details, including identification codes, nicknames, and clinical features like gender, age, SMN1/SMN2 copy number and condition, were described in **Table 3**.

PATIENT'S CODE	CONDITION	SMN1/SMN2 COPY NUMBER	AGE	GENDER	NICKNAME
1890 CL	NON SMA	SMN1: 2 SMN2: 1	9 yrs. 7 mo.	M	CTRL 1
1892 SE	NON SMA	SMN1: 2 SMN2: 1	17 yrs. 3 mo.	F	CTRL 2
1891 SC	NON SMA	SMN1: 2 SMN2: 0	6 yrs. 5 mo.	F	CTRL 3
1279 ZF	SMA type I	SMN1: 0 SMN2: 2	3 mo.	F	SMA 1
1110 RS	SMA type I	SMN1: 0 SMN2: 2	2 mo.	M	SMA 2
1123 DLR	SMA type II	SMN1: 0 SMN2: 3	12 mo.	M	SMA 3

Table 3. Human subjects and patients' details.

4.1 Maintenance

Human fibroblast cell lines were cultured in T75 cm^2 cell culture flasks (Greiner Bio-One, ref. 658175) in Dulbecco's Modified Eagle Medium (DMEM) (Sigma-Aldrich, ref. D5796) with high glucose, supplemented with 10% Fetal Bovine Serum (FBS), 1% L-Glutamine (Sigma-Aldrich, Cat. No. G7513), and 1% penicillin-streptomycin (Gibco, ref. 15140-122). Cells were incubated at 37°C in a controlled atmosphere incubator with 5% CO_2. The culture medium was changed every 3 or 4 days. When they reached 80-90% confluency, cells were detached enzymatically by trypsin 1X and centrifuged at 1,100 rpm for minutes. The cell pellet was resuspended to split the cells into more flasks. Representative images of CTRL and SMA human fibroblasts were shown in **Figure 9**. To thaw human fibroblast cell lines, the vials already preserved in liquid nitrogen

were warmed at 37 °C using the water bath for less than one minute. Once thawed, cells were added to a T25 cm^2 cell culture flask (Greiner Bio-One, ref 690175) with DMEM/high-glucose medium to reach a final volume of 4 ml. To freeze the human fibroblast cell lines, the cells were detached enzymatically using trypsin 1X and centrifuged for 7 minutes at 1100 rpm. The cell pellet was resuspended in freezing medium (90% FBS and 10% DMSO). One ml was distributed in each cryogenic vial (Corning, 2ml tube) and kept at -20 °C for 2 hours, then at -80º for more than 24 hours for a slow freezing process and finally kept in liquid nitrogen.

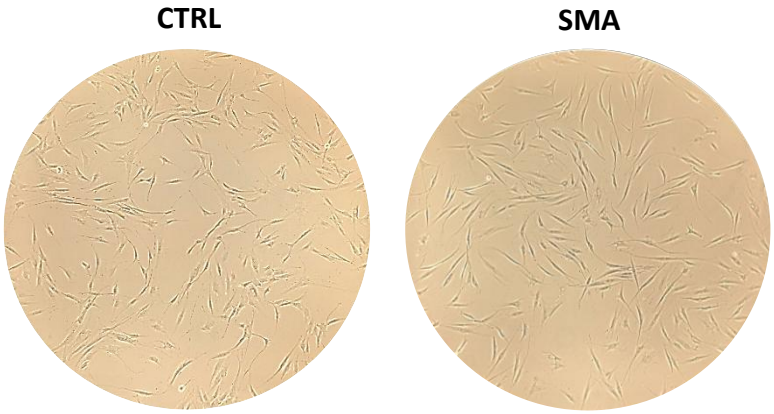

Figure 9. CTRL (1891 SC) and SMA (1110 RS) human fibroblast cell lines by 20X magnification.

4.2 Cell plating and drug treatment

Before any treatments, a thorough morphological evaluation was conducted. The cells were plated using the following ratio: 2,000 cells/well on 96-well plate for 24 hours for MTS assay; 4,000 cells/well on 48-well plate for 72 hours for mitochondrial membrane potential evaluation; 8,000 cells/well on 24-well plate with 1 cm2 glass coverslips coated with poly-d-lysine for IF experiments; lastly, 45,000 cells/well in a 6-well plate for 72 hours for WB analysis. After each different time, TFN or DMSO (vehicle) was added for 48h at 50 µM and 200 µM final concentrations.

4.3 WB analysis of human fibroblasts

Human fibroblasts were rinsed with cold PBS 1X and collected using lysis buffer. The total cell protein lysates were collected in sterile Eppendorf tubes after gentle sonication. The samples were boiled for 5 min at 95° after short centrifugation. The same amount of 15 µg of proteins was always loaded in SDS polyacrylamide gels and transferred onto polyvinylidene difluoride Immobilion-P transfer membrane filters using a semi-dry trans-blot. Membranes were blocked for 1h at RT under shaking. Then, membranes were blotted at 4°C overnight with the following primary antibodies: anti-vinculin (anti-mouse, 1:1,500, #V9131, Sigma Aldrich), anti-SMN (anti-mouse, 1:5,000, #610646, BD Biosciences), anti-Tom20 (anti-rabbit, 1:300; #42406S, Cell Signalling Technology), anti-OXPHOS (anti-rabbit, 1:1,000, #ab110413, Abcam), anti-DRP1 (anti-mouse, 1:1,000, #8570S, Cell Signaling Technology), anti-Mfn2 (anti-rabbit, 1:1,000, #9482S, Cell Signaling Technology), anti-OPA1 (anti-rabbit, 1:1,000, #14739S, Cell Signaling Technology) and anti-LC3B (anti-mouse, 1:1,000, #83506S, Cell Signaling Technology). While tubulin was

used as housekeeping protein to normalize the results of Tom20 and SMN to validate the SMN deficiency among SMA cultures and healthy ones, Tom20 was used to normalize the results of mitochondrial regulators. Anti-mouse and anti-rabbit secondary antibodies (1:10,000, #1706515, #1706516, Bio-Rad) were used to bind primary antibodies and finally blots were developed using LuminataTM ForteWestern HRP Substrate.

4.4 Fluorescence-Activated Cell Sorting (FACS) analysis

Mitochondrial content of human fibroblasts was assessed by Mitotracker probes and flow cytometry or FACS (Fluorescence-Activated Cell Sorting) analysis. The probe used for the mitochondria labeling was MitoTracker Green FM (M7514, Invitrogen by ThermoFischer Scientific). The Mitotracker Green FM is a probe based on carbocyanine, used to stain mitochondria with an excitation spectrum of 490 and an emission spectrum of 516. This type of probe stains live cells but is not retained after aldehyde fixation, staining mitochondria regardless of mitochondrial membrane potential. Human fibroblasts were washed with PBS, treated with trypsin, and left at 37 °C for 3 minutes. MitoTracker Green FM at a final concentration of 50 nM was added and left at 37 °C for 15 min. Labelling was analyzed by Beckman Coulter CyAn ADP High-Performance Flow Cytometer. Each sample was analyzed after being filtered with special filters for sizes less than 50 μm and diluted in PBS. The assay was performed considering about 10,000 cells/events for each analysis. The results have been expressed as mean of fluorescent intensity (MFI), shown by samples based on the amount of probe that stained mitochondria.

4.5 MitoTracker Red CMXRos labelling

The rosamine-based dyes are a subset of xanthene dyes, a class of synthetic dyes characterized by a core structure of a dibenzo-1,4-pyran ring, which lacks carboxyl groups, making them more lipophilic and cell permeable compared to other xanthene dyes, such as the rhodamine-based ones. As fluorescent dyes, they demonstrate a strong ΔΨm-dependency and undergo a step conversion starting from non-fluorescent compounds, and just after oxidation, they acquire a positive charge and sequester inside the mitochondria, where they bind to intramitochondrial components. The MitoTracker Red CMXRos is a rosamine-based dye characterized by an excitation/emission (579/599 nm) that places its fluorescence in the red range. To assess mitochondrial membrane potential changes in SMA human fibroblast cell lines and CTRL ones before and after TFN treatment, cells were plated on 48-well plates (4.000 cells/well) and incubated at 37°C in a controlled atmosphere incubator with 5% CO_2, waiting for confluence. After 48 hours of drug administration, MitoTracker Red CMXRos at a final concentration of 100 nm (#9082, Cell Signaling Technology) and Incucyte Nuclight Rapid NIR Dye (1:2,000; #4804, Sartorius) were added to the growth media and incubated at 37 °C for 30 min in a humidified 5% CO_2 atmosphere. The two labels were visualized and recorded at 599/680 nm using the Sartorius S3 Incucyte Live Cell Imager (Ref 30050303). Moreover, in order to normalize the fluorescence intensity of Mitotracker Red Dye for the number of cells in each well, the following automated analysis was performed through the Incucyte System: Orange Integrated Intensity Per Well / NIR Object Count Per Well (OCU x μm²/Well / 1/Well).

4.6 mACO2 enzymatic activity assay

The Aconitase Assay was performed to evaluate the enzymatic activity of mACO2, using the Cayman Aconitase Assay Kit on enriched mitochondrial protein extracted from human fibroblasts. After removing the medium, cold PBS was added and aspirated to remove any residual medium. The cells were then incubated at 4°C for 10 minutes. Cold PBS was aspirated and added for the scraping phase, in which, through a scraper, cells were recovered and added in Eppendorf to be centrifuged at 800 x g for 10 minutes at 4°C. After discarding the supernatant, the pellet was resuspended in 120 µl of cold Assay Buffer, and the cell suspension was sonicated 20X at one-second bursts. The cell suspension was centrifuged at 20,000 x g for 10 minutes at 4°C, and the supernatant was used for the assay. Black wells were prepared, adding 55 µL of Assay Buffer, 50 µL of Nicotinamide Adenine Dinucleotide Phosphate Reagent, and 50 µL of Isocitric Dehydrogenase. Aconitase positive control wells were prepared by adding 50 µL of Aconitase positive control, 5 µL of Assay Buffer, 50 µL of Nicotinamide Adenine Dinucleotide Phosphate Reagent, and 50 µL of Isocitric Dehydrogenase. Sample wells were prepared by adding 50 µL of sample, 5 µL of Assay Buffer, 50 µL of Nicotinamide Adenine Dinucleotide Phosphate Reagent, and 50 µL of Isocitric Dehydrogenase. Sample Background was prepared by adding 50 µL of sample, 50 µL of Nicotinamide Adenine Dinucleotide Phosphate Reagent, 50 µL of Isocitric Dehydrogenase, and 5 µL of Assay Buffer. The reactions were initiated by adding 50 µL of the diluted substrate solution to all control and sample wells and 50 µL of Assay Buffer to the sample Background wells. Then the absorbance was measured at 340 nm for 30 minutes at 37 °C.

4.7 IF on human fibroblasts

Human fibroblast cell lines were fixed in 4% PFA for 20 min. After PBS 1X washing, fixed human fibroblasts were permeabilized with permeabilizing solution 0.3% Triton-PBS 1X pH 7.4 and left under shaking for 30 min at RT. After two washes with PBS 1X, cells were incubated with blocking solution for unspecific binding sites with 10% Normal Donkey Serum (NDS, Sigma-Aldrich) and 90% 0.3% Triton-PBS 1X pH 7.4 and left under shaking for 30 min at RT. Cells were incubated overnight at 4 °C under shaking in a solution with 10% NDS (Sigma-Aldrich), 90% 0.3% Triton-PBS 1X pH 7.4, and the primary antibody for TOM20 (anti-rabbit, 1:300; #42406S, Cell Signalling Technology) and LC3 (1:500; #83506S, Cell Signalling Technology). After three washes with PBS 1X, human fibroblasts were incubated for 1h at RT under shaking in a solution with 10% NDS (Sigma-Aldrich), 90% 0.3% Triton-PBS 1X pH 7.4, 1:300 secondary anti-rabbit antibody, nsCy3 red for TOM20, 1:300 secondary anti-mouse antibody, ATTO 647 deep red for LC3, and 1:100 DAPI. After three washes with PBS 1X, coverslips were mounted using Mowiol embedding medium. Image acquisition was performed in a LEICA DM6000CSTCS SP5 (Leica Microsystems, Wetzlar, Germany) confocal laser scanning microscope using the blue 405 channel for DAPI, the red 570 channel for TOM20, and the deep red 647 channel for LC3, evaluated both using a 63× magnification oil immersion objective. The mitochondrial morphology analysis of human fibroblasts was performed *in silico* using MiNA toolset, as already described above for human MNs.

4.8 MTS assay for human fibroblasts

The MTS assay (Promega, Ref 3580) was performed to evaluate Teriflunomide's cytotoxicity and IC50 in human fibroblasts. It is a colorimetric method to determine the number of viable cells, based on the use of the combination of a novel tetrazolium compound [3-(4,5-dimethylthiazol-2-yl)-5-(3-carboxymethoxyphenyl)-2-(4-sulfophenyl)-2H-tetrazolium, inner salt; MTS] and an electron coupling reagent (phenazine ethosulfate; PES) to enhance the chemical stability of the whole solution. The MTS compound is bioreduced by cells into a colored formazan soluble in cell culture medium: the quantity of formazan product is directly proportional to the number of living cells in culture (**Fig. 4**). Human fibroblasts were plated on 96-well plates (2,000 cells/well) and incubated at 37°C in a controlled atmosphere incubator with 5% CO_2, waiting for confluence. After 24 hours cells were treated with the drug changing the medium. After 48 hours of treatment, 20µl/well of CellTiter 96® AQueous One Solution Reagent was added and incubated at 37 °C for 2 hours in a humidified 5% CO_2 atmosphere. The absorbance was recorded at 490 nm using a 96-well plate reader (TECAN Infinite 200 Pro P/N microplate reader, Ref 30050303).

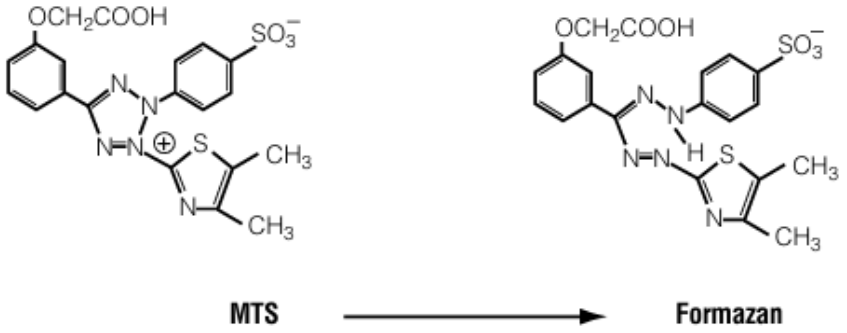

Figure 10. MTS tetrazolium compound structure and its colored formazan product (Saggio di proliferazione cellulare CellTiter 96® AQueous One Solution | Saggio MTS | Saggio MTT).

4.9 MitoTracker Green FM labelling

MitoTracker Green FM is a fluorescent dye with excitation and emission maxima of approximately 490/516 nm, producing green fluorescence. To assess mitochondrial mass changes in SMA human fibroblast cell lines and CTRL ones after TFN treatment, cells were plated on 48-well plates (4,000 cells/well) and incubated at 37°C in a controlled atmosphere incubator with 5% CO_2, waiting for confluence. After 48 hours of drug administration, MitoTracker Green FM at a final concentration of 100 nm (#M7514, Invitrogen) and Incucyte Nuclight Rapid NIR Dye (1:2,000, #4804, Sartorius) were added to the growth media and incubated at 37 °C for 1 h in a humidified 5% CO_2 atmosphere. The two labels were visualized and recorded at 490/680 nm using the Sartorius S3 Incucyte Live Cell Imager (Ref 30050303). Moreover, in order to normalize the fluorescence intensity of Mitotracker Green FM Dye for the number of cells in each well, the following automated analysis was performed through the Incucyte System: Green Integrated Intensity Per Well / NIR Object Count Per Well (OCU x µm²/Well / 1/Well).

4.10 Colocalization rate analysis between TOM20 and LC3

After TFN treatment in human fibroblasts, the colocalization analysis between TOM20 and LC3 signals was performed using the Coloc2 plugin in ImageJ (Fiji). Fluorescence images were acquired under identical settings to avoid bias in signal intensity. Regions of interest (ROIs) of single mitochondria were selected to exclude background and non-specific signals. The Coloc2 plugin was applied to calculate thresholded Manders' overlap coefficients (tM1 and tM2), providing quantitative measures of the fraction of TOM20 signal overlapping with LC3 signal (tM1) and vice versa (tM2), as described by the official documentation on the ImageJ Wiki (Coloc 2). The resulting tM1 and tM2 values were used to determine the rate of colocalization between TOM20 and LC3

5. Statistical analysis

Results have been shown as the mean ± SEM. The obtained data were analyzed using GraphPad Prism (version 8.0.2) by the two-tailed Student's *T*-test for two groups, while for more than two groups by one-way ANOVA followed by Tukey's or Sidak's multiple-comparisons post hoc test. Values were considered significant when $p < 0.05$.

RESULTS

PART I:

Study of mitochondrial network in SMA mouse and human MNs and preliminary screening of a fusion-promoting treatment

1. SMA mouse and human MNs show a significant reduction in the overall mitochondrial content

After 6 days in culture for mouse primary MNs, the characterization of mouse cultures (**wt** and **mut** primary cell) showed the typical MN morphology, as shown in representative phase-contrast images (**Figure 11A**). Concerning iPSC-derived MNs (**CTRL**, **HET**, **SMA I,** and **SMA II** cell lines), after 7 days of differentiation, we assessed the typical MN morphology together with the cell positivity to common mature MNs markers, i.e., Hb9 and ChAT (Lopez-Gonzalez et al, 2012), as illustrated in representative phase-contrast and IF images (**Figure 11C**). All further analyses shown here and in the next paragraphs were performed using MNs from these specified time-points. Moreover, for both primary mouse MNs and differentiated human MNs, we assessed by WB analysis the reduction of SMN protein levels in SMA mouse cells compared to control cells (wt vs mut: 1 vs 0.15, -0.85 ± 0.106, p=0.0013, **Figure 11B**) and in SMA type I and SMA type II human cell lines with respect to heterozygous and control lines (in detail, CTRL vs SMA I: 1 vs 0.17, -0.83 ± 0.1, p<0.0001; CTRL vs SMA II: 1 vs 0.16, 0.84 ± 0.1, p<0.0001; HET vs SMA I: 0.59 vs 0.17, 0.41 ± 0.1, p=0.0071; HET vs SMA II: 0.59 vs 0.16, 0.43 ± 0.1, p=0.0051, **Figure 11D**).

To identify preliminary changes in the mitochondrial network between SMA and non-SMA conditions, WB analysis of two common mitochondrial markers, LONP1 and TOM20, was carried out for mouse and human MNs, respectively. The results showed a lower mitochondrial mass in SMAdelta7 culture with respect to the control one (in detail, wt vs mut: 1 vs 0.85, 0.15 ± 0.03, p=0.0065; **Figure 11E**), and also in SMA type I and II human cell lines compared to the control human cell line (CTRL vs SMA I: 1 vs 0.42, 0.58 ± 0.13, p=0.0038; CTRL vs SMA II: 1 vs 0.32, 0.68 ± 0.13, p=0.0011; **Figure 11F**).

By using different mitochondrial mass markers, we confirmed the significant reduction of the mitochondrial pool in both our models of SMA MNs.

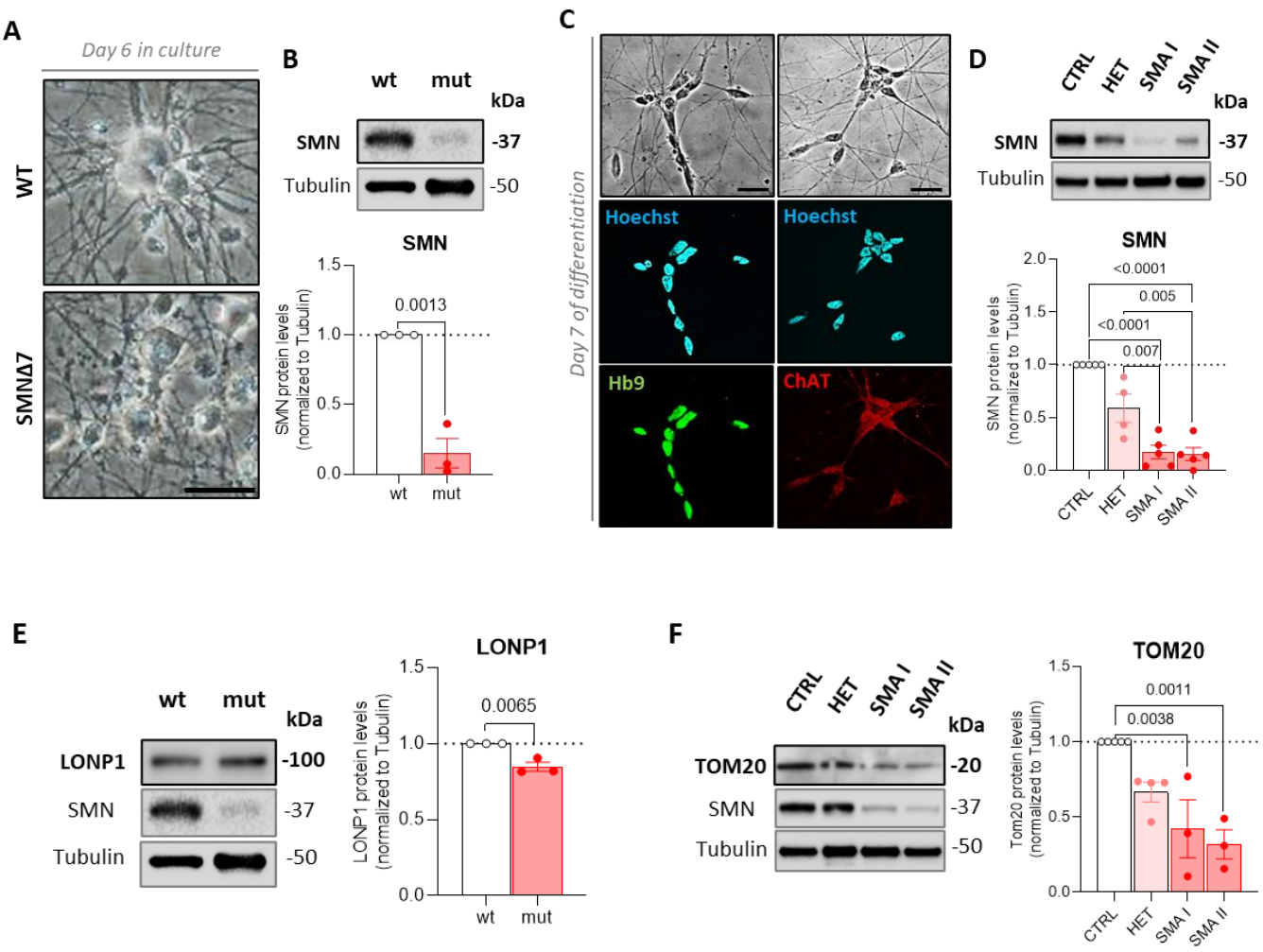

Figure 11. ***Mitochondrial mass analysis in characterized models of SMA mouse and human MNs.*** Representative phase-contrast images of control (wt) and mutant (SMNdelta7) cultures from embryos of the SMNdelta7 mouse model after 6 days in culture. Scale bar: 50 µm (**A**). Graph of the mean ± SEM of SMN protein level quantification in mouse MNs (**B**). Representative phase-contrast images, Hoechst, Hb9, and ChAT stainings by immunofluorescence of human MNs after 7 days of differentiation from iPSCs. Scale bar: 50 µm (**C**). Graph of the mean ± SEM of SMN protein level quantification in human MNs (**D**). Graph of the mean ± SEM of LONP1 protein level quantification in mouse MNs (**E**). Graph of the mean ± SEM of TOM20 protein level quantification in human MNs (**F**). For WB analyses, values were collected from at least three independent experiments. β-Tubulin was used as a loading control. Differences between control (wt) and mutant (mut) values were analysed by using the unpaired t-test, while the values of control (CTRL), heterozygous (HET), SMA type I (SMA I), and SMA type II (SMA II) conditions were analysed by using the ordinary one-way ANOVA with Tukey's multiple comparisons test.

2. Mitochondrial network distribution is altered between soma and neurites in SMA mouse and human MNs

We decided to better visualize the mitochondrial distribution among the two principal MN compartments, soma and neurites, in our SMA MN models. Therefore, the immunostaining for LONP1 and TOM20 mitochondrial markers was performed in mouse (**Figure 12A**) and human

(**Figure 12D**) MNs, respectively. The study of the mitochondrial distribution, which considered the somatic and neuritic compartments as independent, confirmed what it was already seen for other SMA models: indeed, the mitochondrial signal in the area occupied by the neurites of both mutant mouse MNs was significantly reduced compared to WT ones (wt vs mut: 100 vs 31.43, -68.57 ± 14.02, *p*=0.0006; **Figure 12C**) and SMA type I MNs with respect to control MNs (CTRL vs SMA I: 100 vs 59.04, -40.43 ± 10.76, *p*=0.0019; **Figure 12F**).
Interestingly, at the same time, the mitochondrial distribution analysis showed a slight, not significant increased content of mitochondria restricted to the somatic compartment of SMA human MNs (wt vs mut: 100 vs 128.7, +28.7 ± 22.09, *p*=0.19; **Figure 12B**; CTRL vs SMA I: 100 vs 133.7, +33.74 ± 13.55, *p*=0.0162; **Figure 12E**).
Our results, on the one hand, corroborate a mitochondrial transport impairment into the neurites of our SMA MNs models, whose neurites seem to be poor in mitochondria. On the other hand, the distribution analysis preliminarily revealed an abnormal mitochondrial cluster in the somatic space.

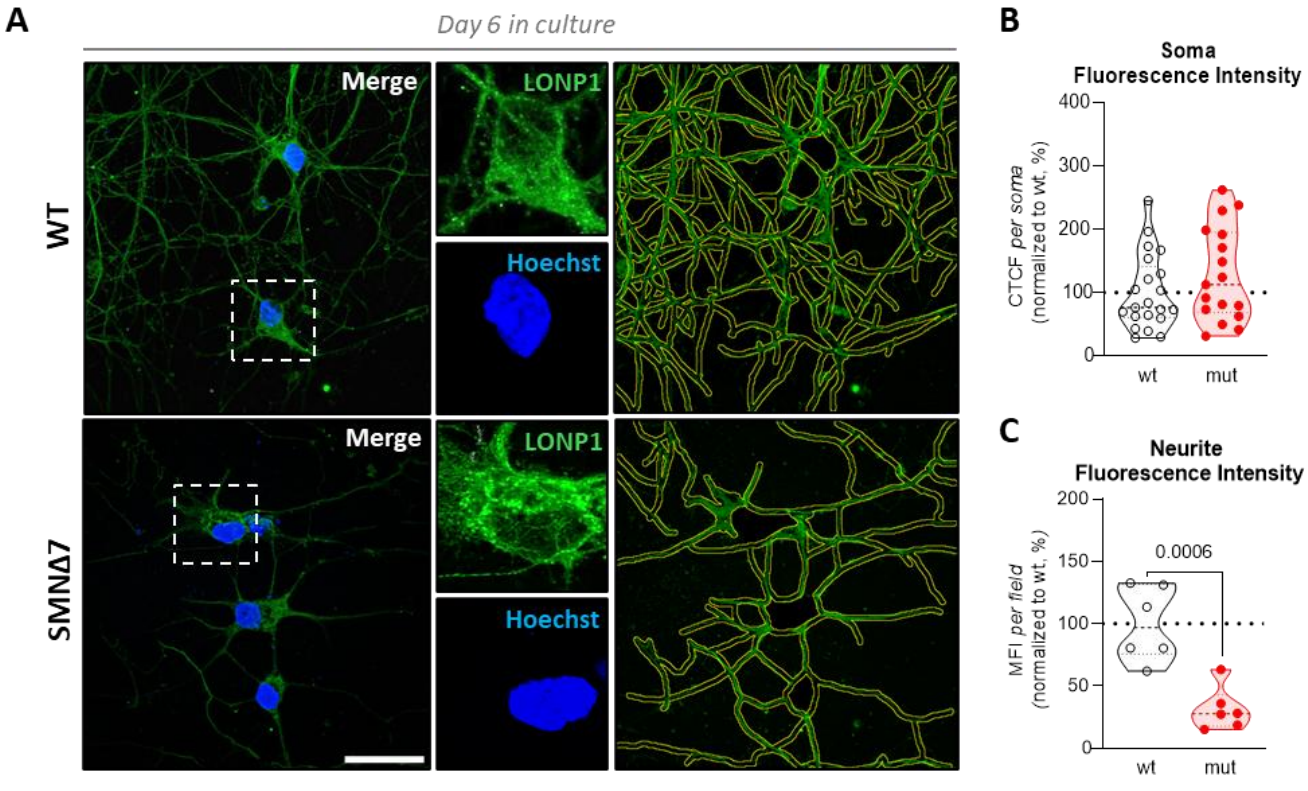

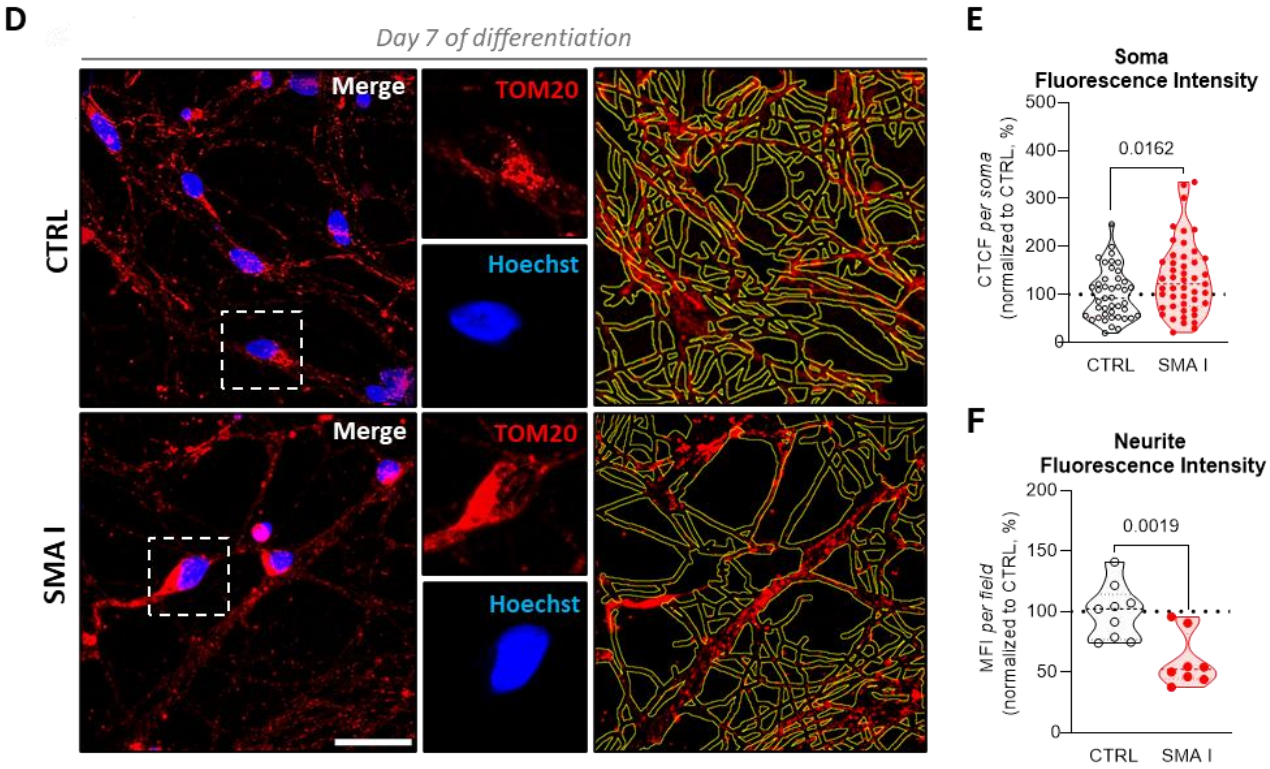

Figure 12. ***Mitochondrial distribution study among soma and neurites in SMA mouse and human MNs.*** For the image panels (**A, D**), from left to right: representative merged images of LONP1 (green) or TOM20 (red) and Hoechst (blue) staining for mitochondria and nuclei, respectively, in wt and mut MNs after 6 days in culture, and CTRL and SMA I MNs after 7 days of differentiation. Scale bar: 30 µm. Representative high magnification images of LONP1 or TOM20 and Hoechst staining for a single soma, and representative images of LONP1 or TOM20 signal for neurites. The graph shows percentage values of relative LONP1 fluorescence levels measured as CTCF for each soma of mouse MNs (**B**). The graph shows percentage values of relative LONP1 fluorescence levels measured as MFI for the neuritic area of mouse MNs (**C**). The graph shows percentage values of relative TOM20 fluorescence levels measured as CTCF for each soma of human MNs (**E**). The graph shows percentage values of relative TOM20 fluorescence levels measured as MFI for each soma of mouse MNs (**F**). Values were collected from three independent experiments. Differences between the values of SMA and non-SMA conditions were analyzed by using the unpaired t-test.

3. Global moderate imbalance toward the fission of mitochondrial dynamic regulators in SMA mouse and human MNs

Since the reduced mitochondrial content and the impaired mitochondrial distribution could be correlated to altered mitochondrial dynamics, the fission-fusion balance state of the mitochondrial network was studied by performing the WB analysis of fission (DRP1, S-OPA1) and fusion (MFN2 and L-OPA1) regulators in both SMA mouse and human MNs.

Regarding fission machinery in mouse MNs, results showed that the expression of DRP1 in the mutant mouse MNs (**Figure 13A**) seemed increased compared to the healthy condition, although with high variability, while the L-OPA1/S-OPA1 ratio was significantly decreased in the mutant

mouse MNs compared to the WT (wt vs mut: 1 vs 0.73, -0.27 ± 0.06, p=0.0428, **Figure 13C**). Regarding the fusion machinery, due to high variability, we only observed a trend toward increased MFN2 expression in the mutant mouse MNs compared to the WT (**Figure 13B**).

In the human model, DRP1 expression was significantly increased in the SMA I human cell line with respect to the CTRL one (CTRL vs SMA I: 1 vs 4.35, +3.35 ± 0.9, p=0.0245, **Figure 13D**), while the L-OPA1/S-OPA1 ratio did not appear to change in SMA human MNs (**Figure 13F**). Regarding the fusion machinery, we observed a trend toward the increased expression of L-OPA1 in SMA I cell lines compared to the CTRL one (**Figure 13F**). In contrast, MFN2 protein levels seemed similar among SMA I and CTRL human cell lines (**Figure 13E**). Western blot analysis of mitochondrial-shaping proteins revealed a complex profile in SMA MNs, with fission markers showing a significant increase in some cases. In contrast, fusion markers exhibited high variability, limiting clear interpretation.

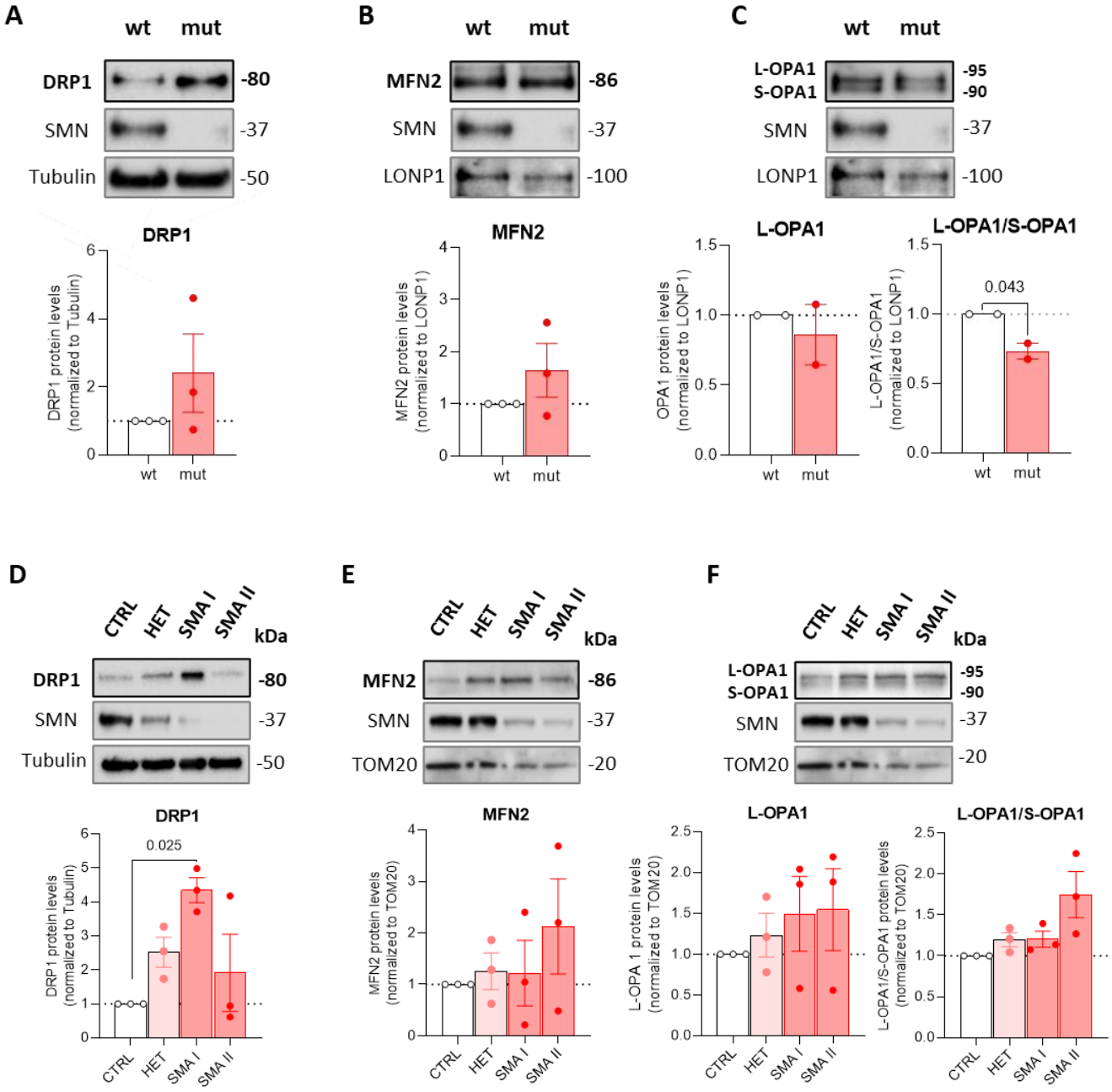

Figure 13. ***Protein levels of mitochondrial dynamics regulators in SMA mouse and human MNs.*** Graphs of the mean ± SEM of three independent experiments of DRP1 (**A**), MFN2 (**B**), L-OPA1, and L-OPA1/S-OPA1 (**C**) protein level quantification in mouse MNs. The β-Tubulin was used as a loading control. LONP1 was used as a mitochondrial marker to normalize the values of mitochondrial proteins. Differences between control (wt) and mutant (mut) values were analyzed by using the unpaired t-test. Graphs of the mean ± SEM of three independent experiments of DRP1 (**D**), MFN2 (**E**), L-OPA1, and L-OPA1/S-OPA1 (**F**) protein level quantification in human MNs. β-Tubulin was used as a loading control. TOM20 was used as a mitochondrial marker to normalize the values of mitochondrial proteins. Differences between the values of control (CTRL), heterozygous (HET), SMA type I (SMA I), and SMA type II (SMA II) conditions were analyzed by using the ordinary one-way ANOVA with Tukey's multiple comparisons test.

4. Differential regulation of mitochondrial fusion and fission between soma and neurites in SMA human MNs

Given the complexity of interpreting protein-level analyses of the regulators of mitochondrial fusion and fission, we decided to investigate the balance state between the two processes using MiNA *in silico* workflow in SMA human MNs. The TOM20/βIII-Tubulin double staining in CTRL and SMA I cell lines allowed for visualizing mitochondria along their cytoskeleton (**Figure 14A**). Moreover, the *in-silico* analysis was separated for the two compartments: representative soma and neurites of healthy and SMA MNs, with their mitochondrial "skeleton" are shown in **Figure 14B** and **Figure 14E**, respectively. In the soma of SMA MNs compared to CTRL ones, mitochondria were more clustered between them since a lower number of Individuals (mitochondria separated from their network) was found (CTRL vs SMA I: 8.36 vs 6.26, -2.101 ± 0.85, p=0.0156, **Figure 14C**). At the same time, the same mitochondria seem longer with respect to mitochondria of CTRL MNs soma, even if this difference was not statistically significant (CTRL vs SMA I: 1.03 vs 1.17, +0.14, ± 0.11, p=0.1837, **Figure 14D**). While in the neuritic area of SMA I MNs, mitochondria appeared significantly shorter than in control MNs (CTRL vs SMA I: 1.65 vs 1.10, -0.55 ± 0.17, p=0.0019, **Figure 14G**).

Taken together, these results suggest that in SMA human MNs, mitochondrial dynamics are unbalanced toward the fusion process in the soma and, on the contrary, toward the fission process in neurites.

In this context, the fusion-promoting compound Teriflunomide (TFN) -previously identified through a high-throughput screening of small molecules capable of enhancing MFN2 expression and inducing mitochondrial elongation (Miret-Casals et al., 2018) - was selected for further experimental investigation.

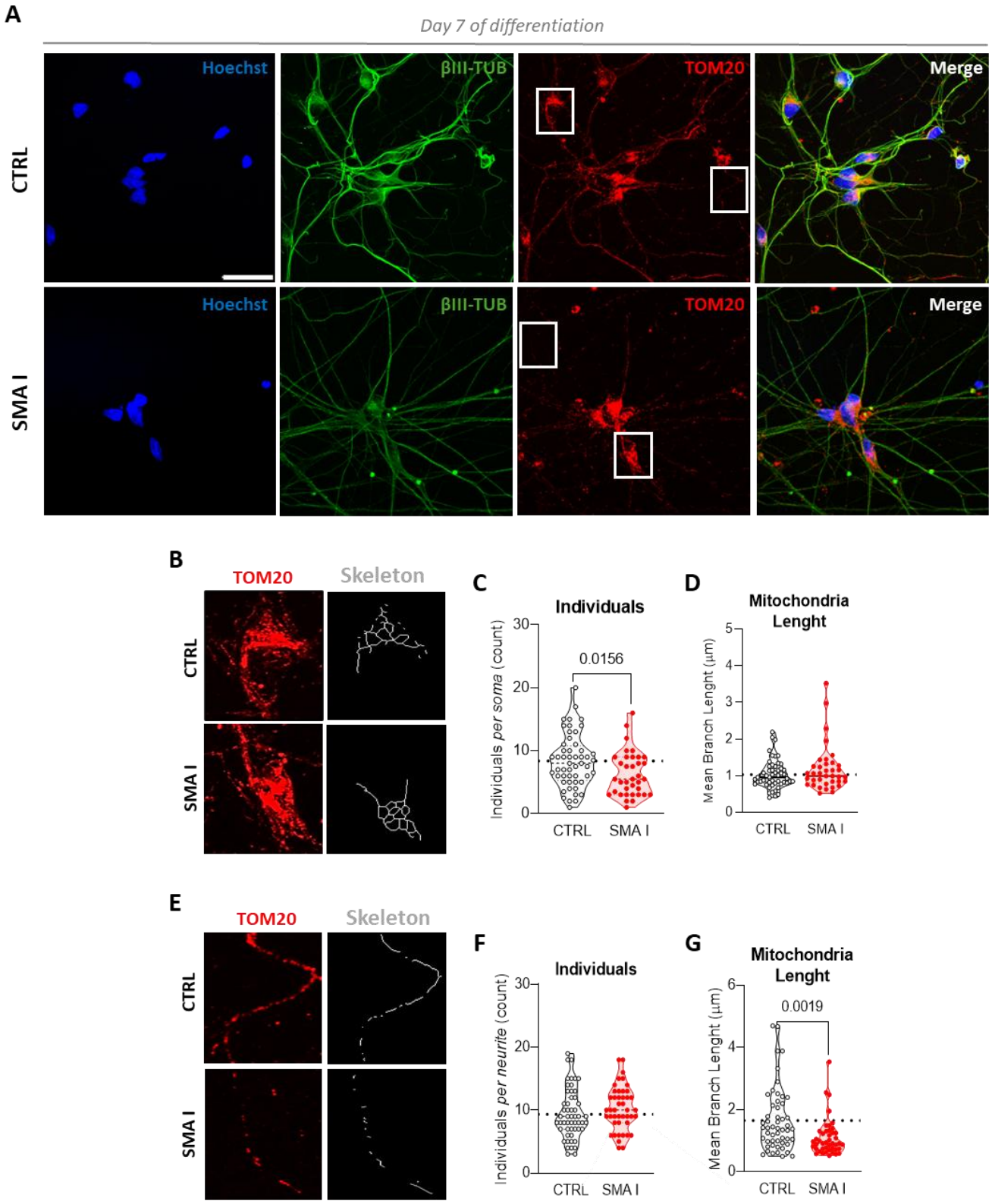

Figure 14. ***Mitochondrial Network Analysis in soma and neurites of SMA human MNs.*** For the image panel (**A**), from left to right: representative Hoechst (blue) staining, beta-III TUBULIN (green) staining, TOM20 (red) staining, and merged images for nuclei, cytoskeleton, and mitochondria in CTRL and SMA I MNs after 7 days of differentiation. Scale bar: 50 µm. Representative high magnification images of TOM20 staining with its skeleton from MiNA analysis for a single soma (**B**) and a single neurite (**E**). The

graph shows the number of individual mitochondria for each soma (**C**). The graph shows the mean mitochondria length for each soma (**D**). The graph shows the number of individual mitochondria for each neurite (**F**). The graph shows the mean mitochondria length for each neurite (**G**). Values were collected from at least three images from three independent experiments. Differences between the values of CTRL and SMA I cell lines were analysed by using the unpaired t-test.

5. TFN, a fusion-promoting drug, increases mitochondrial content and upregulates SMN in SMA human MNs

TFN drug has been tested for its capacity to enhance Mfn2 mRNA and MFN2 protein levels, modulate gene transcription, and act as a mitochondrial fusion promoter. Before evaluating the efficacy of TFN, a cell viability assay was performed by treating human MNs with three different concentrations (25, 50, and 75 μM) for 48 hours (**Figure 15A**), based on a previous screening published by Miret-Casals and coll. (Miret-Casals et al., 2018). The quantification of cell viability was assessed by counting the number of cells after the drug treatment and the DAPI signal: the results were expressed as a percentage of cell reduction compared to the vehicle condition (75 μM DMSO; in detail for the *Cell Viability Assay*, 0 μM = 100 %, 25 μM = 93%, 50 μM = 75%, 75 μM = 43%, **Figure 15B**). The assay demonstrated that among the tested concentrations, 50 μM represented the maximum non-lethal concentration.

Once the 50 μM/48h was selected, the efficacy of the drug in enhancing MFN2 protein levels has been confirmed in CTRL, SMA I, and SMA II cell lines, even if the high variability among the replicates prevented statistical significance (CTRL untreated vs CTRL treated: 1 vs 2.38, +1.38, p=0.8155; SMA I untreated vs SMA I treated: 1 vs 4.04, +3.04, p=0.3153; SMA II untreated vs SMA II treated: 1 vs 2.03, + 1.031, p=0.9345; **Figure 15D**). Interestingly, the increased MFN2 levels after the treatment was also associated with the improved mitochondrial content, as demonstrated by the higher levels of the LONP1 marker in human MNs treated compared to untreated ones (CTRL untreated vs CTRL treated: 1 vs 2.69, +1.69, p=0.7355; SMA I untreated vs SMA I treated: 1 vs 1.21, +0.21, p>0.9999; SMA II untreated vs SMA II treated: 1 vs 2.25, + 1.25, p=0.8985; **Figure 15E**). This latter result seems to suggest that regulating the fission-fusion imbalance can modulate mitochondrial turnover. Moreover, WB analysis revealed that the treatment enhanced the levels of SMN protein, demonstrating a protective effect of the fusion-promoting drug on human MNs. (CTRL untreated vs CTRL treated: 1 vs 1.97, +0.97, p=0.8927; SMA I untreated vs SMA I treated: 1 vs 1.20, +0.20, p<0.9999; SMA II untreated vs SMA II treated: 1 vs 3.35, + 2.35, p=0.2010; **Figure 15F**).

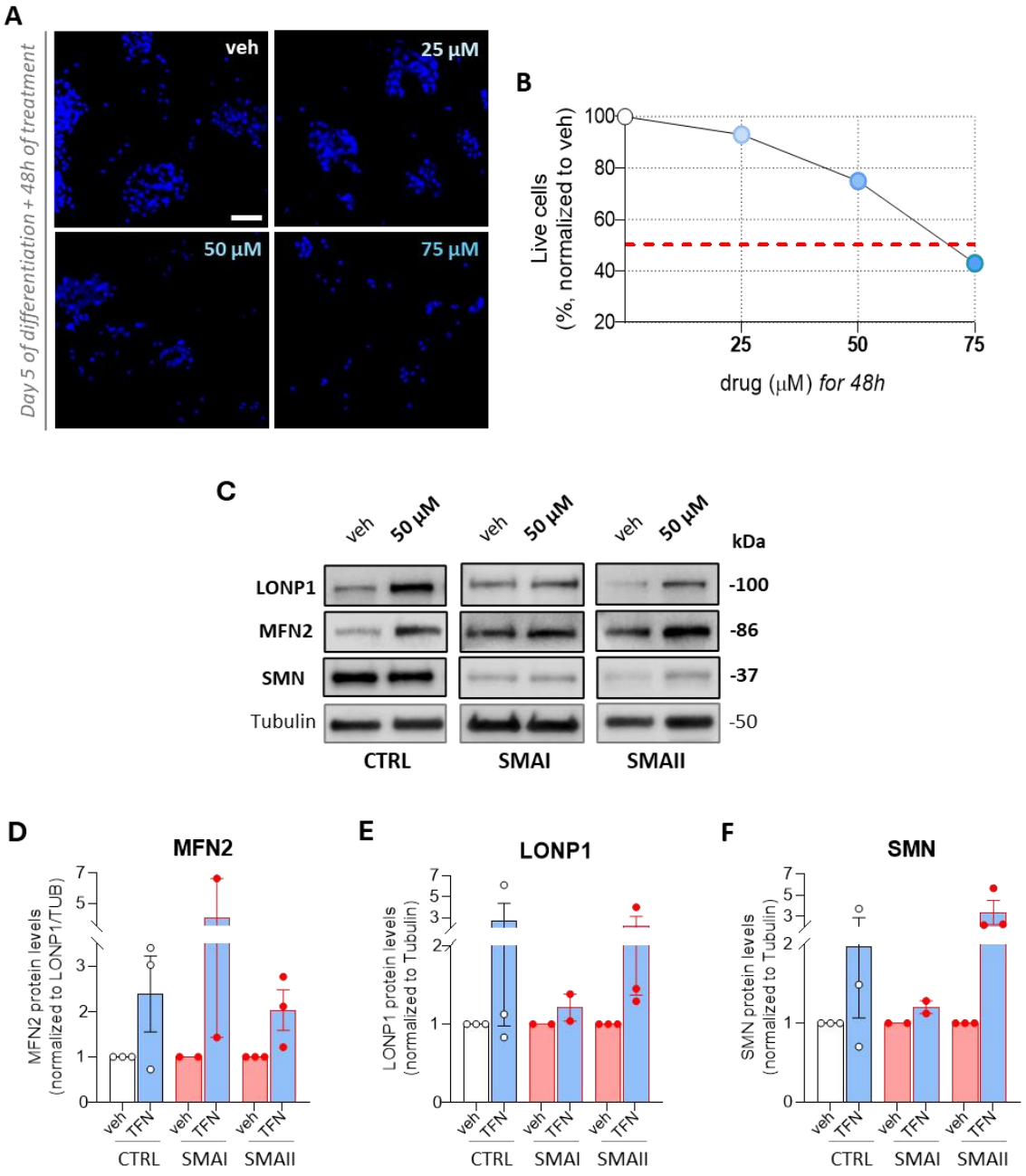

Figure 15. ***Cell viability and protein levels of mitochondrial markers and SMN after treatment in SMA human MNs.*** Representative DAPI immunostaining images of human MNs at 5 days of differentiation after DMSO administration (Veh) and treatment at 25, 50, and 75 µM for 48 hours with TFN. Scale bar: 50 µm (**A**). Cell viability graph showing the percentage of live cells after each treatment (normalized to the veh condition) with an additive red line fixing the 50% cell reduction (**B**). Representative WB of mitochondrial markers and SMN protein of CTRL, SMA I, and SMA II MNs treated with veh and TFN 50 µM for 48 hours (**C**). Graph of the mean ± SEM of MFN2 protein level quantification. The LONP1 was used as a mitochondrial marker to normalize the values of mitochondrial proteins (**D**). Graph of the mean ± SEM of LONP1 protein level quantification. (**E**). Graph of the mean ± SEM of SMN protein level quantification. (**F**). Values were collected from at least three independent experiments. β- Tubulin was used as a loading control. Differences between the values of control (CTRL), SMA type I (SMA I), and SMA type II (SMA II) conditions were analysed by using the ordinary one-way ANOVA with Tukey's multiple comparisons test.

PART II:

Study of mitochondrial network in SMA human fibroblasts and preliminary screening of a fusion-promoting drug

6. SMA human fibroblasts exhibit mitochondrial dysfunctions, despite unaltered mitochondrial content

Based on the alterations in mitochondrial dynamics found in SMA MNs, we decided to investigate such defects also at the peripheral level, using human fibroblasts derived from healthy subjects (**CTRL1**, **CTRL2**, and **CTRL3** cell lines) and SMA patients (**SMA1**, **SMA2**, and **SMA3** cell lines). The characterization of our SMA human fibroblast model was carried out through clinical and genetic features, like the age, the sex, the number of SMN1/SMN2 copies, and the type of SMA, summarized in **Figure 16A.** Moreover, the levels of SMN protein were analyzed by WB analysis: the results confirmed the significantly reduction of SMN protein in SMA cell lines compared to the CTRL ones (CTRL vs SMA: 1 vs 0.52, -0.48 ± 0.14, p=0.0275; in detail for each cell line, CTRL1: 1.23, CTRL2: 0.79, CTRL3: 0.97, SMA1: 0.41, SMA2: 0.61, SMA3: 0.55; **Figure 16B**).

As for mouse and human MNs, a mitochondrial content analysis was performed to identify preliminary network variations between CTRL and SMA human fibroblasts. A high-performance flow cytometer analyzed the labeling and quantified the MFI of the MitoTracker Green probe FM. The quantifications of MFI (**Figure 16C**) highlighted that the mitochondrial mass was comparable between the two groups, and WB analysis of TOM20 (the same marker used for human MNs) confirmed that there were presence no significant changes in mitochondrial content between CTRL and SMA cell lines (CTRL vs SMA: 1 vs 0.71, -0.29, ± 0.17, p=0.1693; in detail for each cell line, CTRL1: 0.77, CTRL2: 1.23, CTRL3: 0.99, SMA1: 0.88, SMA2: 0.75, SMA3: 0.50; **Figure 16D**). Given the lack of differences in mitochondrial mass between SMA and non-SMA conditions, mitochondrial dysfunction was assessed by measuring a key indicator of mitochondrial activity, the mitochondrial membrane potential (**Figure 16E)**. Interestingly, the mitochondrial membrane potential, evaluated by the analysis of Mitotracker Red Intensity, revealed a significant increase in SMA cell lines compared to CTRL cell lines (CTRL vs SMA: 100 vs 153.74, +53.74 ± 19.15, p=0.0485; in detail for each cell line, CTRL1: 122.11, CTRL2: 73.28, CTRL3: 104.61, SMA1: 145.53, SMA2: 136.92, SMA3: 178.76; **Figure 16F**). Moreover, the evaluation of mitochondrial aconitase (mACO2) activity, a mitochondrial enzyme involved in the tricarboxylic acid (TCA) cycle, corroborated the presence of mitochondrial defects in SMA human fibroblasts, at least in two of three patients (CTRL vs SMA: 1.62 vs 1.03, -0.59 ± 0.89; p=0.5442; in detail for each cell line, CTRL1: 1.45, CTRL2: 2.18, CTRL3: 1.24, SMA1: -0.08, SMA2: 2.69, SMA3: 0.49; **Figure 16G**).

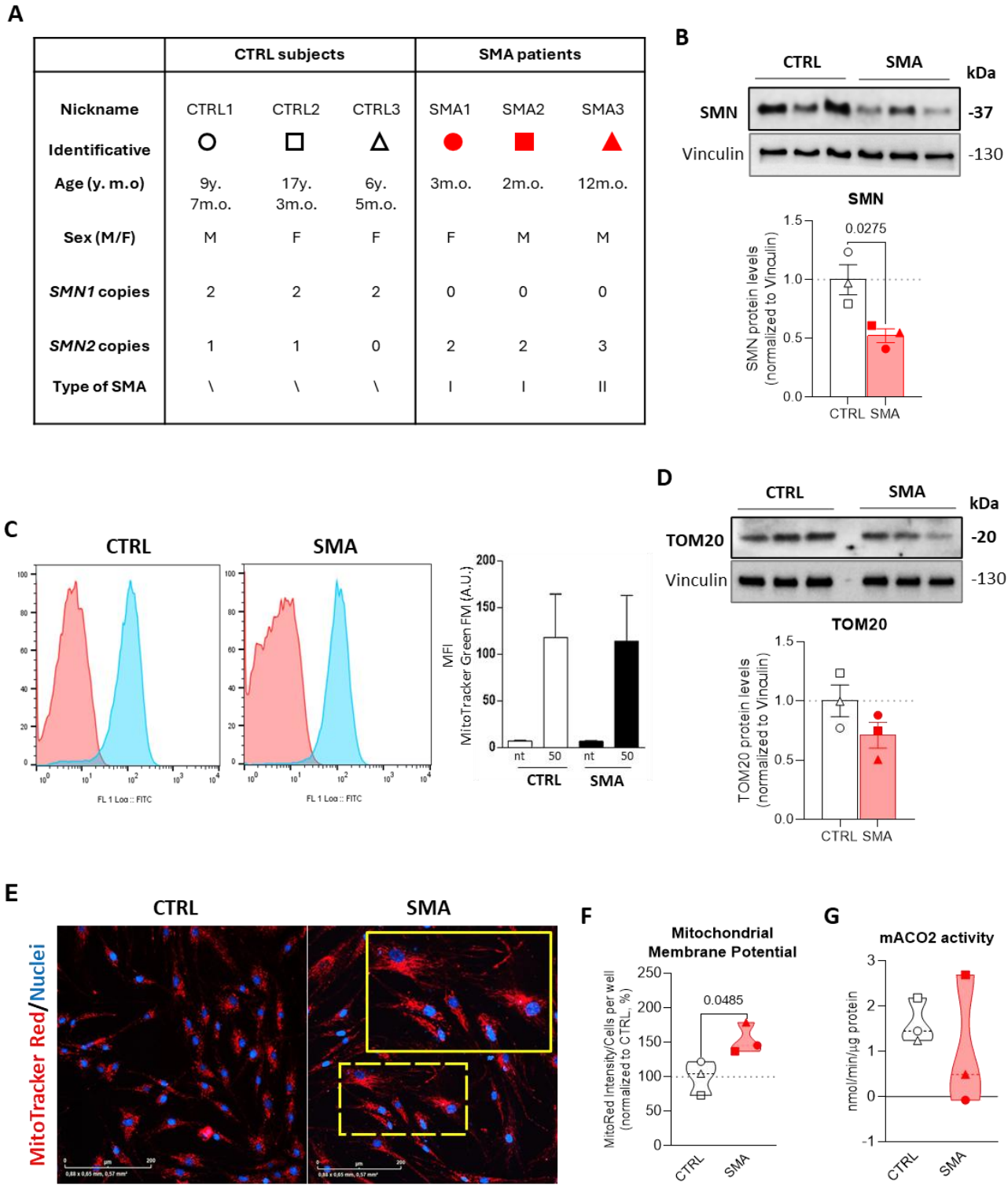

Figure 16. ***Mitochondrial content and activity analysis in a characterized model of SMA human fibroblasts.*** Table summarizing each identifiable symbol and the age, sex, *SMN1/SMN2* copies, and the type of SMA for each CTRL and SMA cell lines (**A**). Graph of the mean ± SEM of the SMN protein level quantification for each CTRL and SMA cell line. The Vinculin was used as a loading control (**B**). Labeling with Mitotracker green probe FM and quantification of MFI between CTRL and SMA human fibroblasts without and with 50 nM of Mitotracker green probe FM. Two-way ANOVA followed by Sidak's multiple

comparisons test, n=3 human subjects per genotype (**C**). Graph of the mean ± SEM of the TOM20 protein level quantification for each CTRL and SMA cell line. Vinculin was used as a loading control (**D**). Representative merged images of live-labeled cells with MitoTracker Red day (red) for active mitochondria and Nuclei (blue) for nuclei in CTRL and SMA human fibroblasts. Scale bar: 200 µm (**E**). The graph shows percentage values of Mitoracker Red Intensity per cell per well for each CTRL and SMA cell line, normalized for the mean of values of CTRL cell lines (**F**). Quantification of the enzymatic activity of mACO2 on enriched mitochondrial protein extraction from CTRL and SMA human fibroblasts expressed in nmol/min/µg protein (**G**). Differences between CTRL and SMA values were always analyzed by using the unpaired t-test.

7. Mitochondrial network fragmentation is moderately increased in SMA human fibroblasts

Although no significant reduction in mitochondrial content was detected in this SMA model, an analysis of the fusion-fission state was performed in SMA human fibroblasts compared to CTRL ones to assess whether the state of network activity dysfunction could be related to changes in its dynamics. As in human MNs, after TOM20 staining, the mitochondrial network morphology was studied by using MiNA *in silico* workflow (**Figure 17A**). Interestingly, the number of mitochondria isolated by their network (Individuals) was increased (more than 50%) in two of three SMA cell lines (CTRL vs SMA: 100 vs 137.43, + 37.43, ± 30.27, p=0.2840; in detail for each cell line, CTRL1: 77.58, CTRL2: 95.75, CTRL3: 126.67, SMA1: 169.79, SMA2: 84.53, SMA3: 157.95; **Figure 17B**). Similarly, a trend of increased mitochondrial area was found in two of three SMA cell lines with respect to the CTRL ones (CTRL vs SMA: 100 vs 124.6, + 24.62, ± 12.50, p=0.1202; in detail for each cell line, CTRL1: 83.46, CTRL2: 109.62, CTRL3: 106.92, SMA1: 126.45, SMA2: 139.81, SMA3: 107.60; **Figure 17C**). Altogether, considering that mitochondrial content is not increased, the increased mitochondrial area is only attributable to the enhanced number of mitochondria fragmented in the SMA condition.

Following the Mitochondrial Network Analysis, which revealed the presence of a fragmented network in SMA human fibroblasts, the WB analysis (**Figure 17D**) of fission (DRP1, S-OPA1) and fusion (MFN2, L-OPA1) regulators was conducted. Regarding fission machinery, results showed that the L-OPA1/S-OPA1 ratio was significantly decreased in the SMA human fibroblasts compared to the CTRL cell lines (CTRL vs SMA: 1 vs 0.77, -0.23 ± 0.07, p=0.0287; in detail for each cell line, CTRL1: 1.03, CTRL2: 1.00, CTRL3: 0.97, SMA1: 0.85, SMA2: 0.83, SMA3: 0.65; **Figure 17G**). However, DRP1 protein levels seemed not to change among SMA and CTRL conditions (CTRL vs SMA: 1 vs 1.11, + 0.11, ± 0.14, p=0.4688; in detail for each cell line, CTRL1: 1.12, CTRL2: 0.86, CTRL3: 1.01, SMA1: 0.99, SMA2: 1.34, SMA3: 0.99; **Figure 17E**). Regarding the fusion machinery, although the expression of MFN2 protein seemed increased in the SMA condition (CTRL vs SMA: 1 vs 1.131, + 0.13 ± 0.20, p=0.55; in detail for each cell line, CTRL1: 1.03, CTRL2: 1.00, CTRL3: 0.97, SMA1: 0.85, SMA2: 0.83, SMA3: 0.65; **Figure 17F**) and L-OPA1 (CTRL vs SMA: 1 vs 1.35, +0.35 ± 0.25, p=0.2366; in detail for each cell line, CTRL1: 1.22, CTRL2: 0.70, CTRL3: 1.08, SMA1: 0.96, SMA2: 1.62, SMA3: 1.48; **Figure 17H**), the variability among the SMA cell lines resulted in the loss of statistical significance.

Moreover, also in SMA human fibroblasts, WB analysis of mitochondrial-shaping proteins revealed an expression pattern, with only one fission marker (S-OPA1) showing a significant increase. In contrast, fusion markers exhibited high variability.

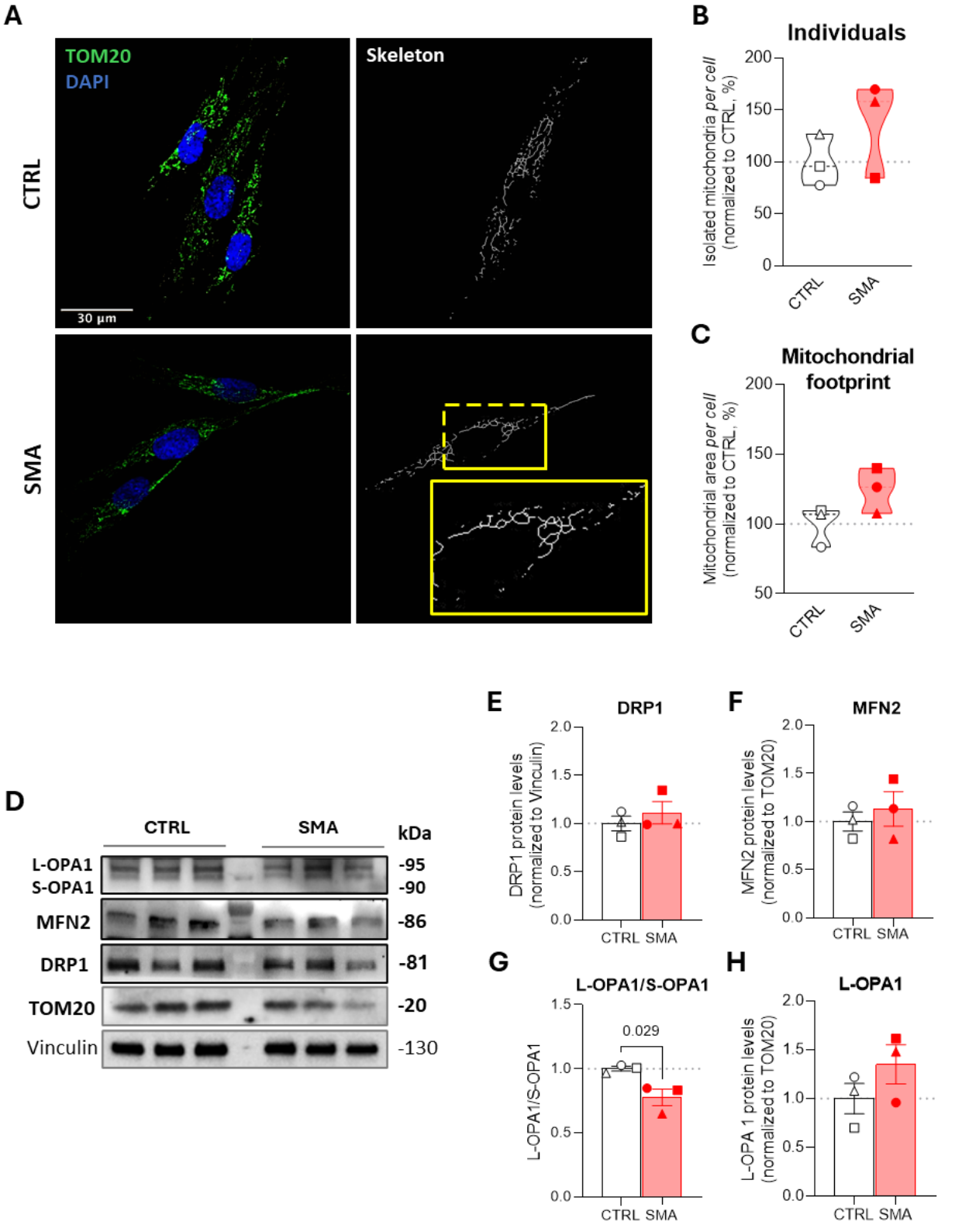

Figure 17. ***Mitochondrial Network Analysis and protein levels of mitochondrial dynamics regulators in SMA human fibroblasts.*** For the image panel (**A**), from left to right: representative merged images for DAPI (nuclei, blue) and TOM20 (mitochondria, green) immunostainings, and "skeletonized" images from MiNA analysis in CTRL and SMA human fibroblasts. Scale bar: 30 μm. The graph shows the percentage of individual mitochondria for each CTRL and SMA cell line (**B**). The graph shows the percentage of mitochondrial area for each CTRL and SMA cell line (**C**). Each percentage is from at least 18 fibroblasts for each cell line. Values were normalized to the mean value of all CTRL cell lines and then expressed as a percentage. Representative WB of mitochondrial dynamics regulators of CTRL and SMA human fibroblasts (**D**). Graph of the mean ± SEM of the DRP1 (**E**), MFN2 (**F**), L-OPA1/S-OPA1 (**G**), and L-OPA1 (**H**) protein level quantification for each CTRL and SMA cell line. The Vinculin was used as a loading control for DRP1. The TOM20 was used as a mitochondrial marker to normalize the values of mitochondrial proteins (MFN2 and L-OPA1). Differences between CTRL and SMA values were always analyzed by using the unpaired t-test.

8. Fusion-promoting drug enhances mitochondrial network fusion in SMA human fibroblasts

Since the moderate imbalance toward the fission found in SMA human fibroblasts and the previous results obtained from SMA human MNs (**Figure 15C**), the TFN drug has also been tested for its function of increasing Mfn2 mRNA and MFN2 protein levels in SMA human fibroblasts. As for MNs, before evaluating the efficacy of the compound, the MTS assay was performed by treating human fibroblasts with seven different concentrations (37.5, 50, 75, 100, 150, 200, and 500 μM) for 48 hours. As reported in the literature for the human skin fibroblast BJ cell line, the IC_{50} value of TFN was not reached within our concentration range (IC50 > 500 μM) (**Figure 18A**) (Adamczuk et al., 2021). Moreover, by considering the effect of the drug on each CTRL and SMA cell line (**Figure 18B**), any difference was found among the cell lines. Based on these results on the TFN safety on our SMA human fibroblast model lines, two different concentrations have been chosen, conventionally, for further analyses. The lower one (C1 = 50 μM) was selected as the same used previously for SMA human MNs, while the higher one (C2 = 200 μM) was selected as the penultimate tested concentration.

Once the treatments at 50 μM (C1) and 200 μM (C2) for 48 hours have been chosen, the efficacy of the drug in enhancing MFN2 protein levels has been confirmed by WB analysis. The trend (V1 vs C1: 1 vs 1.36, +0.36 ± 0.28, p=0.27; V2 vs C2: 1 vs 1.2, +0.2 ± 0.20, p=0.37; **Figure 18C**) shows that both concentrations were able to increase the MFN2 protein levels in SMA human cell lines, although high variability was found among the cell lines. Similarly, L-OPA1 protein levels were enhanced in a dose-dependent manner with both concentrations (V1 vs C1: 1 vs 1.03, +0.03 ± 0.11, p=0.7940; V2 vs C2: 1 vs 1.19, +0.19 ± 0.14, p=0.25; **Figure 18D**). Moreover, to ensure that an increased fission state was not counterbalanced by enhanced fusion state, DRP1 protein levels were evaluated by WB analysis, confirming the reduction of DRP1 protein levels in SMA human fibroblasts treated with C1 and a trend of increased DRP1 protein levels in SMA human fibroblasts treated with C2 (V1 vs C1: 1 vs 0.77, -0.23 ± 0.06, p=0.0197; V2 vs C2: 1 vs 1.17, +0.17 ± 0.16, p=0.3665; **Figure 18E**).

In addition, to further assess the effect of TFN treatment for 48 hours on mitochondrial network morphology of SMA human fibroblasts, the MiNA *in silico* workflow was applied following

TOM20-DAPI immunostaining (**Figure 18F**). The analysis of "skeletonized" fibroblasts revealed a significantly reduced number of mitochondria isolated (Individuals) from their network after the drug administration as opposed to the vehicle condition (veh vs drug: 100 vs 60.23, -39.77 ± 15.81, p=0.0401; **Figure 18G**). Similarly, the efficacy of the fusion-promoting drug was confirmed by the reduction of area occupied by fragmented mitochondria in their network in SMA human fibroblasts with respect to those treated with only vehicle (veh vs drug: 100 vs 60.23, -39.77 ± 15.81, p=0.0401; **Figure 18H**).

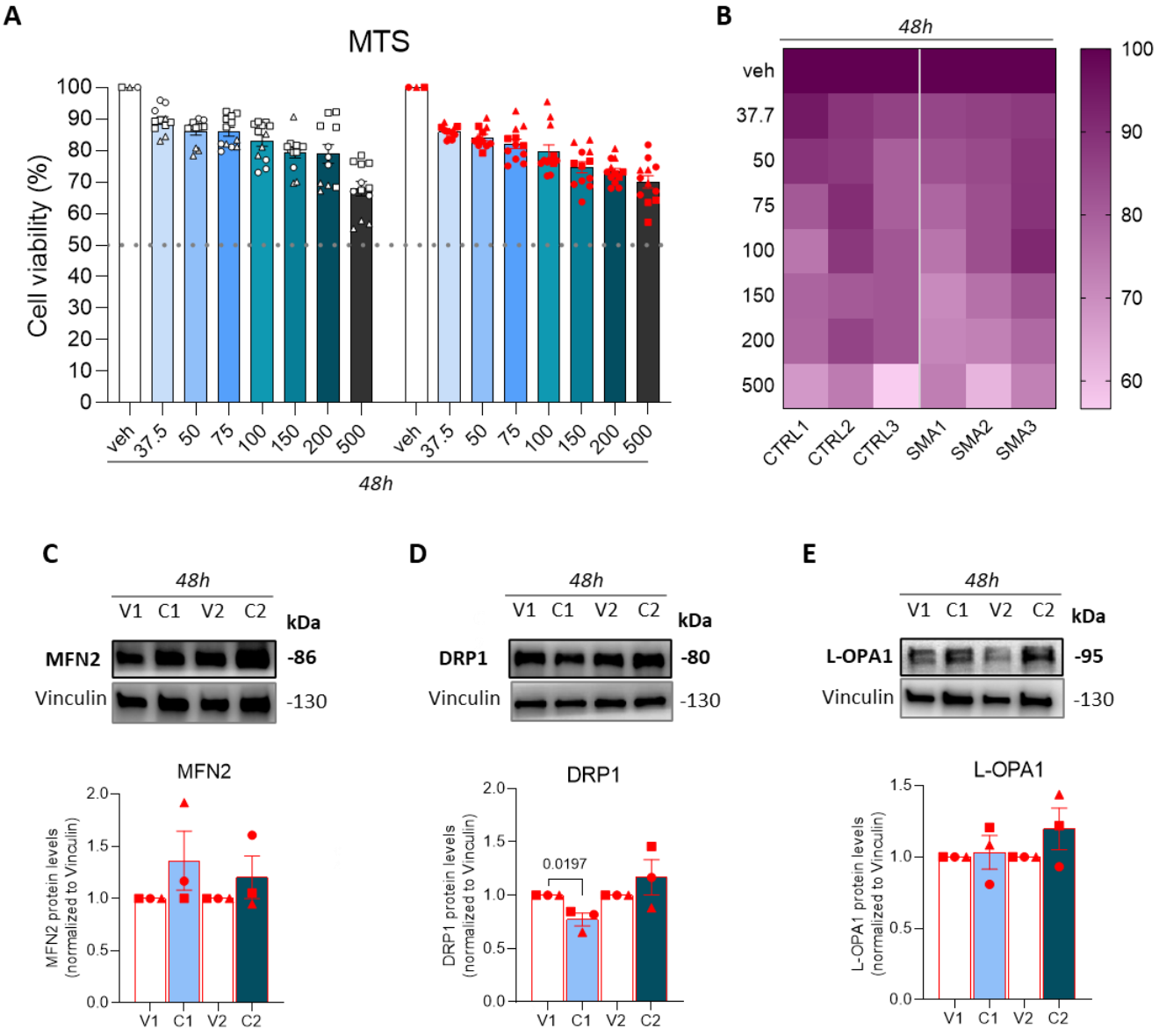

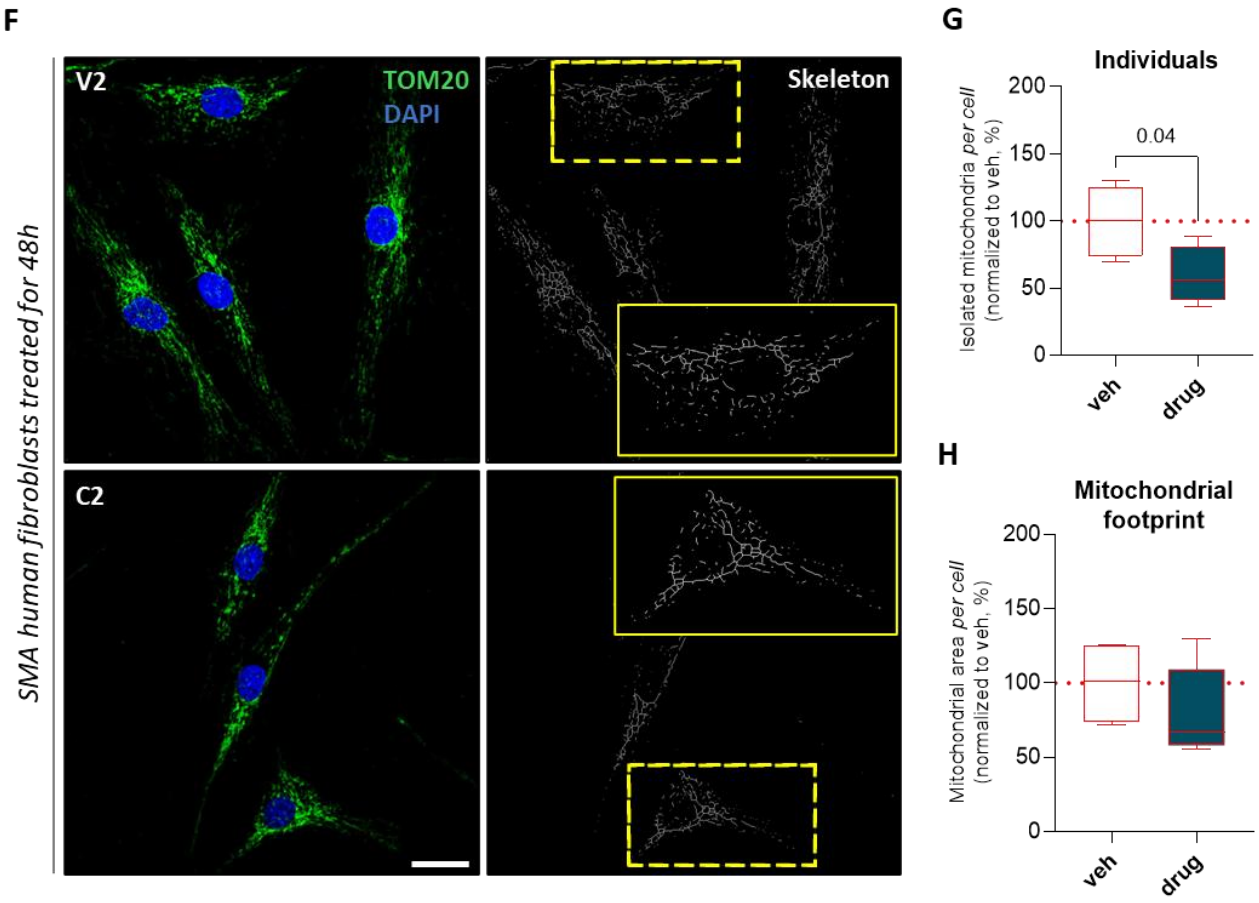

Figure 18. ***Cell viability, protein levels of dynamics regulators, and Mitochondrial Network Analysis after treatment in SMA human fibroblasts.*** MTS assay for the evaluation of cell viability of CTRL and SMA human fibroblast cell lines after the administration of TFN at 37.5-500 µM for 48 hours. The viability of cells treated with DMSO (veh) was considered 100% (**A**). Heatmap showing the comparative effect of each TFN concentration on CTRL and SMA cell lines' viability, according to the color scale in the sidebar on the right (**B**). Graph of the mean ± SEM of the MFN2 (**C**), DRP1 (**D**), and L-OPA1 (**E**) protein levels for each SMA cell line treated for 48 hours with DMSO (V1, V2) and TFN (C1, C2). Vinculin was used as a loading control. For the image panel (**F**), from left to right: representative merged images of DAPI (nuclei, blue) and TOM20 (mitochondria, green) immunostainings, and "skeletonized" images from MiNA analysis of SMA human fibroblasts treated for 48 hours with DMSO (V2) and TFN (C2). Scale bar: 20 µm. The graph shows the percentage of individual mitochondria in SMA cell lines treated for 48 hours with DMSO (V2) and TFN (C2)(**G**). The graph shows the percentage of mitochondria length in SMA cell lines treated for 48 hours with DMSO (V2) and TFN (C2)(**H**). Values were normalized to the corresponding veh condition and differences between the values of SMA cell lines were analyzed by using the unpaired t-test.

9. Enhanced mitochondrial fusion promotes organelle enrichment without suppressing mitophagy in SMA human fibroblasts

Considering the key role of mitochondrial fusion in mitochondrial turnover and the previous results obtained from SMA human MNs (**Figure 15D**), the relationship between the increased fusion state after the treatment and the mitochondrial content was also investigated in SMA human fibroblasts. Therefore, mitochondrial content analysis was assessed by evaluating TOM20 protein levels and MitoTracker Green dye analysis. Interestingly, TOM20 protein levels were increased in a dose-dependent manner by using both the concentrations of the drug compared to the vehicle effect (V1 vs C1: 1 vs 1.17, +0.17 ± 0.06, p=0.0604; V2 vs C2: 1 vs 1.392, +0.39 ± 0.06, p=0.0039; **Figure 19A**). Similarly, the intensity of MitoTracker Green dye was enhanced by using both the concentrations of the drug in a dose-dependent manner (V1 vs C1: 100 vs 107.4, +7.4 ± 9.84, p=0.4592; V2 vs C2: 100 vs 118.8, +18.8 ± 9.17, p=0.0695; **Figure 19B-19C**).
Since mitochondrial fusion is typically associated with the mitophagy inhibition, in contrast with the fission process, the mitophagy state was investigated by assessing LC3B-II protein levels and the colocalization between mitochondria and autophagosome structures. The levels of LC3B-II protein were increased by the administration of the higher TNF concentration (C2), demonstrating the accumulation of autophagosome structures in treated SMA human fibroblasts as opposed to untreated ones (V1 vs C1: 1 vs 1.05, +0.5 ± 0.20, p=0.8005; V2 vs C2: 1 vs 2.96, +1.96 ± 0.907, p=0.0943; **Figure 19D**). Moreover, to confirm that the LC3-positive autophagosome-like structures were indeed interacting with mitochondria, a colocalization analysis was performed using TOM20-LC3 double immunostaining (**Figure 19E**). Actually, the rate of autophagosome structures colocalized with mitochondria (LC3/TOM20), expressed as tM1 (Mander's coefficient), was significantly enhanced by 200 µM concentration in SMA human fibroblasts treated for 48 hours as opposed to those treated with 200 µM of DMSO (veh) (V2 vs C2: 0.35 vs 0.73, + 0.38 ± 0.09, p=0.0138; **Figure 19F**). At the same time, the use of TFN at C2 was related to a trend of increasing colocalization rate of mitochondria with autophagosome structures (TOM20/LC3), expressed as tM2 (Mander's coefficient) (V2 vs C2: 0.35 vs 0.73, + 0.38 ± 0.09, p=0.0138; **Figure 19G**). Taken together, the enhancement of these two parameters indicates the activation of selective mitophagy and the efficiency of mitochondrial turnover.

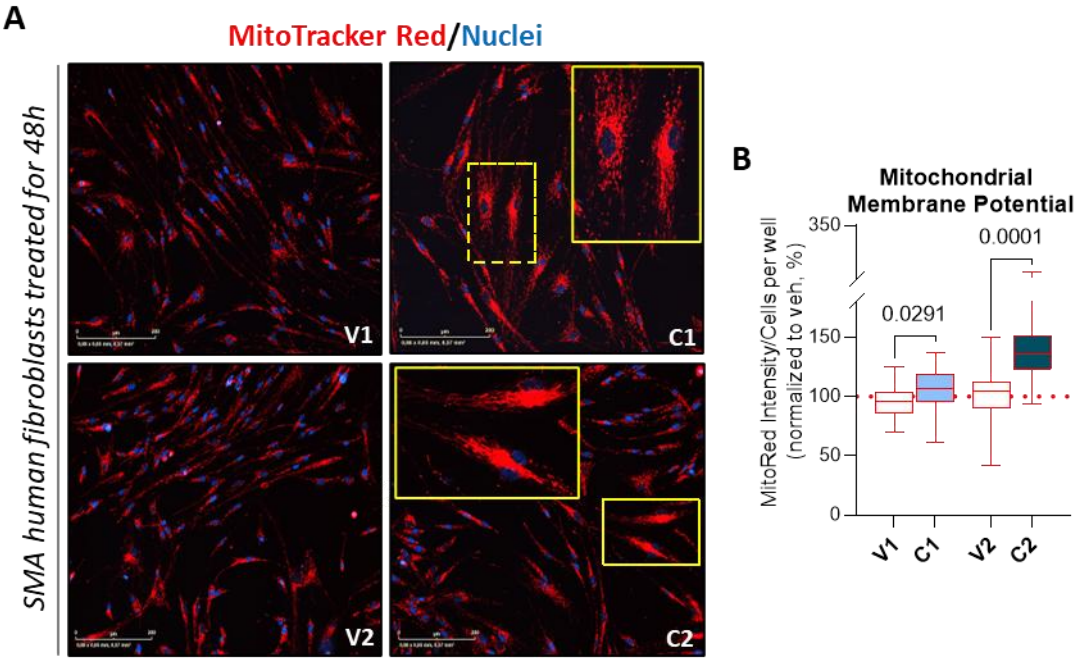

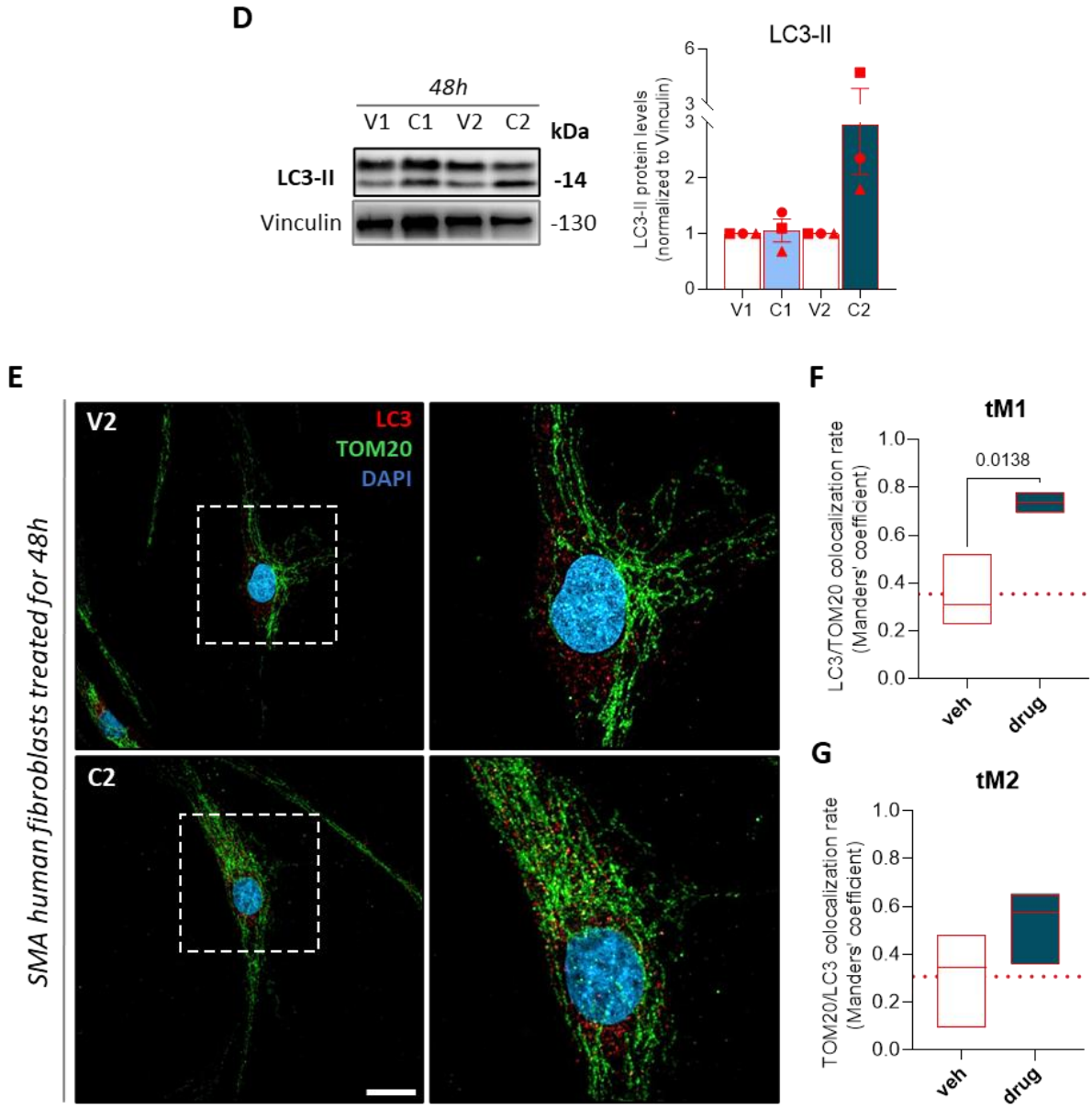

Figure 19. ***Mitochondrial content analysis and mitophagy evaluation after treatment in SMA human fibroblasts.*** Graph of the mean ± SEM of the TOM20 protein level quantification for each SMA cell line. Vinculin was used as a loading control. (**A**). Representative merged images of live-labeled cells with MitoTracker Green dye (green) for mitochondria and Nuclei (blue) for nuclei in SMA human fibroblasts. Scale bar: 200 µm (**B**). The graph shows percentage values of Mitoracker Green Intensity per cell per well(**C**). Graph of the mean ± SEM of the LC3B-II protein level quantification for each SMA cell line. Vinculin was used as a loading control. (**D**). Representative merged images of immunostaining with TOM20 (green) for mitochondria, LC3 (red) for autophagosomes, and DAPI (blue) for nuclei in SMA human fibroblasts treated for 48 hours at V2 or C2; high magnification views of cropped merged images showing the colocalization between TOM20 and LC3 signals. Scale bar: 20 µm (**E**). The graph shows values of colocalization rate (0-1) between LC3 and TOM20 (tM1) (**F**). The graph shows values of colocalization rate (0-1) between TOM20 and LC3 (tM2)(**G**). Values were normalized to the corresponding veh condition and differences between the values of SMA cell lines were analyzed by using the unpaired t-test.

10. Mitochondrial content enhancement boosts membrane potential and upregulates Complex V and SMN in SMA human fibroblasts

Since an improved mitochondrial mass could be related to improved mitochondrial activity, the mitochondrial membrane potential was measured by MitoTracker Red Intensity in live labeled SMA human fibroblasts with MitoTracker Red dye (**Figure 20A**). The result confirms a dosage-dependent positive effect of drug administration compared to the vehicles (V1 vs C1: 100 vs 106, +6 ± 4.83, p=0.0291; V2 vs C2: 100 vs 140.5, +40.54 ± 9.59, p=0.0001; **Figure 20B**). Therefore, due to the strong positive effect of the drug on the mitochondrial function, the Complex V protein levels were analyzed after the treatment. Again, the drug administration acted in a dose-dependent manner, upregulating ATP synthase protein levels compared to DMSO administration alone (V1 vs C1: 1 vs 1.22, +0.22 ± 0.10, p=0.1551; V2 vs C2: 1 vs 2.22, +1.22 ± 0.55, p=0.1555; **Figure 20C**). Finally, given the ameliorative effect of the drug on mitochondrial function and its protective role in preventing the reduction of SMN protein levels already seen in SMA human MNs (**Figure 15E**), SMN protein levels were evaluated after drug administration in SMA human fibroblasts. A dose-dependent positive effect of the drug on SMN protein levels was also observed (V1 vs C1: 1 vs 1.29, +0.29 ± 0.07, p=0.0189; V2 vs C2: 1 vs 1.74, +0.74 ± 0.54, p=0.2428; **Figure 20D**).
These findings highlight that the fusion-promoting drug TFN, in a dose-dependent manner, increases mitochondrial activity and ATP synthase levels, as well as the SMN protein levels, underscoring mitochondrial dynamics as a potential therapeutic target for SMA human fibroblasts and reinforcing the strong correlation between mitochondrial health and SMA pathology.

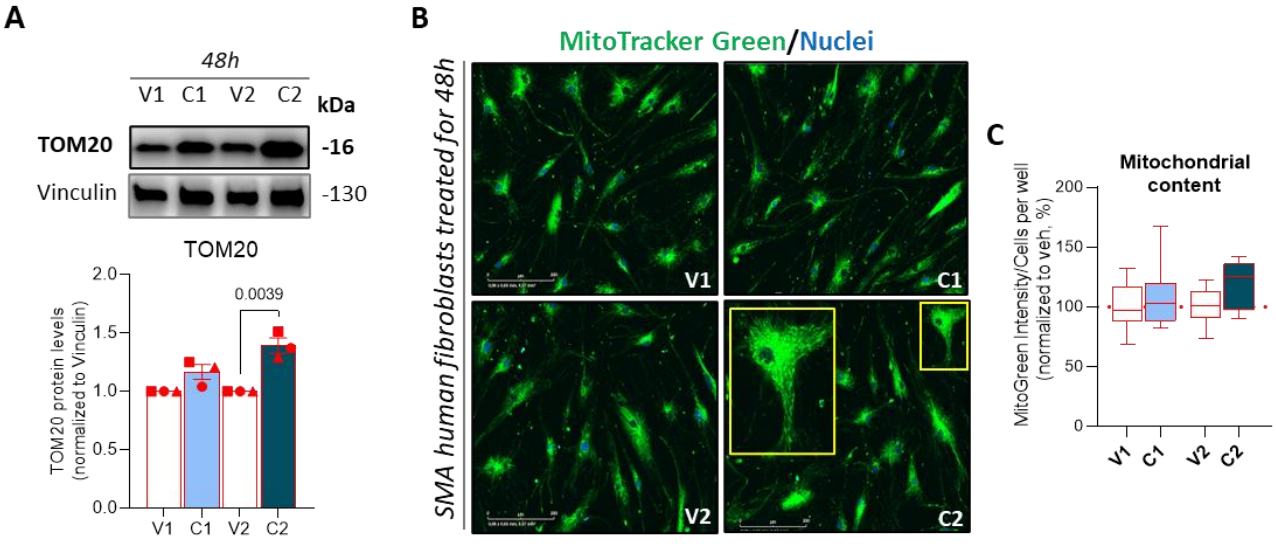

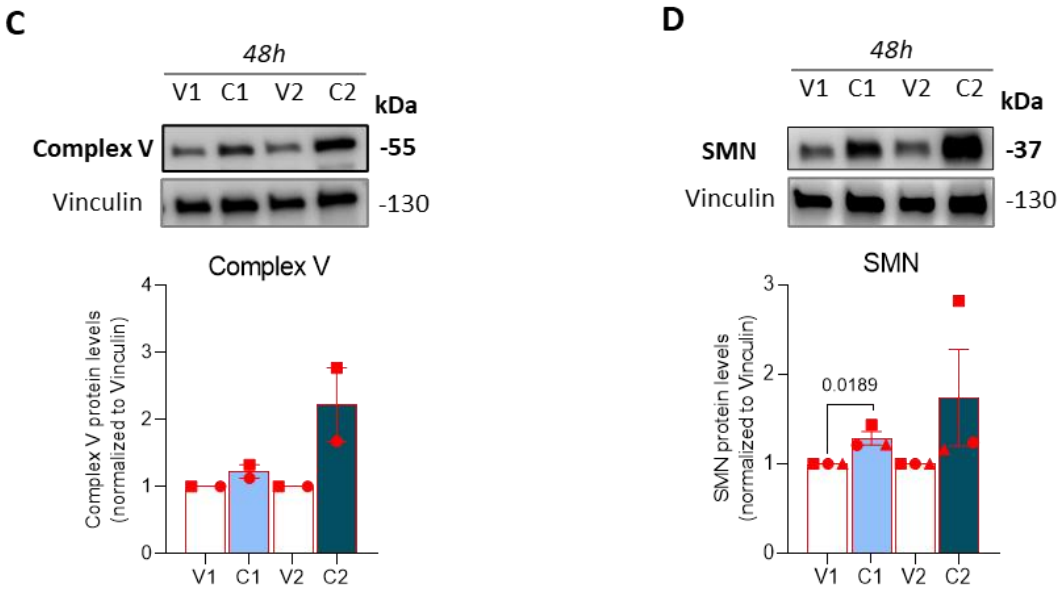

Figure 20. ***Mitochondrial membrane potential and Complex V and SMN protein levels after treatment in SMA human fibroblasts.*** Representative merged images of live-labeled cells with MitoTracker Red dye (red) for active mitochondria and Nuclei (blue) for nuclei in SMA human fibroblasts. Scale bar: 200 µm (**A**). The graph shows percentage values of Mitoracker Red Intensity per cell per well (**B**)**.** Graph of the mean ± SEM of the Complex V (**C**) and SMN (**D**) protein level quantification for each SMA cell line. Vinculin was used as a loading control. Values were normalized to the corresponding veh condition, and differences between the values of SMA cell lines were analyzed by using the unpaired t-test.

DISCUSSION

Nowadays, it is widely recognized that mitochondria play essential roles in the metabolism and physiology of eukaryotic cells. It is noteworthy that in 1898, Carl Benda, employing crystal violet as a specific stain, observed hundreds of tiny bodies within the cytoplasm of eukaryotic cells. Due to their tendency to form long chains and their thread-like appearance, he coined the term "mitochondria," derived from the Greek *mitos,* meaning "thread," and *chondros,* meaning "granule" (Benda, 1898). During the 1900s, accumulating evidence refuted the notion of mitochondria as a static powerhouse of the cell: instead, they came to be increasingly understood as complex and dynamic systems, whose filamentous morphology, described by Benda, reflected the activity of fascinating molecular machineries central to the contemporary mitochondrial biology. Just in 2002, Westermann formalized for the first time the concept of "merging mitochondria matters," since mitochondrial fusion had emerged as a pivotal process for maintaining organellar integrity and bioenergetic efficiency. His work highlighted how balanced fusion and fission events shape the dynamic mitochondrial network, enabling the redistribution of mitochondrial DNA, complementation of gene products, and dissipation of membrane potential across interconnected filaments (Westermann, 2002).

Over the past two decades, this distinctive cellular behavior, called mitochondrial dynamism, has been extensively investigated to elucidate the mechanisms underlying changes in mitochondrial morphology, number, quality, and intracellular distribution. Although not yet fully understood, mitochondrial fusion and fission, also known as mitochondrial dynamics, have emerged as the core processes of the mitochondrial quality control system (Ni et al, 2015). This latter reshapes the mitochondrial network morphology and influences the spatial positioning of mitochondria across distinct subcellular regions, but also continuously repairs and replaces the mitochondrial components, thereby preserving proper function and cellular homeostasis. Indeed, mitochondrial fission facilitates mitochondrial transport and mitophagy by segregating damaged components or entirely eliminating dysfunctional mitochondria. Conversely, mitochondrial fusion promotes the mixing and exchange of intramitochondrial contents, as well as the mitochondrial pool enhancement, thereby enhancing mitochondrial function and bioenergetic efficiency (Youle et al., 2012). Substantial evidence has demonstrated a strong correlation between mitochondrial elongation and optimized oxidative phosphorylation (OXPHOS), elevated ATP production, and reduced susceptibility to mitophagy (Molina et al., 2009; Rambold et al., 2011*).* Overall, a tightly regulated equilibrium between these opposing processes ensures the dynamic remodeling of the mitochondrial network in response to metabolic demands and stress conditions. Disruption of this balance has been implicated in a wide range of pathologies, including neurodegenerative diseases, metabolic syndromes, and cancer (Chen et al., 2023).

In neurodegenerative diseases, altered mitochondrial dynamics have emerged as a central pathological feature. Recent studies have highlighted the role of key regulatory proteins -such as DRP1, MFN2, and OPA1- and their dysregulation has been implicated in conditions including AD, PD, HD and ALS (Kathiresan et al., 2024). In the context of SMA -one of the most common genetic causes of infant mortality, resulting from mutations in the *SMN1* gene and consequent deficiency of the SMN protein- mitochondrial dysfunction has been extensively investigated.

Emerging evidence highlights that SMN depletion affects mitochondrial morphology, dynamics, and bioenergetic capacity, particularly in MNs and skeletal muscle, contributing to disease progression and neuromuscular degeneration (Zilio et al., 2022). As described in the Introduction section, several SMA MN models exhibit mitochondrial alterations linked to mitochondrial dynamics, including reduced mitochondrial content, enhanced fission, impaired axonal trafficking, disrupted mitophagy, and diminished ATP production (Miller et al., 2016; Xu et al., 2016; Thelen et al., 2020)

In our study, to investigate the state of the mitochondrial network in SMA MNs, we employed two different early-stage models: mouse MNs from the SMNΔ7 model cultured for six days and human MNs differentiated from iPSCs of SMA patients cultured for seven days. This choice allows us to distinguish primary mitochondrial defects that may be causally involved in SMA onset, from secondary alterations arising during ongoing neurodegeneration. Both models showed the typical morphology of MNs and the expression of canonical markers of mature MNs, such as Hb9 and ChAT, as seen by the phase-contrast and immunostaining images in **Figure 11A** and **Figure 11C** for SMA mouse and human MNs, respectively. In addition, the marked reduction of SMN protein levels observed in SMA mouse (**Figure 11B**) and human MNs (**Figure 11D**) underscored the robustness and translational relevance of our SMA models. In line with standard approaches for investigating mitochondrial dysfunction, we initially assessed alterations of mitochondrial network content in the SMA condition. As expected, both SMA models (**Figure 11E**, **Figure 11F**) exhibited a significant reduction in mitochondrial enrichment as opposed to non-SMA conditions, thereby confirming previous findings reported in other SMA MN models (Thelen et al., 2020; Fulceri et al., 2021). These results confirm that mitochondrial dysfunction represents a conserved pathological feature across distinct SMA models.

Moreover, neurons are highly polarized cells characterized by functional domains: the somatic and the neuritic compartments. This polarity is essential for neuronal function, governing tightly regulated processes, such as organelle trafficking and cytoskeletal dynamics (Tahirovic et al., 2009). In the context of SMA, where MNs exhibit selective vulnerability, compartment-specific analysis may reveal early and localized mitochondrial defects (**Figure 12A**, **Figure 12D**). Actually, our early-stage SMA models presented a particular mitochondrial distribution: while neurites were poor in mitochondria in SMA mouse (**Figure 12C**) and human (**Figure 12F**) MNs, like the previously cited cellular models, the somatic compartment displayed a visibly enriched mitochondrial content (**Figure 12B**, **Figure 12E**), suggesting compartment-specific accumulation. Additional investigations are needed to clarify whether the observed somatic enrichment reflects just a defective mitochondrial transport along neurites or an adaptive response to increased somatic area energy demands or the interplay of both processes. Indeed, previous studies highlighted that impaired axonal transport in acute neurological disorders results in reduced mitochondrial presence at synapses, whereas increased somatic clustering may reflect compensatory mechanisms to sustain protein quality control and energy production in the soma. Similar phenomena have been described in models of neurodegeneration, where retrograde transport of damaged mitochondria to the soma for degradation coexists with adaptive enrichment to meet stress-induced metabolic demands (Lu et al., 2023).

However, given the central role of mitochondrial dynamics in regulating the spatial distribution of mitochondria within neurons, the protein levels analysis of key fission-fusion regulators displayed a global imbalance favoring fission. In particular, the ratio between long and

short OPA1 isoforms (L-OPA1/S-OPA1) was significantly reduced in SMA mouse MNs (**Figure 13C**), and DRP1 levels were markedly elevated in the SMA type I human MNs (**Figure 13D**). Nevertheless, although fusion-related proteins appeared upregulated, their expression showed high variability, preventing a clear interpretation based solely on western blot data. Consequently, to further investigate the fission-fusion state and to explore whether the observed compartment-specific differences in mitochondrial localization were the mechanistic consequence of an altered fission-fusion balance between the two compartments, we examined the mitochondrial morphology in SMA human MNs (Di Nottia et al., 2021). Interestingly, the mitochondrial network morphology of SMA human MNs (**Figure 14A**) reflected what was found by the distribution study. While in the neurites (**Figure 14E**), mitochondria were shorter due to an increased fragmentation of the network (**Figure 14G**), the soma presented a reduced number of mitochondria isolated by their network (**Figure 14C**), suggesting an increased fusion state and confirming the presence of compartment-specific imbalance of mitochondrial fusion and fission processes. Notably, the increased fusion state observed in the somatic compartment of SMA MNs may reflect the high variability found for fusion regulators by western blot analysis.

The observed overall imbalance in mitochondrial dynamics toward fission may underlie the reduction of mitochondrial content in the neuritic compartment, as excessive fission facilitates mitophagy (Youle et al., 2012; Tomaya et al., 2016). Therapeutic strategies aimed at promoting fusion could therefore confer mitochondrial benefits by stabilizing network integrity within neurites, enhancing bioenergetic efficiency, and potentially delaying neurodegenerative progression. Among the strategies developed to restore mitochondrial fusion under conditions of excessive fission (Chen et al., 2023), we selected a pharmacological compound known to promote mitochondrial fusion. Teriflunomide (TFN), originally approved in 2012 for the treatment of multiple sclerosis (O'Connor et al., 2012), was employed here as a repurposed drug to assess its effects in the context of SMA-related mitochondrial dysfunction. The drug, the main metabolically active form of Leflunomide, is a malononitrilamide that boosts MFN2 mRNA and protein levels (Miret-Casals et al., 2018). Also tested in models of peripheral spinal root explants and acute hippocampal sections in mice, the increased MFN2 levels have been shown to protect from oxidative damage, regulating neuronal activity and mitochondrial dynamics (Malla et al., 2020; Malla et al., 2022).

In our SMA human MN model, the compound was used at the maximum non-lethal concentration, 50 μM (**Figure 15A**, **Figure 15B**), for a two-day treatment, revealing increased MFN2 protein levels (**Figure 15D**) as well as LONP1 protein levels (**Figure 15E**). The simultaneous upregulation of fusion and content mitochondrial markers suggests that the increased fusion state affects the mitochondrial content, redirecting mitochondrial turnover toward the biogenesis of new organelles (Fu et al., 2019). Moreover, in the case of non-dividing cells, such as neurons, which lack the capacity to remove damaged organelles through cell division, stimulating mitochondrial biogenesis becomes essential to sustain their metabolic activity (Cardanho-Ramos et al., 2021). Accordingly, we evaluated the impact of the treatment on SMN protein levels (**Figure 15F**), which increased proportionally to the LONP1 expression, suggesting that enhanced mitochondrial biogenesis may contribute to protection against SMN loss.

Interestingly, similar effects on mitochondrial fusion and content have been reported for other fusion-promoting drugs in other neuronal systems. For example, the mitochondria-targeted peptide SS-31 demonstrated to improve cristae architecture and reduce oxidative stress, resulting in a more

fused mitochondrial network and increased mitochondrial mass in neurons (Birk et al., 2013). Notably, MFN2-targeting compounds such as MASM7, Compound 5, and Piperine (shown in the table 1 of the Introduction section) have also demonstrated the ability to promote mitochondrial fusion and restore mitochondrial content in neuronal models, including sciatic nerves and CMT2A motoneurons (Rocha et al., 2018; Dang et al., 2020; Zhang et al., 2022). Within this broader framework, our findings position the tested compound among the few agents capable of simultaneously enhancing mitochondrial fusion and content in neuronal cells, supporting the idea that restoring mitochondrial dynamics may represent a promising strategy to counteract mitochondrial dysfunctions in SMA motoneurons.

Contrary to what the name of the SMN protein may suggest, the paradigm of SMA as just a MN disease is now outdated. Although MNs seem to be the most sensitive cells to suffer from the low level of SMN, nowadays SMA is considered a multisystemic disease. Indeed, although the selective depletion of SMN protein in spinal MNs is sufficient to mediate a SMA-like murine phenotype, the resultant phenotype is relatively milder when compared with depleting the protein ubiquitously (Park et al., 2010). Regarding SMA-related mitochondrial dysfunctions, fibroblasts have received limited attention. Recently, James et al. conducted a preliminary investigation of mitochondrial function in human fibroblasts from SMA carriers, demonstrating the presence of depolarized mitochondrial membrane potential, increased levels of ROS, and reduced citrate synthase activity (James et al., 2024). However, investigating mitochondrial dynamics in fibroblasts from SMA patients could provide complementary insights into disease mechanisms and therapeutic responses beyond the nervous system and the most affected cellular types.

To characterize the state of the mitochondrial network at peripheral level, we used human fibroblasts from SMA patients. All the clinical and genetic features were summarized in **Figure 16A**. As SMA MNs, SMA human fibroblasts showed the marked reduction of SMN protein levels (**Figure 16B**), confirming also for this model the validity of our SMA human fibroblasts model. Moreover, following an equivalent procedural approach, alterations of the mitochondrial enrichment were first evaluated. In contrast to what was observed in SMA MNs, mitochondrial mass was not significantly different among SMA human fibroblasts and non-SMA conditions (**Figure 16C**, **Figure 16D**). Nevertheless, since an altered mitochondrial activity may occur even in the presence of a preserved mitochondrial pool, mitochondrial activity was assessed, confirming an increased mitochondrial membrane potential (MMP) (**Figure 16E**, **Figure 16F**) and a trend of decreased mACO2 activity (**Figure 16G**) in SMA human fibroblasts. Interestingly, the reduced mACO2 enzyme activity found in our SMA model could be strongly related to the reduced citrate synthase activity demonstrated by the previously cited James et al. in SMA carriers. Indeed, if aconitase activity is reduced, citrate may accumulate in the cell, leading to feedback inhibition of citrate synthases due to excess citrate. Conversely, while reduced MMP could represent a hallmark of dysfunction in SMA carriers, increased $\Delta\Psi m$ may reflect compensatory stress or impaired proton utilization (Zorova et al., 2018).

Surprisingly, an overall imbalance in mitochondrial dynamics toward fission was also found in human SMA fibroblasts. The analysis of mitochondrial network morphology (**Figure 17A**) highlighted a trend of increased number of mitochondria isolated by their network (**Figure 17B**), as well as a trend of enhanced mitochondrial area (**Figure 17C**), suggesting fragmentation of the network. The analysis of protein levels for key regulators of mitochondrial dynamics displayed that the ratio between long and short OPA1 isoforms (L-OPA1/S-OPA1) was significantly reduced

in SMA human fibroblasts (**Figure 17G**). Unlike MNs, the coexistence of increased mitochondrial fission with preserved organelle content suggests a dynamic remodelling of the mitochondrial network than a net loss of mitochondria (Chen et al., 2009). The absence of content reduction could indicate an early imbalance in dynamics where this remodeling phase toward fragmentation precedes mitochondrial degradation.

However, although SMA human fibroblasts did not exhibit a reduction in mitochondrial mass, promoting fusion may stabilize network morphology, blocking the shift toward fragmentation, facilitating inter-mitochondrial complementation, mitigating oxidative stress, and optimizing bioenergetic output (Yao et al., 2019). Moreover, given the intercellular metabolic crosstalk, targeting mitochondrial fusion beyond the CNS may yield broader therapeutic benefits in the context of SMA. In this light, evaluating the effects of TFN in SMA human fibroblasts -despite their preserved mitochondrial content- offers an interesting perspective, particularly when considering systemic drug administration.

In SMA human fibroblasts, two different TFN concentrations were tested, C1 (50 μM) and C2 (200 μM), for a two-day treatment, to assess potential differential outcomes. Neither tested concentration exceeded the maximum non-lethal threshold (**Figure 18A**), and no significant differences in viability were observed among the human cell lines (**Figure 18B**), thereby confirming the absence of cytotoxic effects at the tested doses. The TFN administration upregulated the MFN2 protein levels (**Figure 18C**) in SMA human fibroblasts, confirming its primary effect of boosting the expression of MFN2, which is involved in the fusion of the outer mitochondrial membrane. Interestingly, DRP1 levels decreased at C1 but showed a partial increase at C2 (**Figure 18D**), indicating that excessive fusion may trigger a compensatory upregulation of the fission molecular driver. This response likely represents a homeostatic mechanism for the cell aimed at rebalancing mitochondrial dynamics when one process becomes predominant (Adebayo et al., 2021). The fusion-promoting drug also partially enhanced protein levels of L-OPA1 (**Figure 18E**), involved in the fusion of the inner mitochondrial membrane, highlighting the effectiveness of the treatment in enhancing not only outer membrane remodeling but all the fusion machinery. Moreover, the analysis of mitochondrial network morphology of SMA human fibroblasts treated with TFN (**Figure 18F**) showed a significantly reduced number of mitochondria isolated by their network (**Figure 18G**), as well as a trend of decreased mitochondrial area (**Figure 18H**). Taken together, these results pinpoint the enhanced fusion state and the reduction of network fragmentation after treatment.

Similarly to what was observed in MNs, the treatment promoting mitochondrial fusion was associated with an increased mitochondrial content (**Figure 19A**, **9B,** and **9C**), further highlighting how the regulation of mitochondrial dynamics can positively influence mitochondrial turnover, here resulting in organelle enrichment. Notably, this result underscores a key aspect: the fusion-enhancing treatment appears to be independent of the baseline mitochondrial content. This implies that mitochondrial enrichment can occur even in models, like SMA human fibroblasts, that do not exhibit a significant reduction in organelle pool. Moreover, this enrichment seems to be proportional to the drug dosage. However, since an imbalance in mitochondrial dynamics favoring fusion can be associated with a reduction in the selective degradation of mitochondria (Zanfardino et al., 2025), an additional analysis was conducted to investigate whether the observed enrichment in mitochondrial content might instead result from an impairment of mitophagy in SMA human fibroblasts. Interestingly, TFN treatment once again increased the number of autophagosomes in

a dose-dependent manner (**Figure 19D**), suggesting an enhanced production of organelles involved in the autophagic process. Moreover, the colocalization analysis between autophagosomes and mitochondria revealed a significant increase following drug administration in SMA human fibroblasts (**Figure 19E**), suggesting an enhancement of selective mitochondrial degradation. Further analyses are required to determine whether the accumulation of mitochondria-associated autophagosomes truly reflects an active mitophagic flux. Nonetheless, the fusion-promoting compound appears to stimulate mitochondrial turnover, enhancing the biogenesis of new mitochondria without impairing their degradation.

Physiologically, mitochondrial biogenesis is an adaptive cellular response to increased energy demand, and the number of mitochondria correlates with the metabolic activity of the cell (Popov, 2020). In a manner comparable to the physiological adaptation to elevated energy requirements, the compound promoted mitochondrial activity in SMA human fibroblasts, evaluated through the mitochondrial membrane potential (**Figure 20A**, **20B**). The dose-dependent nature of this effect supports the hypothesis that the increase in mitochondrial content drove it. The role of ATP synthase is particularly intriguing in mitochondrial health -not only as a key enzyme in ATP production and a direct indicator of mitochondrial activity- but also as a regulator of mitochondrial fusion, as described in detail in the Introduction section (Arselin et al., 2004). Indeed, the fusion-promoting drug increases the expression of Complex V in proportion to the dose (**Figure 20C**), likely due to its involvement in the fusion process itself, but also plausibly by enhancing ATP production. Further analyses are required to confirm whether ATP synthesis is effectively increased in SMA human fibroblasts treated with TFN. Finally, mirroring the protective effect of TFN against the reduction of SMN protein levels in SMA human MNs, the treatment seemed to preserve SMN expression in SMA human fibroblasts (**Figure 20D**), highlighting the compound's consistent ability to counteract SMN protein loss across different SMA models.

In this context, the effects of TFN in SMA human fibroblasts parallel the robust mitochondrial remodeling described for mitofusin activators in peripheral CMT2A models. Such remodeling has been demonstrated not only in motoneurons and sciatic nerves treated with MASM7 and related agonists, but also in MFN2-mutant MEFs, where Compound 5 restores mitochondrial fusion, architecture, and distal organelle content (Franco et al., 2020). This convergence across distinct peripheral systems reinforces the idea that pharmacological stimulation of mitofusin expression and/or activity can generically re-establish mitochondrial dynamics in compromised backgrounds.

Further investigations are certainly required to better characterize the effects of TFN, particularly in relation to its dose-dependent impact on SMA human fibroblasts. The regulation of mitochondrial dynamics is a highly sensitive process, and an excessive shift toward fusion may ultimately prove detrimental rather than protective over time.

In summary, both of our SMA models, MNs and fibroblasts, exhibit alterations in mitochondrial dynamics, with an imbalance toward fission. At the central level, in SMA mouse and human MNs, this shift is associated with a reduction in mitochondrial content within the neuritic compartment, whereas at the peripheral levels, in SMA human fibroblasts, it likely reflects an earlier stage preceding mitochondrial degradation. Importantly, even in this latter model, we identified defects in mitochondrial functionality, which may benefit from the action of a pharmacological agent capable of modulating mitochondrial dynamics. Given their crucial role in maintaining mitochondrial homeostasis, already extensively discussed, our findings underscore the therapeutic potential of targeting mitochondrial dynamics as a strategy to counteract cellular

dysfunction in SMA. Notably, treatment with TFN, which promotes mitochondrial fusion within the network, proved effective in increasing mitochondrial content by stimulating biogenesis of new organelles and in counteracting the reduction of SMN protein in SMA human MNs. Similarly, in SMA human fibroblasts, enhanced mitochondrial fusion resulted in increased mitochondrial content, together with improvements in mitochondrial membrane potential, ATP synthase levels, and SMN protein expression (**Figure 21**).

Nevertheless, our study presents certain limitations that also provide valuable insights into how future investigations may be directed. Regarding the treatment in SMA human MNs, a more detailed characterization of the drug's effects at the level of each compartment (somatic and neuritic) should be performed. Indeed, in the soma we already identified an imbalance of mitochondrial dynamics favoring fusion, and further analyses are required to determine whether a compartment-specific state of hyperfusion has been induced following TFN treatment.Moreover, functional assays are still lacking to demonstrate whether the increased mitochondrial pool is accompanied by enhanced activity. In SMA human fibroblasts, the drug was tested in a model that, unlike SMA MNs, does not display a pronounced imbalance toward fission but rather a tendency. This represents both a limitation and a strength of our study, as positive -also functional- effects were observed after treatment, clarifying how TFN may act independently of the basal conditions of the model. However, the concentrations tested in SMA human fibroblasts did not reach the IC50 of the drug and were chosen conventionally. Therefore, future studies are needed to investigate the impact of higher drug concentrations on mitochondrial homeostasis in this SMA model.

Overall, the beneficial effects of the compound across two distinct SMA models -each characterized by different mitochondrial network conditions- suggest that boosting MFN2 may represent a viable therapeutic strategy. This is particularly promising in the context of combinatorial therapies alongside already approved SMA treatments. In this perspective, further studies will be essential to identify an optimal concentration for systemic administration, which could offer the advantage of oral delivery, as is the case for teriflunomide in the treatment of MS.

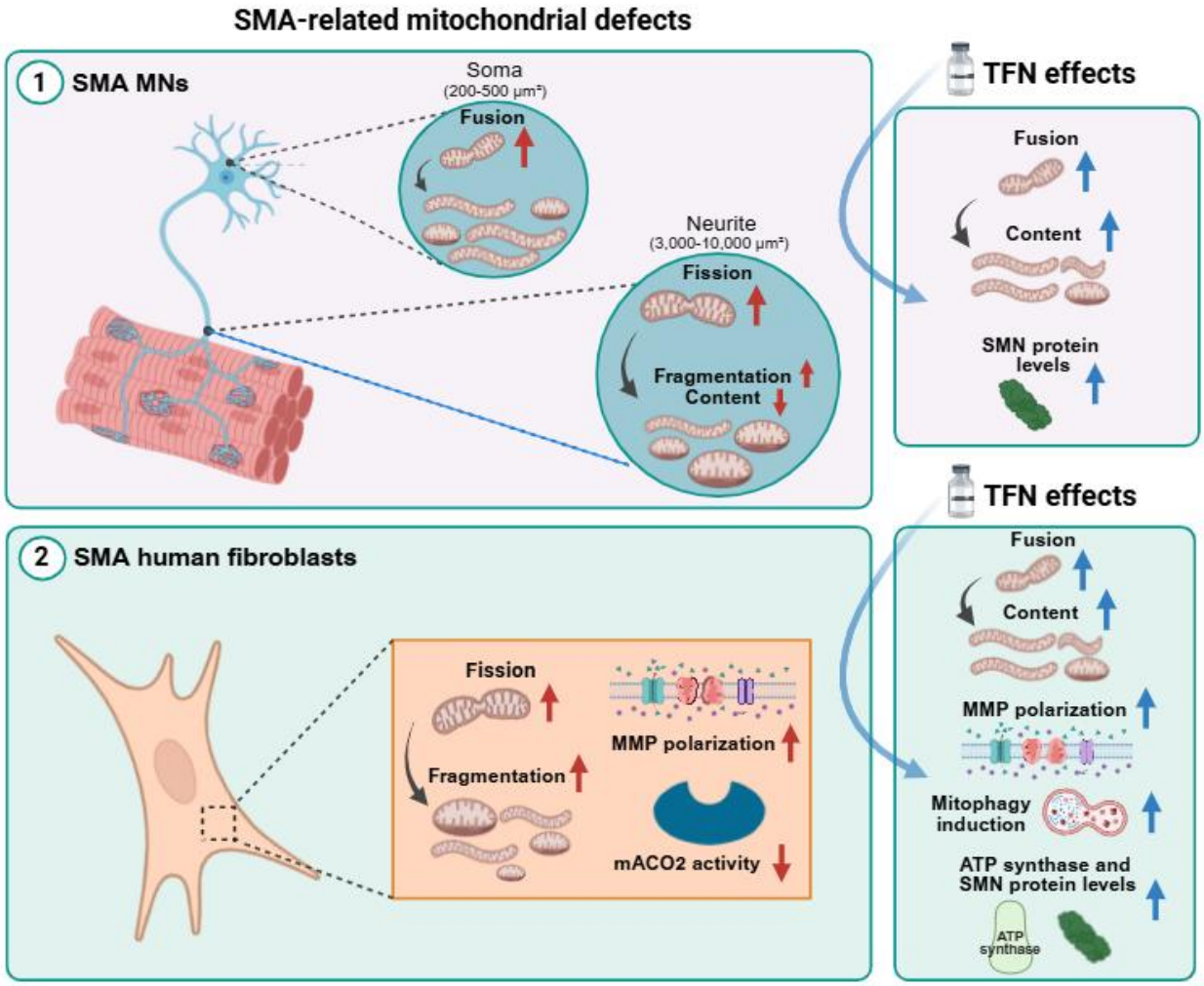

Figure 21. ***Mitochondrial dysfunctions related to SMA MNs and human fibroblasts and the beneficial effect of TFN compound.*** Upper left: mitochondrial defects observed in SMA MNs. Lower left: mitochondrial dysfunction detected in SMA human fibroblasts. Right panels: TFN treatment effects in both models.

REFERENCES

Adamczuk G, Humeniuk E, Iwan M, Natorska-Chomicka D, Adamczuk K, Korga-Plewko A. The Mitochondria-Independent Cytotoxic Effect of Leflunomide on RPMI-8226 Multiple Myeloma Cell Line. *Molecules*. 2021;26(18):5653. https://doi.org/10.3390/molecules26185653

Adebayo M, Singh S, Singh AP, Dasgupta S. Mitochondrial fusion and fission: The fine-tune balance for cellular homeostasis. *FASEB J*. 2021;35(6):e21620. https://doi.org/10.1096/fj.202100067R

Angelova PR, Abramov AY. Role of mitochondrial ROS in the brain: from physiology to neurodegeneration. *FEBS Lett*. 2018;592(5):692-702. https://doi.org/10.1002/1873-3468.12964

Arnold WD, Kassar D, Kissel JT. Spinal muscular atrophy: diagnosis and management in a new therapeutic era. *Muscle Nerve*. 2015;51(2):157-167. https://doi.org/10.1002/mus.24497

Arselin G, Vaillier J, Salin B, et al. The modulation in subunits e and g amounts of yeast ATP synthase modifies mitochondrial cristae morphology. *J Biol Chem*. 2004;279(39):40392-40399. https://doi.org/10.1074/jbc.M404316200

Azzouz M, Le T, Ralph GS, et al. Lentivector-mediated SMN replacement in a mouse model of spinal muscular atrophy. *J Clin Invest*. 2004;114(12):1726-1731. https://doi.org/10.1172/JCI22922

Bahat A, Gross A. Mitochondrial plasticity in cell fate regulation. *J Biol Chem*. 2019;294(38):13852-13863. https://doi.org/10.1074/jbc.REV118.000828

Behringer EJ, Segal SS. Impact of Aging on Calcium Signaling and Membrane Potential in Endothelium of Resistance Arteries: A Role for Mitochondria. *J Gerontol A Biol Sci Med Sci*. 2017;72(12):1627-1637. https://doi.org/10.1093/gerona/glx079

Bertini E, Burghes A, Bushby K, et al. 134th ENMC International Workshop: Outcome Measures and Treatment of Spinal Muscular Atrophy, 11-13 February 2005, Naarden, The Netherlands. *Neuromuscul Disord*. 2005;15(11):802-816. https://doi.org/10.1016/j.nmd.2005.07.005

Bessou P, Emonet-Dénand F, Laporte Y. Motor fibres innervating extrafusal and intrafusal muscle fibres in the cat. *J Physiol*. 1965;180(3):649-672. https://doi.org/10.1113/jphysiol.1965.sp007722

Birk AV, Liu S, Soong Y, et al. The mitochondrial-targeted compound SS-31 re-energizes ischemic mitochondria by interacting with cardiolipin. *J Am Soc Nephrol*. 2013;24(8):1250-1261. https://doi.org/10.1681/ASN.2012121216

Bordet T, Berna P, Abitbol JL, Pruss RM. Olesoxime (TRO19622): A Novel Mitochondrial-Targeted Neuroprotective Compound. *Pharmaceuticals (Basel)*. 2010;3(2):345-368. https://doi.org/10.3390/ph3020345

Boulisfane N, Choleza M, Rage F, Neel H, Soret J, Bordonné R. Impaired minor tri-snRNP assembly gene differential splicing defects of U12-type introns in lymphoblasts derived from a type I SMA patient. *Hum Mol Genet*. 2011;20(4):641-648. https://doi.org/10.1093/hmg/ddq508

Briscoe J, Pierani A, Jessell TM, & Ericson J. A homeodomain protein code specifies progenitor cell identity and neuronal fate in the ventral neural tube. *Cell*. 2000; 101(4), 435–445. https://doi.org/10.1016/S0092-8674(00)80853-3

Brzustowicz LM, Lehner T, Castilla LH, et al. Genetic mapping of chronic childhood-onset spinal muscular atrophy to chromosome 5q11.2-13.3. *Nature.* 1990; 344(6266): 540–541. https://doi.org/10.1038/344540a0

Burghes AH, Beattie CE. Spinal muscular atrophy: why do low levels of survival motor neuron protein make motor neurons sick? *Nat Rev Neurosci*. 2009;10(8):597-609. https://doi.org/10.1038/nrn2670

Burke RE, Levine DN, Tsairis P, Zajac FE 3rd. Physiological types and histochemical profiles in motor units of the cat gastrocnemius. *J Physiol*. 1973;234(3):723-748. https://doi.org/10.1113/jphysiol.1973.sp010369

Cagalinec M, Safiulina D, Liiv M, et al. Principles of the mitochondrial fusion and fission cycle in neurons. *J Cell Sci*. 2013;126(Pt 10):2187-2197. https://doi.org/10.1242/jcs.118844

Cardanho-Ramos C, Morais VA. Mitochondrial Biogenesis in Neurons: How and Where. *Int J Mol Sci*. 2021; 22(23):13059. https://doi.org/10.3390/ijms222313059

Cartegni L, Krainer AR. Correction of disease-associated exon skipping by synthetic exon-specific activators. *Nat Struct Biol*. 2003;10(2):120-125. https://doi.org/10.1038/nsb887

Chandrasekhar A. Turning heads: development of vertebrate branchiomotor neurons. *Dev Dyn*. 2004;229(1):143-161. https://doi.org/10.1002/dvdy.10444

Chaytow H, Faller KME, Huang YT, Gillingwater TH. Spinal muscular atrophy: From approved therapies to future therapeutic targets for personalized medicine. *Cell Rep Med*. 2021;2(7):100346. https://doi.org/10.1016/j.xcrm.2021.100346

Chaytow H, Huang YT, Gillingwater TH, Faller KME. The role of survival motor neuron protein (SMN) in protein homeostasis. *Cell Mol Life Sci*. 2018;75(21):3877-3894. https://doi.org/10.1007/s00018-018-2849-1

Chen H, Chan DC. Mitochondrial dynamics--fusion, fission, movement, and mitophagy--in neurodegenerative diseases. *Hum Mol Genet*. 2009;18(R2):R169-R176. https://doi.org/10.1093/hmg/ddp326

Chen W, Zhao H, Li Y. Mitochondrial dynamics in health and disease: mechanisms and potential targets. *Signal Transduct Target Ther*. 2023;8(1):333. https://doi.org/10.1038/s41392-023-01547-9

Cogliati S, Frezza C, Soriano ME, et al. Mitochondrial cristae shape determines respiratory chain supercomplexes assembly and respiratory efficiency. *Cell*. 2013;155(1):160-171. https://doi.org/10.1016/j.cell.2013.08.032

Dang X, Zhang L, Franco A, et al. Discovery of 6-Phenylhexanamide Derivatives as Potent Stereoselective Mitofusin Activators for the Treatment of Mitochondrial Diseases. *J Med Chem*. 2020;63(13):7033-7051. https://doi.org/10.1021/acs.jmedchem.0c00366

Dasen JS, De Camilli A, Wang B, Tucker PW, Jessell TM. Hox repertoires for motor neuron diversity and connectivity gated by a single accessory factor, FoxP1. *Cell*. 2008;134(2):304-316. https://doi.org/10.1016/j.cell.2008.06.019

Day JW, Howell K, Place A, et al. Advances and limitations for the treatment of spinal muscular atrophy. *BMC Pediatr*. 2022;22(1):632. https://doi.org/10.1186/s12887-022-03671-x

Dennis MY, Harshman L, Nelson BJ, et al. The evolution and population diversity of human-specific segmental duplications. *Nat Ecol Evol*. 2017;1(3):69. https://doi.org/10.1038/s41559-016-0069

Di Nottia M, Verrigni D, Torraco A, Rizza T, Bertini E, Carrozzo R. Mitochondrial Dynamics: Molecular Mechanisms, Related Primary Mitochondrial Disorders and Therapeutic Approaches. *Genes (Basel)*. 2021;12(2):247. https://doi.org/10.3390/genes12020247

DUBOWITZ V. INFANTILE MUSCULAR ATROPHY. A PROSPECTIVE STUDY WITH PARTICULAR REFERENCE TO A SLOWLY PROGRESSIVE VARIETY. *Brain*. 1964;87:707-718. https://doi.org/10.1093/brain/87.4.707

ECCLES JC, ECCLES RM, IGGO A, LUNDBERG A. Electrophysiological studies on gamma motoneurones. *Acta Physiol Scand*. 1960; 50:32-40. https://doi.org/10.1111/j.1748-1716.1960.tb02070.x

Finkel R, Bertini E, Muntoni F, Mercuri E; ENMC SMA Workshop Study Group. 209th ENMC International Workshop: Outcome Measures and Clinical Trial Readiness in Spinal Muscular Atrophy 7-9 November 2014, Heemskerk, The Netherlands. *Neuromuscul Disord*. 2015;25(7):593-602. https://doi.org/10.1016/j.nmd.2015.04.009

Finkel RS, Mercuri E, Darras BT, et al. Nusinersen versus Sham Control in Infantile-Onset Spinal Muscular Atrophy. *N Engl J Med*. 2017;377(18):1723-1732. https://doi.org/10.1056/NEJMoa1702752

Foust KD, Wang X, McGovern VL, et al. Rescue of the spinal muscular atrophy phenotype in a mouse model by early postnatal delivery of SMN [retracted in: Nat Biotechnol. 2022 Nov;40(11):1692. doi: 10.1038/s41587-022-01497-7]. *Nat Biotechnol*. 2010;28(3):271-274. https://doi.org/10.1038/s41587-022-01497-7

Frezza C, Cipolat S, Martins de Brito O, et al. OPA1 controls apoptotic cristae remodeling independently from mitochondrial fusion. *Cell*. 2006;126(1):177-189. https://doi.org/10.1016/j.cell.2006.06.025

Fu W, Liu Y, Yin H. Mitochondrial Dynamics: Biogenesis, Fission, Fusion, and Mitophagy in the Regulation of Stem Cell Behaviors. *Stem Cells Int*. 2019;2019:9757201. https://doi.org/10.1155/2019/9757201

Fulceri F, Biagioni F, Limanaqi F, et al. Ultrastructural characterization of peripheral denervation in a mouse model of Type III spinal muscular atrophy. *J Neural Transm (Vienna)*. 2021;128(6):771-791. https://doi.org/10.1007/s00702-021-02353-9

Gallo Cantafio ME, Torcasio R, Viglietto G, Amodio N. Non-Coding RNA-Dependent Regulation of Mitochondrial Dynamics in Cancer Pathophysiology. *Non-Coding RNA*. 2023; 9(1):16. https://doi.org/10.3390/ncrna9010016

Gray MW, Burger G, Lang BF. Mitochondrial evolution. *Science*. 1999;283(5407):1476-1481. https://doi.org/10.1126/science.283.5407.1476

Hellbach N, Peterson S, Haehnke D, et al. Impaired myogenic development, differentiation and function in hESC-derived SMA myoblasts and myotubes. *PLoS One*. 2018;13(10):e0205589. https://doi.org/10.1371/journal.pone.0205589

Hoffmann J. Ueber chronische spinale Muskelatrophie im Kindesalter, auf familiärer Basis. *Dtsch Z Für Nervenheilkd*. 1893; 3:427–470. https://doi.org/10.1007/BF01668496

Jeong SY, Seol DW. The role of mitochondria in apoptosis. *BMB Rep*. 2008;41(1):11-22. https://doi.org/10.5483/bmbrep.2008.41.1.011

Kandel ER, Schwartz JH, Jessell TM. *Principles of Neural Science*. 4th ed. New York, NY: McGraw-Hill; 2000.

Kariya S, Park GH, Maeno-Hikichi Y, et al. Reduced SMN protein impairs maturation of the neuromuscular junctions in mouse models of spinal muscular atrophy. *Hum Mol Genet*. 2008;17(16):2552-2569. https://doi.org/10.1093/hmg/ddn156

Kathiresan DS, Balasubramani R, Marudhachalam K, et al. Role of Mitochondrial Dysfunctions in Neurodegenerative Disorders: Advances in Mitochondrial Biology. *Mol Neurobiol*. 2025;62(6):6827-6855. doi:10.1007/s12035-024-04469-x. https://doi.org/10.1007/s12035-024-04469-x

Kong L, Wang X, Choe DW, et al. Impaired synaptic vesicle release and immaturity of neuromuscular junctions in spinal muscular atrophy mice. *J Neurosci*. 2009;29(3):842-851. https://doi.org/10.1523/JNEUROSCI.4434-08.2009

Kraus F, Roy K, Pucadyil TJ, Ryan MT. Function and regulation of the divisome for mitochondrial fission. *Nature*. 2021;590(7844):57-66. https://doi.org/10.1038/s41586-021-03214-x

KUGELBERG E, WELANDER L. Heredofamilial juvenile muscular atrophy simulating muscular dystrophy. *AMA Arch Neurol Psychiatry*. 1956;75(5):500-509. https://doi.org/10.1001/archneurpsyc.1956.02330230050005

Lane N, Martin W. The energetics of genome complexity. *Nature*. 2010;467(7318):929-934. https://doi.org/10.1038/nature09486

Lee RH, Heckman CJ. Bistability in spinal motoneurons in vivo: systematic variations in persistent inward currents. *J Neurophysiol*. 1998;80(2):583-593. https://doi.org/10.1152/jn.1998.80.2.583

Lefebvre S, Burglen L, Reboullet S, et al. Identification and characterization of a spinal muscular atrophy-determining gene. *Cell*. 1995; 80(1): 155–165. https://doi.org/10.1016/0092-8674(95)90460-3

Li J, Donath S, Li Y, Qin D, Prabhakar BS, Li P. miR-30 regulates mitochondrial fission through targeting p53 and the dynamin-related protein-1 pathway. *PLoS Genet*. 2010;6(1):e1000795. https://doi.org/10.1371/journal.pgen.1000795

Lin MT, Beal MF. Mitochondrial dysfunction and oxidative stress in neurodegenerative diseases. *Nature*. 2006;443(7113):787-795. https://doi.org/10.1038/nature05292

Liu Q, Dreyfuss G. A novel nuclear structure containing the survival of motor neurons protein. *EMBO J*. 1996;15(14):3555-3565. https://doi.org/10.1002/j.1460-2075.1996.tb00725.x

López-González R, Velasco I. Therapeutic potential of motor neurons differentiated from embryonic stem cells and induced pluripotent stem cells. *Arch Med Res*. 2012;43(1):1-10. https://doi.org/10.1016/j.arcmed.2012.01.007

Lorson CL, Hahnen E, Androphy EJ, Wirth B. A single nucleotide in the SMN gene regulates splicing and is responsible for spinal muscular atrophy. *Proc Natl Acad Sci U SA*. 1999;96(11):6307-6311. https://doi.org/10.1073/pnas.96.11.6307

Lu D, Feng Y, Liu G, et al. Mitochondrial transport in neurons and evidence for its involvement in acute neurological disorders. *Front Neurosci*. 2023;17:1268883. https://doi.org/10.3389/fnins.2023.1268883

Lunn MR, Wang CH. Spinal muscular atrophy. *Lancet.* 2008; 371(9630):2120–2133. https://doi.org/10.1016/S0140-6736(08)60921-6

Lutz AK, Exner N, Fett ME, et al. Loss of parkin or PINK1 function increases Drp1-dependent mitochondrial fragmentation. *J Biol Chem*. 2009;284(34):22938-22951. https://doi.org/10.1074/jbc.M109.035774

Ma K, Chen G, Li W, Kepp O, Zhu Y, Chen Q. Mitophagy, Mitochondrial Homeostasis, and Cell Fate. *Front Cell Dev Biol*. 2020;8:467. https://doi.org/10.3389/fcell.2020.00467Maden M**.** Retinoic acid in the development, regeneration and maintenance of the nervous system. *Nature Reviews Neuroscience*. 2007; 8(10), 755–765. https://doi.org/10.1038/nrn2212

Malla B, Cotten S, Ulshoefer R, et al. Teriflunomide preserves peripheral nerve mitochondria from oxidative stress-mediated alterations. *Ther Adv Chronic Dis*. 2020;11:2040622320944773. https://doi.org/10.1177/2040622320944773

Malla B, Liotta A, Bros H, et al. Teriflunomide Preserves Neuronal Activity and Protects Mitochondria in Brain Slices Exposed to Oxidative Stress. *Int J Mol Sci*. 2022;23(3):1538. https://doi.org/10.3390/ijms23031538

Martin W, Müller M. The hydrogen hypothesis for the first eukaryote. *Nature*. 1998;392(6671):37-41. https://doi.org/10.1038/32096

Mazzoni EO, Mahony S, Closser M, et al. Synergistic binding of transcription factors to cell-specific enhancers programs motor neuron identity. *Nat Neurosci*. 2013;16(9):1219-1227. https://doi.org/10.1038/nn.3467

Melki J, Abdelhak S, Sheth P, et al. Gene for chronic proximal spinal muscular atrophies maps to chromosome 5q. *Nature.* 1990; 344(6268): 767–778. https://doi.org/10.1038/344767a0

Mendell JR, Al-Zaidy S, Shell R, et al. Single-Dose Gene-Replacement Therapy for Spinal Muscular Atrophy. *N Engl J Med*. 2017;377(18):1713-1722. https://doi.org/10.1056/NEJMoa1706198

Miller N, Shi H, Zelikovich AS, Ma YC. Motor neuron mitochondrial dysfunction in spinal muscular atrophy. *Hum Mol Genet*. 2016; 25(16):3395–3406. https://doi.org/10.1093/hmg/ddw262

Miret-Casals L, Sebastián D, Brea J, et al. Identification of New Activators of Mitochondrial Fusion Reveals a Link between Mitochondrial Morphology and Pyrimidine Metabolism. *Cell Chem Biol*. 2018;25(3):268-278.e4. https://doi.org/10.1016/j.chembiol.2017.12.001

Molina AJ, Wikstrom JD, Stiles L, et al. Mitochondrial networking protects beta-cells from nutrient-induced apoptosis. *Diabetes*. 2009;58(10):2303-2315. https://doi.org/10.2337/db07-1781

Monani UR, Lorson CL, Parsons DW, et al. A single nucleotide difference that alters splicing patterns distinguishes the SMA gene SMN1 from the copy gene SMN2. *Hum Mol Genet*. 1999;8(7):1177-1183. https://doi.org/10.1093/hmg/8.7.1177

Monani UR, Sendtner M, Coovert DD, et al. The human centromeric survival motor neuron gene (SMN2) rescues embryonic lethality in Smn(-/-) mice and results in a mouse with spinal muscular atrophy [published correction appears in Hum Mol Genet. 2007 Nov 1;16(21):2648. Rossol, W [corrected to Rossoll, W]]. *Hum Mol Genet*. 2000;9(3):333-339. https://doi.org/10.1093/hmg/9.3.333

Monani UR. Spinal muscular atrophy: a deficiency in a ubiquitous protein; a motor neuron-specific disease. *Neuron*. 2005;48(6):885-896. https://doi.org/10.1016/j.neuron.2005.12.001

Muntoni F, Bertini E, Comi G, et al. Long-term follow-up of patients with type 2 and non-ambulant type 3 spinal muscular atrophy (SMA) treated with olesoxime in the OLEOS trial. *Neuromuscul Disord*. 2020;30(12):959-969. https://doi.org/10.1016/j.nmd.2020.10.008

Ni HM, Williams JA, Ding WX. Mitochondrial dynamics and mitochondrial quality control. *Redox Biol*. 2015; 4:6-13. https://doi.org/10.1016/j.redox.2014.11.006

Nieuwenhuys R, Voogd J, Van Huijzen C, et al. *The Human Central Nervous System*. 4th ed. New York, NY: Springer; 2008.

Nunnari J, Suomalainen A. Mitochondria: in sickness and in health. *Cell*. 2012;148(6):1145-1159. https://doi.org/10.1016/j.cell.2012.02.035

O'Connor P, Wolinsky JS, Confavreux C, et al. Randomized trial of oral teriflunomide for relapsing multiple sclerosis. *N Engl J Med*. 2011;365(14):1293-1303. https://doi.org/10.1056/NEJMoa1014656

Otera H, Wang C, Cleland MM, et al. Mff is an essential factor for mitochondrial recruitment of Drp1 during mitochondrial fission in mammalian cells. *J Cell Biol*. 2010;191(6):1141-1158. https://doi.org/10.1083/jcb.201007152

Park GH, Maeno-Hikichi Y, Awano T, et al. Reduced survival of motor neuron (SMN) protein in motor neuronal progenitor functions cell autonomously to cause spinal muscular atrophy in model mice expressing the human centromeric (SMN2) gene. *J Neurosci*. 2010;30(36):12005-19. https://doi.org/10.1523/JNEUROSCI.2208-10.2010

Passini MA, Bu J, Richards AM, et al. Antisense oligonucleotides delivered to the mouse CNS ameliorate symptoms of severe spinal muscular atrophy. *Sci Transl Med*. 2011;3(72):72ra18. https://doi.org/10.1126/scitranslmed.3001777

Peeters K, Chamova T, Jordanova A. Clinical and genetic diversity of SMN1-negative proximal spinal muscular atrophies. *Brain*. 2014;137(Pt 11):2879-2896. https://doi.org/10.1093/brain/awu169

Philippidou P, Walsh CM, Aubin J, Jeannotte L, Dasen JS. Sustained Hox5 gene activity is required for respiratory motor neuron development. *Nat Neurosci*. 2012;15(12):1636-1644. https://doi.org/10.1038/nn.3242

Popov LD. Mitochondrial biogenesis: An update. *J Cell Mol Med*. 2020;24(9):4892-4899 https://doi.org/10.1111/jcmm.15194

Purves D, Augustine GJ, Fitzpatrick D, et al. *Neuroscience*. 3rd ed. Sunderland, MA: Sinauer Associates; 2004.

Rambold AS, Kostelecky B, Elia N, Lippincott-Schwartz J. Tubular network formation protects mitochondria from autophagosomal degradation during nutrient starvation. *Proc Natl Acad Sci U S A*. 2011;108(25):10190-10195. https://doi.org/10.1073/pnas.1107402108

Rexed B. A cytoarchitectonic atlas of the spinal cord in the cat. *Journal of Comparative Neurology*. 1954; 100 (2): 297-379. https://doi.org/10.1002/cne.901000205

Ripolone M, Ronchi D, Violano R, et al. Impaired Muscle Mitochondrial Biogenesis and Myogenesis in Spinal Muscular Atrophy. *JAMA Neurol*. 2015;72(6):666-75. https://doi.org/10.1001/jamaneurol.2015.0178

Rocha AG, Franco A, Krezel AM, et al. MFN2 agonists reverse mitochondrial defects in preclinical models of Charcot-Marie-Tooth disease type 2A. *Science*. 2018;360(6386):336-341. https://doi.org/10.1126/science.aao1785

Rochette CF, Gilbert N, Simard LR. SMN gene duplication and the emergence of the SMN2 gene occurred in distinct hominids: SMN2 is unique to Homo sapiens. *Hum. Genet*. 2001; 108:255–66. https://doi.org/10.1007/s004390100473

Rossoll W, Jablonka S, Andreassi C, et al. Smn, the spinal muscular atrophy-determining gene product, modulates axon growth and localization of beta-actin mRNA in growth cones of motoneurons. *J Cell Biol*. 2003;163(4):801-812. https://doi.org/10.1083/jcb.200304128

Shen Q, Yamano K, Head BP, et al. Mutations in Fis1 disrupt orderly disposal of defective mitochondria. *Mol Biol Cell*. 2014;25(1):145-159 https://doi.org/10.1091/mbc.E13-09-0525

Singh NK, Singh NN, Androphy EJ, Singh RN. Splicing of a critical exon of human Survival Motor Neuron is regulated by a unique silencer element located in the last intron. *Mol Cell Biol*. 2006;26(4):1333-1346. https://doi.org/10.1128/MCB.26.4.1333-1346.2006

Skordis LA, Dunckley MG, Yue B, Eperon IC, Muntoni F. Bifunctional antisense oligonucleotides provide a trans-acting splicing enhancer that stimulates SMN2 gene expression in patient fibroblasts. *Proc Natl Acad Sci U S A*. 2003;100(7):4114-4119. https://doi.org/10.1073/pnas.0633863100

Sockanathan S, Perlmann T, Jessell TM. Retinoid receptor signaling in postmitotic motor neurons regulates rostrocaudal positional identity and axonal projection pattern. *Neuron*. 2003;40(1):97-11. https://doi.org/10.1016/s0896-6273(03)00532-4

Standring S, ed. *Gray's Anatomy: The Anatomical Basis of Clinical Practice*. 42nd ed. London, UK:Elsevier; 2020.

Stanga S, Caretto A, Boido M, Vercelli A. Mitochondrial Dysfunctions: A Red Thread across Neurodegenerative Diseases. *Int J Mol Sci*. 2020;21(10):3719. https://doi.org/10.3390/ijms21103719

Stifani N. Motor neurons and the generation of spinal motor neuron diversity. *Front Cell Neurosci*. 2014; 8:293. https://doi.org/10.3389/fncel.2014.00293

Tábara LC, Segawa M, Prudent J. Molecular mechanisms of mitochondrial dynamics. *Nat Rev Mol Cell Biol*. 2025;26(2):123-146 https://doi.org/10.1038/s41580-024-00785-1

Tahirovic S, Bradke F. Neuronal polarity. *Cold Spring Harb Perspect Biol*. 2009;1(3):a001644. https://doi.org/10.1101/cshperspect.a001644

Thelen MP, Wirth B, Kye MJ. Mitochondrial defects in the respiratory complex I contribute to impaired translational initiation via ROS and energy homeostasis in SMA motor neurons. *Acta Neuropathol Commun*. 2020;8(1):223. https://doi.org/10.1186/s40478-020-01101-6

Thielen FW, Heine RJSD, Berg SVD, Ham RMTT, Groot CAU. Towards sustainability and affordability of expensive cell and gene therapies? Applying a cost-based pricing model to estimate prices for Libmeldy and Zolgensma. *Cytotherapy*. 2022;24(12):1245-1258. https://doi.org/10.1016/j.jcyt.2022.09.002

Toyama EQ, Herzig S, Courchet J, et al. Metabolism. AMP-activated protein kinase mediates mitochondrial fission in response to energy stress. *Science*. 2016;351(6270):275-281. https://doi.org/10.1126/science.aab4138Trigo D, Avelar C, Fernandes M, Sá J, da Cruz E Silva O. Mitochondria, energy, and metabolism in neuronal health and disease. *FEBS Lett*. 2022;596(9):1095-1110. https://doi.org/10.1002/1873-3468.14298

Tsuchida T, Ensini M, Morton SB, et al. Topographic organization of embryonic motor neurons defined by expression of LIM homeobox genes. *Cell*. 1994;79(6):957-970. https://doi.org/10.1016/0092-8674(94)90027-2

Verhaart IEC, Robertson A, Wilson IJ, et al. Prevalence, incidence and carrier frequency of 5q-linked spinal muscular atrophy – a literature review. *Orphanet J Rare Dis.* 2017; 12(1):124. https://doi.org/10.1186/s13023-017-0671-8

WADKINS CL, LEHNINGER AL. The adenosine triphosphate-adenosine diphosphate exchange reaction of oxidative phosphorylation. *J Biol Chem*. 1958;233(6):1589-1597

Wang ZB, Zhang X, Li XJ. Recapitulation of spinal motor neuron-specific disease phenotypes in a human cell model of spinal muscular atrophy. *Cell Res*. 2013;23(3):378-393. https://doi.org/10.1038/cr.2012.166

Werdnig G. Two early infantile hereditary cases of progressive muscular atrophy simulating dystrophy, but on a neural basis. 1891. *Arch Neurol*. 1971; 25(3):276–278. https://doi.org/10.1001/archneur.1971.00490030102014

Wijngaarde CA, Blank AC, Stam M, Wadman RI, van den Berg LH, van der Pol WL. Cardiac pathology in spinal muscular atrophy: a systematic review. *Orphanet J Rare Dis*. 2017;12(1):67. https://doi.org/10.1186/s13023-017-0613-5

Xie LL, Shi F, Tan Z, Li Y, Bode AM, Cao Y. Mitochondrial network structure homeostasis and cell death. *CancerSci.* 2018;109(12):3686-369. https://doi.org/10.1111/cas.13830

Xu CC, Denton KR, Wang ZB, Zhang X, Li XJ. Abnormal mitochondrial transport and morphology as early pathological changes in human models of spinal muscular atrophy. *Dis Model Mech*. 2016;9(1):39-49. https://doi.org/10.1242/dmm.021766

Yao CH, Wang R, Wang Y, Kung CP, Weber JD, Patti GJ. Mitochondrial fusion supports increased oxidative phosphorylation during cell proliferation. *Elife*. 2019;8:e41351. https://doi.org/10.7554/eLife.41351

Yong J, Wan L, Dreyfuss G. Why do cells need an assembly machine for RNA-protein complexes?. *Trends Cell Biol*. 2004;14(5):226-232. https://doi.org/10.1016/j.tcb.2004.03.010

Youle RJ, van der Bliek AM. Mitochondrial fission, fusion, and stress. *Science*. 2012;337(6098):1062-1065. https://doi.org/10.1126/science.1219855

Zhang L, Dang X, Franco A, Zhao H, Dorn GW II. Piperine Derivatives Enhance Fusion and Axonal Transport of Mitochondria by Activating Mitofusins. *Chemistry*. 2022; 4(3):655-668. https://doi.org/10.3390/chemistry4030047

Zhou J, Zheng X, Shen H. Targeting RNA-splicing for SMA treatment. *Mol Cells*. 2012;33(3):223-228. https://doi.org/10.1007/s10059-012-0005-6

Zorova LD, Popkov VA, Plotnikov EY, et al. Mitochondrial membrane potential. *Anal Biochem*. 2018;552:50-59. https://doi.org/10.1016/j.ab.2017.07.009